STRETCHABLE MICRONEEDLE ELECTRODE ARRAY FOR STIMULATING AND MEASURING INTRAMUSCULAR ELECTROMYOGRAPHIC ACTIVITY

A Dissertation
Presented to
The Academic Faculty

by

Gareth Sacha Guvanasen

In Partial Fulfillment
of the Requirements for the Degree
Doctor of Philosophy in the
School of Electrical and Computer Engineering

Georgia Institute of Technology
December 2015

STRETCHABLE MICRONEEDLE ELECTRODE ARRAY FOR STIMULATING AND MEASURING INTRAMUSCULAR ELECTROMYOGRAPHIC ACTIVITY

Approved by:

Dr. Stephen P. DeWeerth, Advisor
School of Electrical and
Computer Engineering
Georgia Institute of Technology

Dr. T. Richard Nichols, Co-Advisor
School of Applied Physiology
Georgia Institute of Technology

Dr. Robert J. Butera
School of Electrical and
Computer Engineering
Georgia Institute of Technology

Dr. Boris I. Prilutsky
School of Applied Physiology
Georgia Institute of Technology

Dr. Pamela T. Bhatti
School of Electrical and
Computer Engineering
Georgia Institute of Technology

Dr. Arthur W. English
School of Medicine
Emory University

Date Approved: October 2, 2015

ACKNOWLEDGEMENTS

The environment in which I have worked and studied at Georgia Tech has been one of support, intellectual curiosity, ambition, and comradery. As such, it is too difficult to thank everyone who has assisted my research, but I would like to express my great appreciation of a few individuals.

I am indebted to my advisors, Professor Stephen P. DeWeerth and Professor T. Richard Nichols. Under their guidance, I have learned to become a better communicator, a better scientist – and a better person. I have learned how to think critically of my work and that of others, while maintaining "the big picture" in mind. I will forever remember their lessons and their mentorship.

In some ways, Dr. Swaminathan Rajaraman has acted as my third research advisor. I am very thankful for his tutelage in microfabrication, guidance in overcoming the challenges of graduate-school life, and assistance in the development of the neuroprosthetic device presented herein.

I would also like to thank the other members my committee: Dr. Pamela T. Bhatti, Dr. Robert J. Butera, Dr. Arthur W. English, and Dr. Boris I. Prilutsky, for advising me in the fields of physiology, histology, and electrical engineering, which enabled me to more thoroughly characterize and evaluate the capabilities of my neuroprosthetic device.

There are many within the Neurolab, the Nichols' Lab, and at Axion Biosystems who have provided considerable assistance with device fabrication and animal experiments, and I am incredibly thankful for their time and efforts. Listed, are a few of these individuals: Yogi Patel, Chris Tuthill, Ricardo Aguilar, Jason White, Bill Goolsby, Chancellor Shafor, Ashton Cheek, Dr. Mark Lyle, Jeffrey Bair, Dr. Irrum Niazi, Elma Kajtaz, and Dr. Liang Guo. Thank you.

Lastly, I would like to thank my mother, father, and Uncle Peter; who have served as sources of inspiration, encouragement, love, and guidance throughout my life.

The research presented herein was supported in part by US NIH Grants EB006179, HD32571, and SBIR NS071894-01, for which I am sincerely grateful.

TABLE OF CONTENTS

LIST OF TABLES

LIST OF FIGURES

SUMMARY

The advancement of technologies that interface with electrically excitable tissues, such as the cortex and muscle, has the potential to lend greater mobility to the disabled, facilitate the study of the central and peripheral nervous systems, and transform how people interact with technological devices. Myoelectric interfaces are currently limited in their signal fidelity, spatial resolution, and interfacial area. Such interfaces are either implanted in muscle [1] or applied to the surface of the muscle [2] or skin [3]. Thus far, the former technology has been limited in its applications due to the stiffness (several orders of magnitude greater than muscle) of its substrates, such as silicon and polyimide, whereas the latter technology suffers from poor spatial resolution and signal quality due to the physical separation between the electrodes and the signal source. We have developed a stretchable microneedle electrode array (sMEA) that can function while stretching and flexing with muscle tissue, thereby enabling multi-site muscle stimulation and electromyography (EMG) measurement across a large interfacial area.

The scope of this research encompassed: (i) the development of a stretchable and flexible array of penetrating electrodes for the purposes of stimulating and measuring the electrical activity of excitable tissue, (ii) the characterization of the electrical, mechanical, and biocompatibility properties of this electrode array, (iii) the measurement of regional electrical activity of muscle via the electrode array, (iv) the study of the effect of spatially distributed stimulation of muscle on the fatigue and ripple of muscle contractions, and (v) the assessment of the extent to which the stretch response of electrically stimulated muscle behaves in a physiological manner.

CHAPTER I

INTRODUCTION

Prosthetics that measure and stimulate the electrical activity of muscle, in particular, possess three advantages over devices that interface with nerves, the spinal cord, and the cortex. One, they reduce the risk of damage to the central and peripheral nervous systems [4], [5]. Two, they facilitate the study of the spatial activation of muscle. And three, they may allow for the activation of paralyzed muscle through electrical stimulation in a more physiological fashion [6], [7].

Unfortunately, existing myoelectric interfaces are limited in their signal fidelity, spatial resolution, and interfacial area and are thus restricted in the extent to which they can observe muscle activity or control muscle contractions. Such interfaces are either implanted in muscle [1] or applied to the surface of the muscle [2] or skin [3]. Thus far, the former technology has been limited in its applications due to the stiffness of its substrates, whereas the latter technology suffers from poor spatial resolution and signal quality due to the physical separation between the electrodes and the signal source. Therefore, there remains a need for prosthetic devices that are capable of measuring and stimulating muscle activity with high signal fidelity and spatial resolution across a large area.

1.1 Neurophysiology

To produce neuroprosthetic devices that are capable of reproducing the physiological recruitment of muscle, it is necessary to understand (i) how muscle is recruited under normal physiological conditions, (ii) the mechanisms through which the electrical activity of muscle tissue is measured, and (iii) how muscle fibers are activated through the electrical stimulation of tissue.

1.1.1 Physiological Recruitment of Muscle

The wide variety of motor tasks produced through muscular systems is achieved by the differential activation of muscles, muscle compartments, and muscle fibers [8]–[13]. Running will require the recruitment of different muscles than swimming, a range of shoulder movements will activate different deltoid muscle compartments preferentially [14], [15], and particular motor units/muscle fibers may be recruited depending on whether it is necessary to lift a pencil or a piano [16].

When a muscle contracts, its muscle fibers will generally be recruited in order of their contractile force, from weak to strong [16]. This physiology enables animals to produce fine motor movements with weak Type I fibers, and forceful contractions with strong Type II fibers; however, muscles do not always utilize this order of recruitment. Muscles can be compartmentalized into regions innervated by different nerve branches [17], [18], and some of these compartments may be more greatly recruited than others depending on the task performed [10], [19], regardless of its muscle fiber composition. The deltoid muscle, for example, is composed of seven compartments [19], groups of which may be preferentially activated depending on whether it is necessary to perform shoulder extension or shoulder adduction.

1.1.2 Measuring Electromyographic Activity

The action potentials of muscle fibers produce transient changes in the ion concentrations of the proximal extracellular environment. If a conductive electrode is placed in/on muscle, in the vicinity of this ion flux, the change of these ion concentrations during an action potential will attract/repel the electrons within an electrode to generate a measureable electric current along the electrode's trace, thus enabling the activity of muscle to be electrically observed [20]. Because the diameter of Type II muscle fibers is larger than that of Type I, the ionic resistance along Type II fibers is lower and action potentials travel along those fibers more rapidly [21], [22].

Additionally, wider muscle fibers will also produce action potentials of greater amplitude [22]. Thus, assuming a Type I muscle fiber and a Type II muscle fiber are equidistant from an electrode, the action potentials of Type I would be electrically observed to be longer in duration and shorter in amplitude than those of Type II. As the detecting electrode is moved further away from a muscle fiber, however, the observed action potentials will fall exponentially in amplitude. Additionally, muscle tissue will serve in a similar capacity to a low-pass filter, where the high frequency components of the muscle fiber's electrical activity will be more greatly attenuated as the distance between the electrode and muscle fiber is increased [23]. Although muscle fiber types may differ in their electrical properties, it is difficult to identify muscle fiber types via EMG because the distances between the electrode and the muscle fibers are unknown.

1.1.3 Electrically Stimulating Muscle Tissue

When electrically stimulating muscle to induce the tissue to contract, the motor nerves are more likely to be activated by the stimuli than the muscle fibers because muscle fibers have a higher electric threshold for activation than the motor nerves [24]. As to which motor nerves are recruited by the stimuli is dependent on the proximity of the nerves to the stimulating electrode, the size of the nerves, and the electrical stimulus. In general, the motor nerves closer to the electrode will be activated at a lower level of stimulation than those that are further away; and larger nerves will be more readily activated than smaller nerves [25]. It has been theorized that this axonal size order of recruitment is due to larger axons possessing nodes of Ranvier that are further apart, which enable their axonal membrane potentials to change more rapidly in response to electrical stimulation [26].

As stated in Section 2.1.1, motor units will be physiologically recruited in the order of their contractile force, from weak to strong, or by the compartment in which they are located. Thus, if a single electrode is used to stimulate muscle, it will likely activate

different muscle fiber types and muscle regions than those that would be activated physiologically. This difference in muscle fiber recruitment creates two challenges for neuroprosthetic systems designed to return motor function through electrical stimulation: (i) electrically stimulated muscles will fatigue more easily and (ii) less fine motor control is achieved via muscle stimulation.

1.2 Muscle Stimulation/Measurement Technologies and Applications

Electrodes that can measure electromyographic (EMG) activity as well as stimulate muscles to contract may be utilized to diagnose neuromuscular disorders, enable the paralyzed to gain greater mobility, study the physiological recruitment of muscle, or facilitate the control of technological devices via the measurement of muscle contractions. Some functional electrical stimulation (FES) systems measure the EMG activity of working muscle and electrically stimulate nerves or paralyzed muscle based on this activity. In so doing, such systems enable the paralyzed (e.g. individuals who have spinal cord injuries, nerve damage, or have suffered a stroke) to contract lame muscle and perform a greater range of motor tasks. One of the earliest FES systems was designed to correct for foot drop in hemiplegic patients [27] – during the swing phase of locomotion the system would stimulate the common peroneal nerve to dorsiflex the ankle and prevent the foot from dragging on the ground. More recently, FES has been utilized to return motor function to upper extremities (e.g. arms and hands). The Freehand System, for example, measures the EMG activity of the active muscles in the forearm and neck (through two epimysial electrodes) and correspondingly stimulates the paralyzed muscles of the forearm and hand (via 12 intramuscular/epimysial electrodes) to enable the spinal-cord injured to perform basic hand grasps and gestures [28]. Another research group has developed a robotic prosthetic arm, to be used by amputees, which can be controlled through the contraction of residual muscle [29]. Subjects who receive this robotic arm also undergo surgery to have the nerves that would normally innervate the amputated

limb transferred to residual muscle. This surgery enables subjects to contract the residual muscle with greater precision, the electrical activity of which is measured via electrodes placed on the surface of the skin and serves as the control input for the robotic arm.

Those who have received the FES Freehand System implant have been able to perform a wide variety of daily tasks, including: eating with a fork, drinking from a glass, and brushing their teeth [28], however, these individuals have limited control over their fingers and their muscles are easily fatigued by the electrical stimulation. Although this technology has undoubtedly transformed the lives of the recipient amputees, the speed and accuracy with which the robotic prosthetic arm estimates the desired motor tasks still requires improvement. Surface electrodes are one cause for the arm's slow performance and inaccurate estimates – the skin physically separates such electrodes from the muscle signal sources, reducing the signal fidelity and increasing the muscle crosstalk within the measured EMG signals.

Existing myoelectric prosthesis may use more than one hundred surface electrodes to measure EMG activity [30] or a dozen intramuscular electrodes to measure and stimulate muscle activity [31]. Although both systems have proven effective for use in neuroprosthetic devices, both have their drawbacks. Surface electrode arrays may be applied across a large area of the skin, and thus measure the EMG activity of multiple muscles and neuromuscular compartments; however, their physical separation from the muscle signal sources reduces the spatial resolution and the fidelity of these EMG signals. Conversely, intramuscular electrodes may stimulate and measure the activity of muscle with excellent spatial resolution and signal fidelity, but only so many may be implanted before their use becomes impractical. Thus, a more ideal solution would be to use arrays of intramuscular electrodes.

The substrates of intramuscular electrode arrays have typically been composed of polyimide [30], parylene [32], or SU-8 [33]. These materials facilitate mass-production processes, however, their stiffness reduces the interfacial area across which the electrode

arrays may be applied without causing significant damage to the muscle tissue. Additionally, when these electrode arrays are implanted for a prolonged period of time, their capacity to measure and stimulate muscle activity diminishes as a result of scar-tissue encapsulation induced by the micro-vibrations that occur between the device and the tissue [34].

Polydimethylsiloxane (PDMS) has been utilized as a substrate in microelectrode arrays for application on muscle tissue and the spinal cord. This material is biocompatible [35] and possesses a Young's Modulus three orders of magnitude lower than the materials of traditional intramuscular electrode arrays [36], thus it should cause less scar-tissue encapsulation and may be applied across a greater interfacial area. Not only must the substrate of the microelectrode array be stretchable, but its conductive traces must also maintain a low resistance during high tensile strain. Research groups have patterned vaporized metal on PDMS to form conductive traces and flat electrodes, however, their fabrication processes can create multiple challenges: (i) they may be time consuming and require the use of expensive equipment, (ii) they may have low device yields [2], and (iii) they may produce metal traces that form discontinuities when stretched beyond a 2% tensile strain [37]. Research studies have observed that muscle may change in length by as much as 25% [38], [39], thus the ideal neuromuscular device must be capable of operating under such strain without placing too much stress on muscle. Given the aforementioned challenges presented by existing metal-patterned PDMS technologies and the requirements for a functional microelectrode array, alternative methods must be utilized to produce highly stretchable traces, at low cost, and with high yield.

One research group has used a conductive PDMS (cPDMS) to produce stretchable traces in an epidural electrode array [40], the traces of which have been shown to maintain conductance up to a 100% tensile strain [41]. This device, however, is not ideal for multi-site muscle stimulation and EMG measurement because (i) its electrodes are flat and (ii) its wires are bonded to cPDMS with conductive epoxy. Flat electrodes will

measure and stimulate tissue across a larger area than penetrating electrodes, and thus will have less spatial resolution. Additionally, bodily fluids may easily get between the flat electrodes and muscle, thereby increasing the resistance and reducing the contact between the electrodes and the tissue. Although conductive epoxy may form an effective electrical bond between cPDMS traces and wires, the material is impractical for bonding wires to cPDMS traces of high density and narrow width. Thus, there is still very much a need for a stretchable electrode array that can penetrate tissue to provide high spatial resolution electrical stimulation and measurement across the surface of an expansive area of excitable tissue.

1.3 Dissertation Structure

This dissertation comprises five body chapters and one appendix. Chapters 2, 3, and 4 discuss the research performed to develop and characterize a stretchable microneedle electrode array (sMEA), and its application for the stimulation and measurement of the regional electrical activity of muscle. The appendix is an article published in the Journal of Microelectromechanical Systems that presents my research pertaining to the fabrication of polydimethylsiloxane (PDMS) stencils molded by 3D-printed templates.

Chapter 1: Discusses the principles of electrophysiology and the motivation for the development of an sMEA.

Chapter 2: Describes and illustrates the procedure for fabricating sMEAs, and presents the characterization of the device's electrical, mechanical, cytocompatibility, and biocompatibility properties.

Chapter 3: Characterizes the capabilities/limitations of the sMEA to selectively activate skeletal muscle, spatially distribute charge to reduce the ripple and fatigue of muscle contractions, and reproduce the physiological stretch response of muscle.

Chapter 4: Analyzes regional EMG activity measured through the electrodes of the sMEA, and compares the properties of the EMG signals to the known muscle fiber composition of the underlying muscle tissue.

Chapter 5: Summarizes the research presented within this dissertation relating to sMEAs, and discusses how the technology may be utilized to study the neuromuscular system, and applied to return mobility to the disabled or reduce the symptoms of neurological disorders.

Appendix A: Presents a method by which to mold PDMS stencils with templates produced by 3D printers, and the application of the stencils to the patterning of vaporized metal and cell cultures.

CHAPTER II

FABRICATION AND CHARACTERIZATION OF A STRETCHABLE MICRONEEDLE ELECTRODE ARRAY

We have developed a stretchable microneedle electrode array (sMEA) to stimulate and measure the electrical activity of muscle across multiple sites. The technology provides the signal fidelity and spatial resolution of intramuscular contacts across a large area of tissue. Our sMEA is composed of a polydimethylsiloxane (PDMS) substrate, conductive-PDMS traces, and stainless-steel penetrating electrodes. The device was produced utilizing a highly scalable, microfabrication process. The traces and microneedles maintained a resistance of less than 10 kΩ when stretched up to a ~56% tensile strain, which allows for the full range of physiological stretch of feline muscle. The device and its constituent materials were cytocompatible for 28 days in vitro. When implanted in vivo, the device measured electromyographic (EMG) activity with clear compound motor unit action potentials. The sMEA also maintained a stable connection with moving muscle while electrically stimulating the tissue. This technology has direct application to wearable sensors, neuroprostheses, and electrophysiological studies of animals and humans.

2.1 Introduction

Electrophysiological interfaces enable the modulation and measurement of the electrical activity of excitable tissues for scientific studies [42], [43] and for a wide range of clinical applications: returning motor function to paralyzed individuals [27], [28], [31], reducing pain [44], regulating heart rhythms [45], managing symptoms of movement disorders [46], improving glycemic control [47]. These interfaces can be applied throughout the neuromuscular system (e.g. cortex, nerves, or muscle) to modulate and measure broad movement-related patterns, or to provide direct control over specific

muscle elements. The most appropriate prosthesis will depend on the acceptable tradeoff between modulating/measuring neuromuscular tissue and the invasiveness of the interface.

Individuals who suffer from debilitating neurological disorders, which originate in the cortex, are strong candidates for cortical neuroprostheses. Cortical stimulation has been demonstrated to reduce the symptoms of those suffering from Parkinson's [46], epilepsy [48], and clinical depression [49]. Although stimulating the motor cortex can drive muscle contractions as well, it is inefficacious if the subject suffers from a spinal cord injury or nerve damage. Additionally, the neuronal complexity of the motor cortex limits the resolution by which muscles can be controlled. Therefore, in instances in which it is necessary to precisely control or measure the activity of muscles, it is better to use neuroprostheses that interface peripherally. Neuroprosthetic devices applied to nerves and muscle have returned motor function to paralyzed individuals [28], [31], enabled the restoration of bladder control [50], reduced the severity of gait abnormalities [27], and have been used in the diagnosis of neuromuscular disorders [51].

The stimulation and measurement of muscle activity can be performed transcutaneously, epimysially (on muscle), or intramuscularly. Surface electrodes placed on skin are commonly used because they are less invasive and surgery is not required for their application. Although this technology is very convenient, it places tissue between the electrodes and the sites of interest within muscle. This intervening tissue reduces the spatial and temporal resolution of both muscle stimulation and measurement. As a result, the measured electromyographic (EMG) activity attributable to the muscle over which the surface electrode is applied, may be as little as 36% of the measured signal [52]. In contrast, EMG activity measured via intramuscular electrodes is entirely attributable to the muscles in which the electrodes are implanted [53], [54]. The tissue between surface electrodes and muscle reduces the EMG signal bandwidth from 1 kHz, as measured through intramuscular electrodes, to less than 400 Hz [55], and prevents the effective

identification of motor unit action potentials. The skin, furthermore, restricts the application of surface electrodes to large superficial muscles, while intramuscular electrodes may be used to stimulate and measure the activity of any muscle.

To adequately control and observe a muscle's regional electrical activity, multiple electrodes (e.g. an electrode array) must be applied to a single muscle. Ideally, the spatial resolution of the electrode interface should match that of the muscle's organization. Muscles can be composed of multiple compartments [17]–[19], hundreds of muscle units [56], and hundreds to thousands of muscle fibers [57]. Additionally, regions of muscle can be differentially recruited depending on the motor task performed [10], [19]. Given the spatial and temporal resolution limitations of surface electrodes, matching the spatial resolution of a muscle's activity would require the use of more invasive technologies, such as an array of intramuscular electrodes.

If an array is intramuscular, it must be capable of stretching and conforming to the surface of muscle tissue. Research studies have observed that muscle may change in length by as much as ±25% [39], [38]. Unfortunately, the substrates of intra-muscular electrode arrays have typically been composed of rigid or inelastic materials, such as silicon [36] or parylene [1]. The stiffness of these materials reduces the interfacial area across which the electrode arrays may be applied without causing significant damage to the muscle tissue. Moreover, when these electrode arrays are implanted for a prolonged period of time, their capacity to measure and stimulate muscle activity diminishes as a result of scar-tissue encapsulation, primarily induced by the micro-motions that occur between the device and the tissue due to the mismatch in their mechanical properties [34]. An alternative material, polydimethylsiloxane (PDMS), has been utilized as a substrate in electrode arrays for application on muscle tissue [2] and the spinal cord [58], [59]. This material is biocompatible [35], lends itself to soft lithography [60], and possesses a Young's modulus (~1 MPa) at least three orders of magnitude lower than the substrate materials of traditional intramuscular electrode arrays [2]. Consequently, it has

the potential to cause less scar-tissue encapsulation and be applied across a greater interfacial area.

Not only must the substrate of an intramuscular electrode array be stretchable, but its conductive traces must also maintain a low resistance under physiological tensile strains. The most common approach to defining conductive traces on PDMS is to pattern vaporized metal films on PDMS to form wires and electrodes [61], [62]. This fabrication process, however, can create multiple challenges: (i) it is time consuming and requires the use of expensive equipment (e.g. e-beam evaporators and sputter metal coaters), (ii) it may have low device yields [2], and (iii) most importantly, it may produce metal traces that form discontinuities when stretched beyond a 2% tensile strain [37]. Stretchable electrode arrays that penetrate tissue have recently been developed [63], however, their traces are composed of a room-temperature liquid indium/gallium alloy, which is highly toxic [64]. Conductive PDMS (cPDMS), composed of silver flakes and PDMS mixed at a 4:1 weight ratio [65], has proven to be moldable and highly stretchable. Additionally, the material facilitates the encapsulation of three-dimensional objects, such as electrodes that can be used to penetrate tissue.

This project focused on the development of stretchable microneedle electrode arrays (sMEA) that can provide high spatial resolution and high signal fidelity muscle stimulation and measurement across a large interfacial area of muscle. In producing sMEAs to work with a range of muscle sizes, we: (i) developed a scalable sMEA fabrication process; (ii) characterized the mechanical, electrical, and cytocompatibility properties of our sMEAs; and (iii) implanted our devices into *in vivo* preparations to assess their ability to measure EMG activity, their stability on moving muscle, and their biocompatibility (e.g. the inflammatory response and fibrosis).

2.2 Fabrication of the sMEA

We have developed a scalable, stretchable microneedle electrode array (sMEA) –

here we describe one such device that was designed to cover the entire posterior surface of the feline's lateral gastrocnemius (LG) muscle, to enable electrical stimulation and measurement of that muscle's EMG activity (Fig. 2.1). This muscle was selected because it contains multiple neuromusculular compartments and is of high curvature, which makes it an excellent tissue on which to test the sMEA's electrical and mechanical properties. Four sMEA designs were developed to accommodate different sizes of muscles – two contained 16 microneedle electrodes, one was designed with 24 microneedle electrodes (Fig. 2.2), and a fourth was developed for rat muscle and contained 4 microneedles (Fig. 2.3). The fabrication process for the sMEAs, involved four major steps (Fig. 2.4): (a) designing and etching the sMEA's microneedles, (b) producing the negative micromold for the device, (c) micromolding the sMEA, and (d) packaging the device.

2.2.1 Fabrication and Optimization of the Microneedles

The electrodes of the sMEA were either laser micromachined or photochemically milled (PCM) from 100-μm thick 316L stainless steel. The stainless steel was laser micromachined utilizing an infrared laser (Resonetics, Inc.) with a 50-μm beam of a wavelength of 1047 nm and acid pickled with 9% nitric acid and 2.3% hydrofluoric acid, to remove oxide debris, and clean/sharpen the tips of the microneedles. We have achieved a tip geometry of ~40 μm by acid pickling and sonicating the microneedles for 10 minutes. Although laser micromachining is an effective process for producing microneedles, we used photochemical milling most heavily because its precision and cost efficacy enabled us to test a wide range of microneedle designs. The microneedle electrodes were designed so that the needle could be bent orthogonal to the plane of the base of the electrode to build a three-dimensional structure.

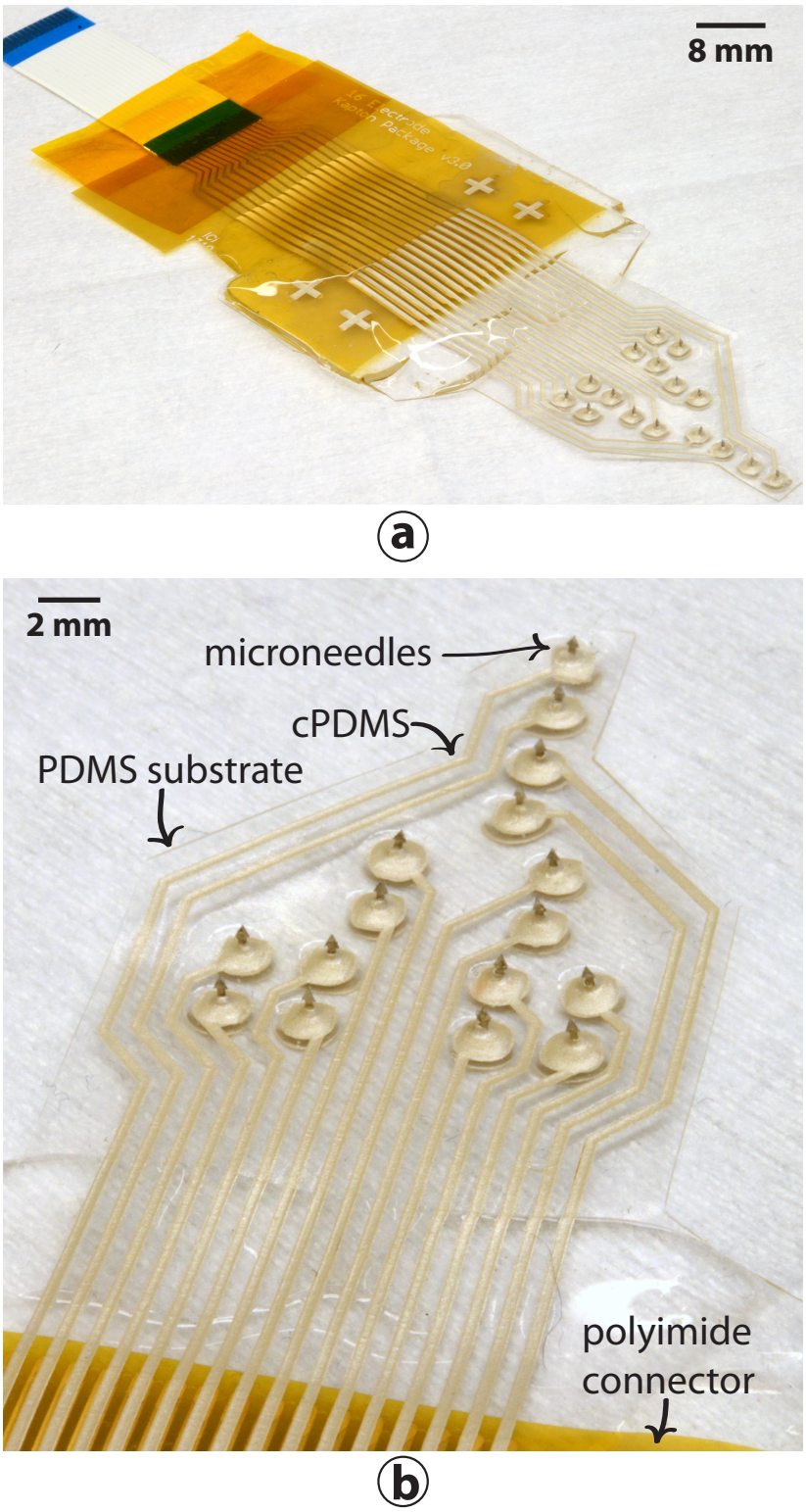

Figure 2.1: The most recently developed (a) stretchable microneedle electrode array (sMEA) – that contains (b) 16 microneedle electrodes, barbed to adhere the device to muscle tissue. The electrode layout of this sMEA was designed to interface across the superficial surface of a feline's lateral gastrocnemius muscle.

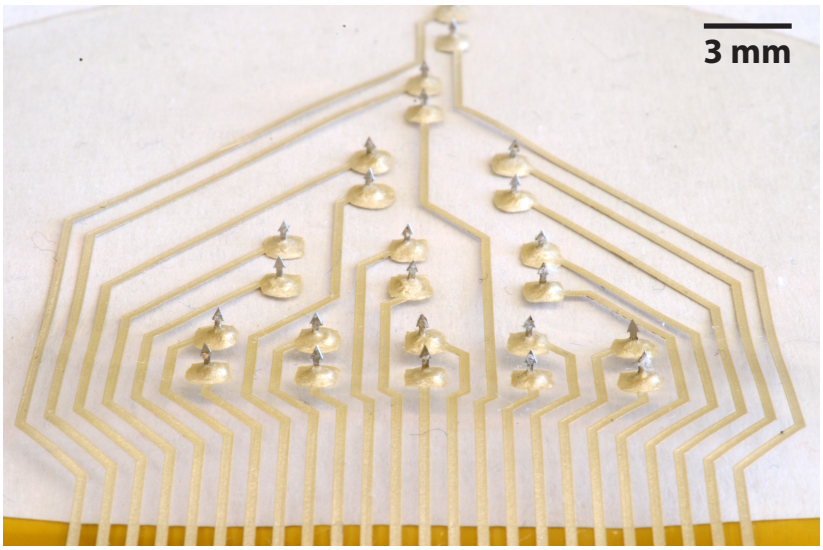

Figure 2.2: A 24-electrode sMEA – designed to interface with the surface of the lateral gastrocnemius muscles of large felines.

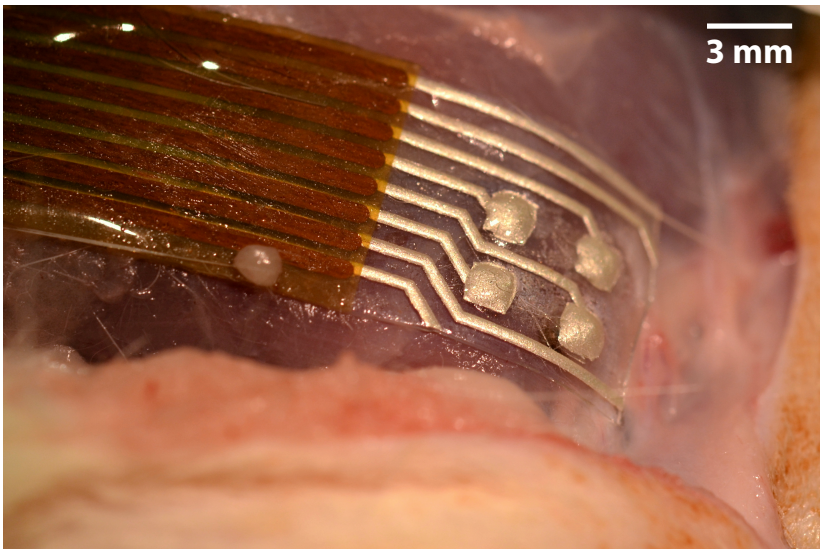

Figure 2.3: A miniature sMEA with four microneedle electrodes, implanted in a rat's biceps femoris muscle.

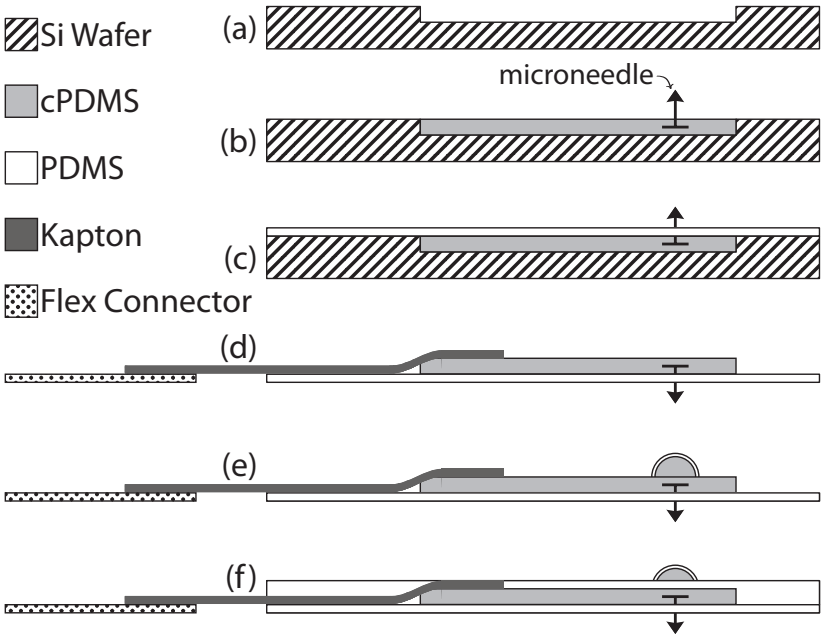

Figure 2.4: An illustration of the fabrication process for a stretchable microneedle electrode array (sMEA). Both the substrate and the conductive traces are composed of PDMS to facilitate device stretching and conformability to tissue. The PDMS interface was laminated and packaged with a polyimide sheet and a flat-flexible connector cable to provide a reliable multi-channel connection to electrical equipment.

To find a microneedle electrode design optimal for adhesion to muscle tissue, eleven different designs of arrowhead-shaped microneedles that varied in their shaft and barb widths were fabricated (Fig. 2.5). From these designs, eleven sMEAs were produced using a PCM process, each containing sixteen 1.5-mm tall electrodes of a single design. To characterize the epimysial adhesion of the eleven sMEAs, a pull-off test was conducted using an axial compression/tension testing system (EnduraTEC ELF 3200 Uniaxial Testing System, Bose). At one end, the sMEAs were attached to a force transducer connected to the upper arm of the tension system. At the other end, the microneedle electrodes of the sMEAs were implanted into immobilized poultry muscle (Fig. 2.6), which was utilized to evaluate the mechanical engagement of microneedle electrodes to muscle tissue. The sMEAs were pulled orthogonal to the plane of the poultry tissue at a fixed velocity of 0.3 mm/s for 1.5 minutes, or until separated from the tissue. Three trials were performed for each microneedle design and the peak forces were

recorded.

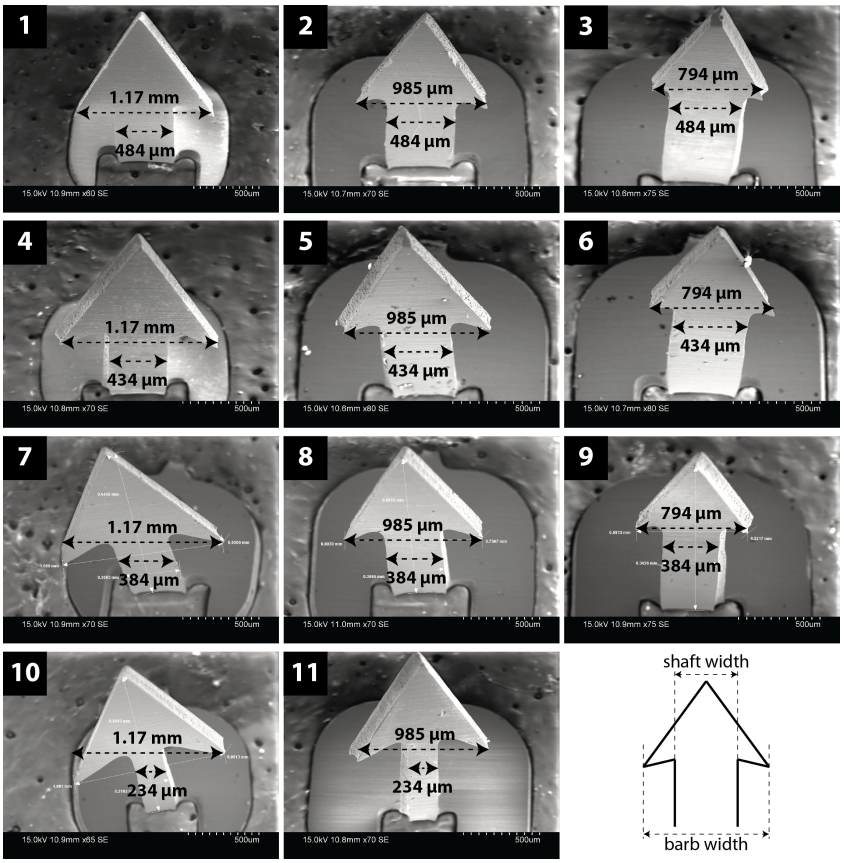

Figure 2.5: Scanning electron microscope images of the eleven electrode designs. These electrodes were 794 to 1170 µm in barb width, and 234 – 484 µm in shaft width. The purpose of producing multiple electrode designs was to find a near-optimal electrode shape for sMEA adherence to muscle tissue.

Microneedle electrode design 3 required the least force to remove the sMEA from the muscle tissue, at 0.81 N, and design 11 required the greatest force, at 2.41 N (Fig. 2.7), an ~200% improvement in sMEA adhesion to tissue compared to electrode design 3. Design 9, however, was observed to require a similar peak force, on average, as design 11 and had the greatest level of consistency among all of the microneedle designs tested. In general, the force required to remove the sMEAs from muscle tissue increased as the shaft width of the microneedles was reduced. Additionally, at a given shaft width, the microneedles with arrowheads 985 and 794 µm in width adhered better than those 1170

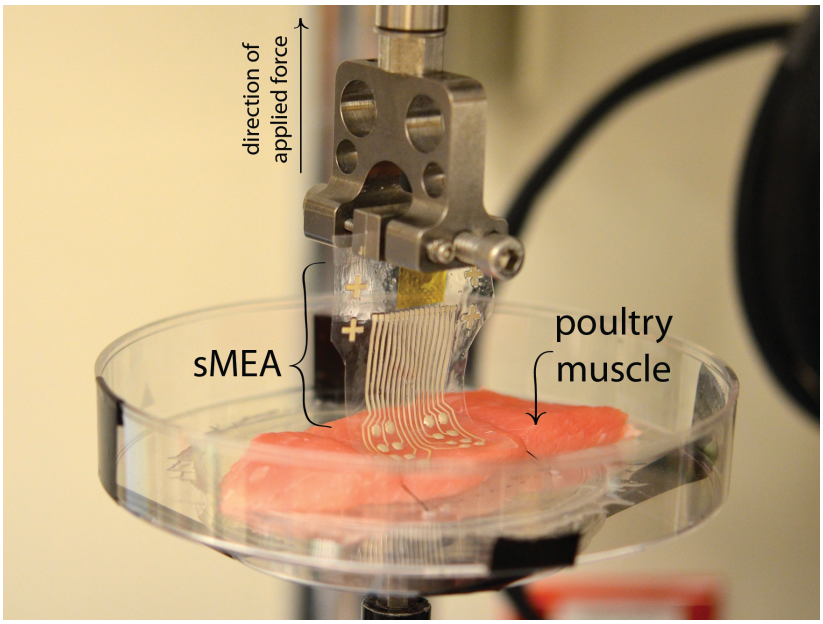

Figure 2.6: The adhesion pull-off test used to measure the force required to remove an sMEA from muscle tissue. Eleven sMEAs were produced, each with a different electrode design. These sMEAs were implanted in immobilized muscle tissue, and at one end pulled orthogonal to the plane of the muscle until the sMEAs' electrodes detached. The force required to remove the sMEAs' electrodes from muscle was recorded.

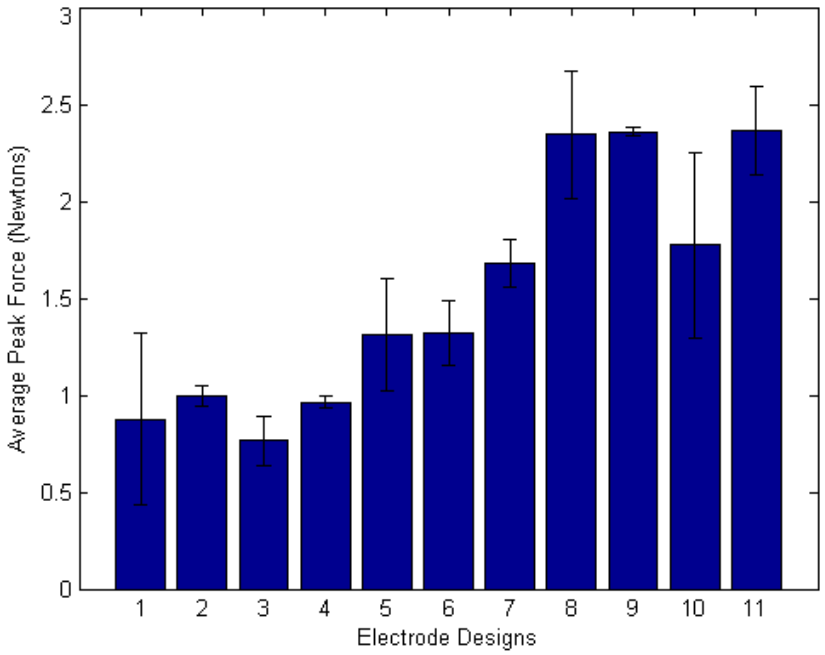

Figure 2.7: The average peak-pull force, and their respective standard errors, necessary to remove each sMEA from muscle tissue. Electrode designs 8, 9, and 11 required the greatest amount of force to detach sMEAs, with those electrodes, from muscle.

μm in width. This suggests that the smaller arrowheads facilitate insertion of the microneedles into tissue, while narrower shaft widths increase the length of the arrowhead that may be utilized to adhere the microneedle to tissue. These results demonstrate that the optimization of the shape of sMEA microneedles can significantly improve the interfacial contact between a neuroprosthetic device and tissue. With such optimized microneedle electrodes, the reliability of muscular stimulation and recording can be improved, and tissue damage as a result of device removal can be reduced.

2.2.2 Fabrication of the Negative Mold

Silicon-wafers were patterned via inductively coupled plasma (ICP) etching technology to produce negative molds, with which to form the conductive traces of the sMEAs (Fig. 2.4a). Each silicon-wafer (4-inch diameter, 550-μm thickness) was cleaned in a piranha solution (i.e. 75% sulfuric acid and 25% hydrogen peroxide) for 10 mins, rinsed in deionized water for 5 mins, cleaned in buffered hydrofluoric acid for 1 min, and rinsed in deionized water for another 5 mins. The purpose of this multi-step procedure is to remove organic materials, native oxides, and loose particles from the wafer to facilitate material adhesion and uniform film deposition. Once the wafer was prepared, a layer of negative photoresist (NR9-3000PY, Futurrex, Inc.) was spin coated (G3P8 Spin Coater, Specialty Coating Systems) onto the wafer to a thickness of ~6 μm. The pattern of the electrode-trace design (e.g. length, width, and pitch) was produced utilizing AutoCAD (Autodesk, Inc.) and printed on a high-resolution transparency (Fineline Imaging). This design was transferred to the photoresist-covered silicon-wafer via UV lithography (365-nm wavelength and a 1150-mJ/cm2 dose). The photoresist was developed in a resist developer (RD6, Futurrex, Inc.) for 30-35 seconds to reveal the negative of the electrode-trace design. The exposed silicon was subsequently etched using an ICP system to produce 100-μm deep trenches with smooth vertical sidewalls. An acetone bath was used to remove the photoresist from the etched wafer. After which, a sputter coater was used

to deposit a separation layer of Ti/Au (50 nm of Ti and 500 nm of Au) on the wafer's surface, to facilitate the removal of micromolded features from the silicon wafer. A non-silicone mold release layer (Knock Out, SLIDE®) was also spray coated onto the wafer to assist with the demolding process. The silicon micromold trenches closely followed the design specifications and measured ~500-um wide and ~100-µm deep.

2.2.3 Molding the sMEA

The traces of the sMEA are composed of a conductive polydimethylsiloxane (cPDMS) that contains PDMS and silver flakes (Silver Flakes #102, Ferro Corporation) mixed at a 1:4 weight ratio [65]. The PDMS was prepared by mixing Sylgard 184 (Dow Corning) base and curing agent at a 10:1 weight ratio.

The traces of the sMEA were fabricated by squeegee printing the mixed cPDMS into the cavities of the silicon micromold. At this stage, the cPDMS would contain air bubbles that could increase the resistance of the traces. To remove these air bubbles, the cPDMS filled micromold was placed in a vacuum chamber (e.g. a bell-jar vacuum system) for 45 minutes, after which the excess cPDMS was removed via squeegee printing. The base of the microneedle electrodes was covered in cPDMS and inserted into appropriate locations on the mold (Fig. 2.4b). Together, the microneedles, cPDMS, and silicon-wafer were placed in a 150 °C oven for 15 minutes, to cure the cPDMS material and make it conductive.

The substrate of the sMEA was produced by spin coating a 300-µm thick layer of PDMS onto the wafer and curing the PDMS at 100 °C for 45 minutes (Fig. 2.4c). After which, the sample, consisting of the PDMS layers, cPDMS, and microneedle electrodes, was demolded from the wafer for packaging.

2.2.4 Packaging the sMEA

To connect the sMEA with electrical equipment (e.g. signal generators and data acquisition systems) and enable the stimulation/measurement of bioelectric activity, the sMEA was packaged with a polyimide sheet and a flat-flexible connector cable. This was achieved by laminating the molded device to the other two components, insulating the back of the device, and reinforcing the bond between the polyimide sheet and the sMEA. This process provides the sMEA a durable connector for interfacing with electrical equipment, and is constant in production time regardless of the number of channels in the sMEA.

The uninsulated backside of the sMEA, in which the cPDMS traces were still exposed, was laminated to a polyimide sheet (1-mil thick) with metal traces (Fig. 2.4d). The metal traces on the polyimide sheet had been defined via metal lift-off or a thick film subtractive process (standard for flex PCB vendors), and were designed to mate with the cPDMS traces of the sMEA (~500-μm wide, 1.5-mm pitch) and the flat-flexible connector cable. The polyimide sheet, the connector cable, and the sMEA were bonded together in a lamination press (Hydraulic Unit Model #3912, Carver) at 135 °C and 750 psi for 60 minutes. After the sMEA had been bonded to the polyimide sheet and connector cable, the placement of microneedles in the sMEA was further reinforced via the application of additional cPDMS and Sylgard 186 (Dow Corning). Droplets of cPDMS were applied to the back of the electrodes and cured in an oven at 150 °C for 15 minutes, after which, droplets of Sylgard 186 were further applied to reinforce the electrode placement and this was cured at 100 °C for 25 minutes (Fig. 2.4e). Lastly, the backside of the sMEA was insulated with Sylgard 184 (Dow Corning), and the resistances between the traces and their corresponding sMEA terminals were measured, to confirm that the PDMS effectively insulates the cPDMS traces. Reinforcement droplets were added to the fabrication procedure after it was observed that the microneedles could push through the backside of the sMEA, when implanted in muscle.

To reinforce the electrical bond between the sMEA and the polyimide sheet, the connection between the two was en-capsulated in Sylgard 184 and cured at 100 °C for 35 minutes (Fig. 2.4f). This step was performed in four stages (i.e. back, front, left side, and right side) to minimize the development of air bubbles trapped in the PDMS.

2.3 Experimental Methods and Results

The mechanical, electrical, and cytological/biological compatibility properties of the sMEA device were characterized to determine how the sMEA would perform in experiments and implantations. This required the (1) measurement of the resistance of the device's traces under various levels of tensile strain, (2) evaluation of the impedance spectra of its electrodes/traces, and assessment of the (3) cytocompatibility and (4) biocompatibility of the device's materials. The device was also applied to *in vivo* preparations to (5) determine the stability of the device on moving muscle and (6) confirm that it is capable of measuring regional EMG activity.

2.3.1 Resistance v. Tensile Strain

To effectively electrically interface with excitable tissue the sMEA must maintain contact with the tissue reliably, through both muscle lengthening and shortening. When interfacing with tissue, however, three problems may occur: the traces of the device may break or become non-conductive, the device may buckle and detach from the tissue, or the device may tear the tissue.

In order to study potential failure modes, it is necessary to evaluate the device's reliability on contracting/lengthening tissue as well as measure how the resistance of the device's traces is affected by tensile strain. To test the functionality of the sMEA under tensile strain, test strips were fabricated and their electrical resistances measured when stretched to different lengths. The test strips were 24 mm in length, 100-μm thick, 500-μm and 1000-μm wide, with pads 2-mm wide and 2-mm long. These studies were

performed on test strips, with and without microneedles, and were produced following the sMEA fabrication process described in Section II.C.

The test traces were stretched by clamping their ends/microneedles to micromanipulators (Siskiyou, Inc.) and gradually increasing the distance separating the two. The distance between the micromanipulators was increased in ~0.75-mm increments while the resistance of the test traces was measured continuously. Two experiments were performed for each test-trace type, one in which the test traces were gradually stretched to the point of failure, and the other in which the test traces were repeatedly stretched to a 40% tensile strain and returned to their resting length. The purpose of the latter experiment was to determine how the resistance *v.* tensile strain relationship would change with repeated stretches.

It was observed that the 500-µm wide cPDMS test traces without microneedles, on average (n = 3), could maintain a resistance below ~10 kΩ to ~63% tensile strain (Fig. 2.8). The 500-µm wide test traces with microneedles, however, broke within the tensile

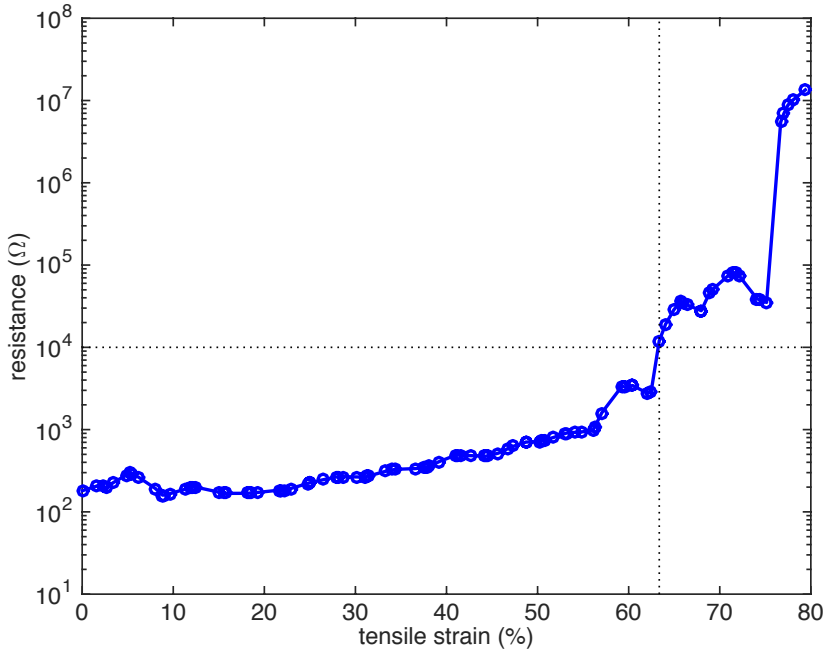

Figure 2.8: The average (n = 4) resistance v. tensile strain relationship for 500-µm wide cPDMS test traces that were not fabricated with microneedles. At a tensile strain of ~63%, the electrode/trace resistance approximates the impedance of an sMEA/saline interface (~10 kΩ).

strain range of 56-61% (n = 3) at the interconnecting area between the cPDMS and the microneedles. Before breaking, however, the 500-µm wide traces embedded with microneedles maintained a resistance below 1 kΩ. When the test traces with microneedles were stretched and released repeatedly to a 40% tensile strain, we observed that they were able to maintain a resistance below 1 kΩ for the majority of the time (Fig. 2.9). Unexpectedly, the resistance would spike above 1 kΩ when the traces were returned to their resting length.

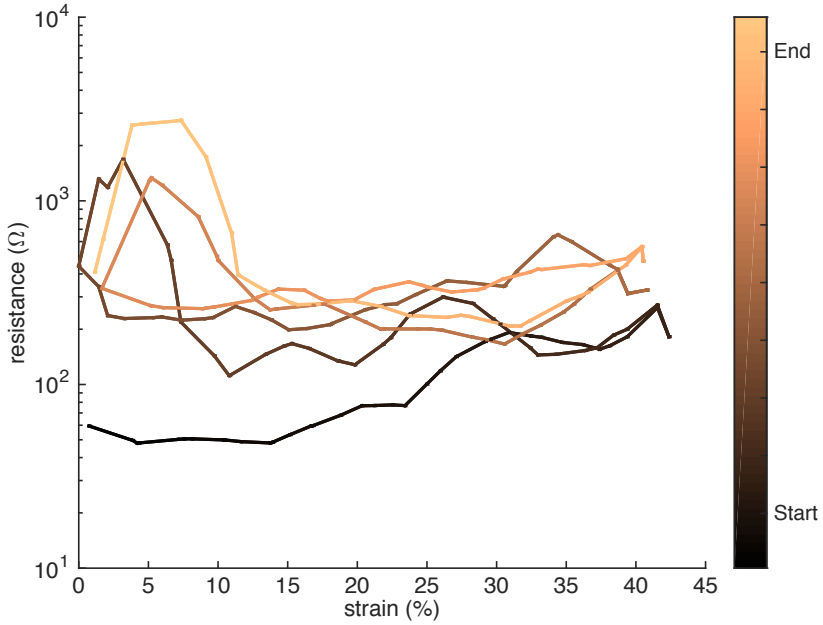

Figure 2.9: The average (n = 3) resistance of 500-µm wide cPDMS test traces, with embedded microneedles, when repeatedly stretched to a 40% tensile strain. The color indicates the moment at which the resistance and tensile strain measurements were taken, with dark colored points measured at the start of the tensile strain test and light colored points measured at the end. The resistance of these traces was principally maintained below 1 kΩ, however, when returning the test traces to their original length a spike in resistance would be observed.

2.3.2 Impedance Spectra of sMEA Electrodes

The impedance spectra of the electrodes on the sMEA needs to be closely matched in order to: (i) easily compare the EMG activities measured across the electrodes; and (ii) uniformly distribute electrical charge across the muscle via the electrodes. We measured the impedance spectra of the sMEA's electrodes with a

Stanford Research SR785 (Stanford Research Systems, Sunnyvale, CA) two-channel dynamic signal analyzer that provided the impedance magnitude and phase of each electrode trace across a frequency range of 10 Hz – 100 kHz. One probe of the dynamic signal analyzer was connected to a silver ground electrode placed in a bath of cellular conducting media (Hank's Balanced Salt Solution, Invitrogen Corporation, Carlsbad, CA) and the other probe was connected to one of the sixteen terminals of the sMEA. The electrode-face of the sMEA was placed face down in the conducting media bath, and the impedance spectrum of each electrode/trace was measured by connecting their respective terminals to the signal analyzer probe. Cellular conducting media was used in this study to emulate the ionic environment that the device would encounter in a physiological implantation.

Intramuscular EMG activity lies predominately within the frequency domain of 20 Hz to 1 kHz [55], [66]. At a frequency of 1 kHz the average resistance of the sMEA's impedance spectra (Fig. 2.10) was approximately 7.6 ± 2.2 kΩ, and below this frequency the impedance spectra was maintained below 38 kΩ. This indicates that the sMEA's electrodes/traces have sufficiently low impedance for measuring EMG activity. The impedance spectra data illustrated in Figure 1.10, was collected from an sMEA that had previously been used in acute *in vivo* experiments, which confirms the reusability of the device.

2.3.3 Effect of an Aqueous Environment on sMEA Impedance

If the sMEA were implanted in muscle tissue chronically, the humidity, high temperature, and aqueous nature of the tissue might cause the device's electrodes/traces to increase in impedance or to become nonconductive. To test the electrodes under such an environment, an sMEA was fabricated, placed in a saline solution, and stored at 35 °C and 95% relative humidity, for 28 days. The impedance spectra of the device's

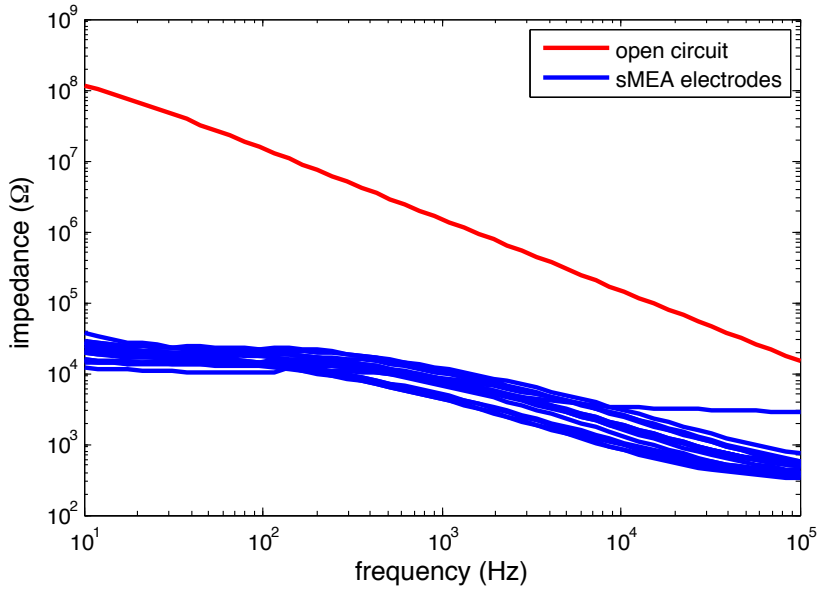

Figure 2.10: The impedance spectra of the sMEA's traces when interfacing with a saline solution. Within the frequency domain of intramuscular EMG activity (20 – 1000 Hz), the impedance was maintained below 38 kΩ, with an average impedance of ~7.6 kΩ ± 2.2 kΩ at 1 kHz.

electrodes/traces were measured on days 0 and 28, following the same procedure as described in Section III.B. The test sMEA was fabricated with eight electrodes, using the process described in Section II.C, however, instead of laminating the polyimide sheet to a flat-flexible connector cable, eight wires were bonded to the polyimide sheet with conductive epoxy. The polyimide sheet, wires, and PDMS connection were encapsulated in PDMS. The sMEA was submerged in a container of saline with the wires protruding from the solution, and together they were placed in an incubator with the aforementioned environmental settings. Over the course of 28 days the exposed tips of the copper wires oxidized, so before measuring the impedance spectra, the ends of the wires were stripped to remove the cuprous oxide.

The impedance spectra of the eight sMEA electrodes on day 28 were fairly similar to those measured on day 0 (Fig. 2.11). At a frequency of 1 kHz, the average impedance dropped by ~310 ± 230 Ω over the 28 days of the study. Although this drop in

impedance was unexpected, the study demonstrates that the sMEA can operate in an *in vivo* environment for a prolonged period of time.

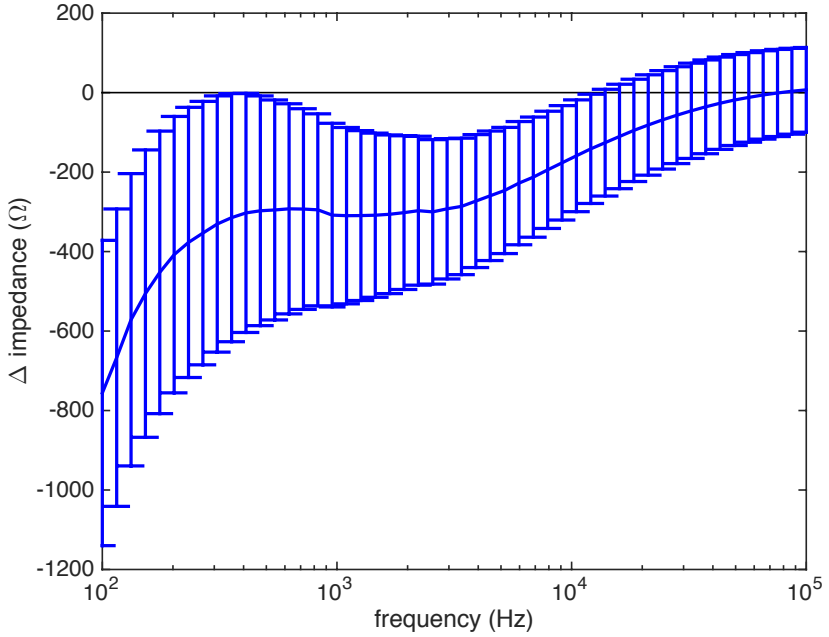

Figure 2.11: The mean impedance spectra of the sMEA's electrodes/traces when interfacing with a saline solution, on Days 0 and 28 of the device's storage in saline. The error bars illustrate the standard deviation from the mean (n = 8). Minimal change was observed in the impedance spectra of the sMEA's traces after the device had been stored in a saline solution, at 35 °C and 95% relative humidity, for 28 days.

2.3.4 Cytocompatibility of the sMEA

It is critical for implantable neuroprosthetic devices to be cytocompatible (i.e. nontoxic to cells) and that they cause minimal damage to tissue. As a preliminary measure before a biocompatibility assessment, a cytocompatibility test was conducted to determine the effect of the sMEA's materials on the health of living cells. Although these studies do not provide insight into the inflammatory response of tissue to an implanted device, they can test the cytotoxicity of a device.

Cortical cell cultures were grown in three test environments: (i) on top of conductive PDMS that was sandwiched between two layers of regular PDMS, (ii) on top of conductive PDMS that was bonded to regular PDMS on one side, and (iii) on top of polystyrene to provide a control. Three samples were created for each test environment.

The effect of the materials on the morphological growth of the cell cultures was observed at 7, 14, 21, and 28 days *in vitro* (DIV). On the 28th DIV, the adenosine triphosphate (ATP) levels of the cell cultures were measured using a CellTiter-Glo Luminescent Cell Viability Assay, which produces a luminescence that is proportional to the amount of ATP present – and a plate reading luminometer (FilterMax F5 Multi-Mode Microplate Reader, Molecular Devices) was used to measure this luminescence. This assay was chosen because considerable research had established ATP levels as a quantitative indicator of cell metabolic activity and cell count [67].

Throughout this 28-day cytocompatibility study, the cryopreserved rat-cortical-cell cultures, from all three test environments, were observed to exhibit excellent morphological growth. The adenosine triphosphate (ATP) levels of these cultures were measured at 28 DIV, and little difference was observed between the ATP levels of the cultures grown on the polystyrene controls to those grown on the sMEA materials (Fig. 2.12). This finding suggests that the sMEA described herein is cytocompatible for at least

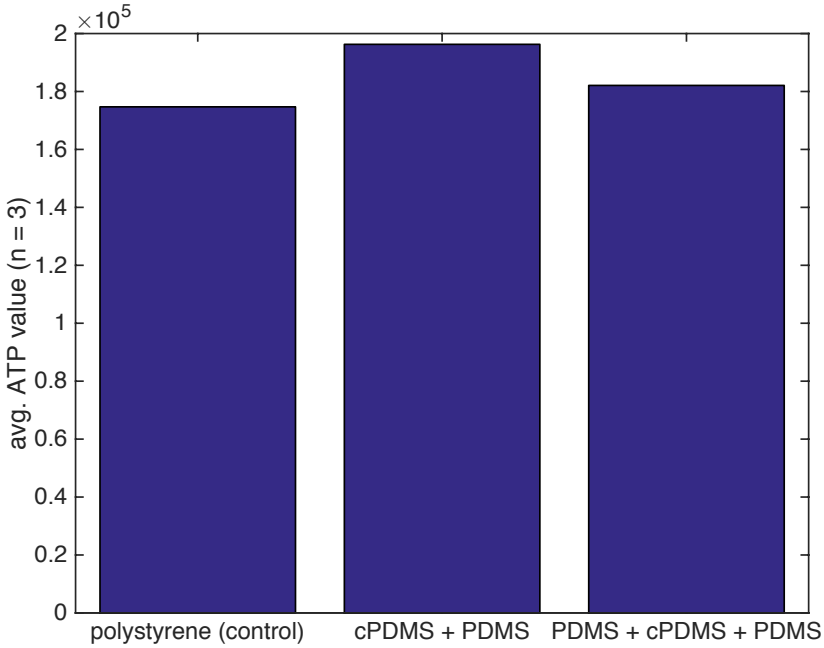

Figure 2.12: The mean (n = 3) ATP levels of cortical cell cultures grown on three different materials for 28 days. The cortical cell cultures grown on the polystyrene control produced similar levels of ATP to those grown on cPDMS bonded to PDMS, and cPDMS sandwiched by PDMS.

28 days and may be utilized to study neuromuscular tissues and neuropathologies.

2.3.5 Biocompatibility of the sMEA

The biocompatibility of the sMEA was evaluated by analyzing the muscle tissue of rats that had received an implantation of the sMEA, or its constituent materials, for a 35-day period. The implants were placed on the surface of the rats' biceps femoris muscles. To isolate the effects individual materials of the sMEA may have on muscle tissue, the twelve rats used in this study were divided into four groups of three: (i) received bilateral implantations of sMEAs without connector cables, (ii) received bilateral implantations of sMEAs without microneedles, polyimide sheets, or connector cables, (iii) received bilateral implantations of PDMS strips, and (iv) received surgery, but no implantations. The sMEAs implanted in this study measured 25 mm in length, 10 mm in width, 0.4-mm thick, and contained four 1.5-mm tall microneedle electrodes (Fig. 2.3). The microneedles of the sMEAs were configured in a 2 x 2 orientation and were separated by 2 mm, lengthwise and widthwise. During the 35 days that sMEA or its materials were implanted, no surgeries or experiments were performed on the rats.

2.3.5.1 Implantation of sMEA and Materials

To prepare the rats for surgery, the rats were anesthetized with isoflurane (5% vol), the fur on their hind legs and abdomen was shaved, and alcohol/chlorhexidine was applied three times successively. The rats were covered with sterile drapes that contained a hole for the site of surgery. Two incisions, approximately 25-mm long, were made above the abdominal external oblique muscle and above the gluteus medius muscle, after which the skin was blunt dissected to expose the biceps femoris muscles. These incision sites were chosen to place distance between the implant and the site of surgery. The incisions were closed with wound clips. The rats were given prophylactic antibiotics (cefazolin, 60 mg/kg) to reduce the risk of infection; and sustained release buprenorphine (1 mg/kg, SC), and ketoprofen (5 mg/kg, SC) to reduce the pain caused by the surgery.

The rats were observed daily to ensure that they successfully recovered from their surgeries.

2.3.5.2 Dissection and Preparation of Muscle Tissue

The rats were anesthetized with isoflurane (5% vol), and euthanized via saline and paraformaldehyde (4% vol) perfusion. If the rat had received implants, the implants and the connective tissue that had grown around the implants were removed. The biceps femoris muscles were dissected and stored in a 30% sucrose in PBS solution at 4 °C, until the tissue sank to the bottom of the container. After which, half the volume of the solution was replaced with optimal cutting temperature compound (OCT), and the muscle was stored in this solution for 2 hours at 4 °C. Following this, the tissue was transferred to a 100% OCT solution and stored at 4 °C for 1 hour. Each muscle was embedded in a block of OCT gel, and frozen for cryosectioning (CM3050 S Research Cryostat, Leica Camera AG). The muscle was sectioned transversely to a thickness of 10 um. The muscle sections were reacted with a standard hematoxylin and eosin stain (H&E) stain and a CD68 pan-macrophage marker, to quantify the presence of fibrosis and inflammation, respectively. The CD68 stain was applied to the muscle sections as described by Mokarram et al. [68]. The muscle sections reacted with CD68, were also incubated with DAPI for 10 minutes, to mark all cells within the muscle sections.

2.3.5.3 Analysis of Muscle Sections

Images of the muscle sections were captured at a 4x and 10x magnification using a fluorescent microscope (Eclipse 80i Advance Research Microscope, Nikon Corp.). The images analyzed from the CD68 stained muscle sections were of the edges and the inner regions of the muscle that contained the greatest concentration of CD68+ cells (Fig. 2.13). The images analyzed from the H&E stained muscle sections were of the surface of the muscle tissue that came into contact with the implant and had the greatest amount of connective tissue intact (Fig. 2.13). Muscle sections dissected from the control group were analyzed at the edge of the muscle on which an implant would have been implanted.

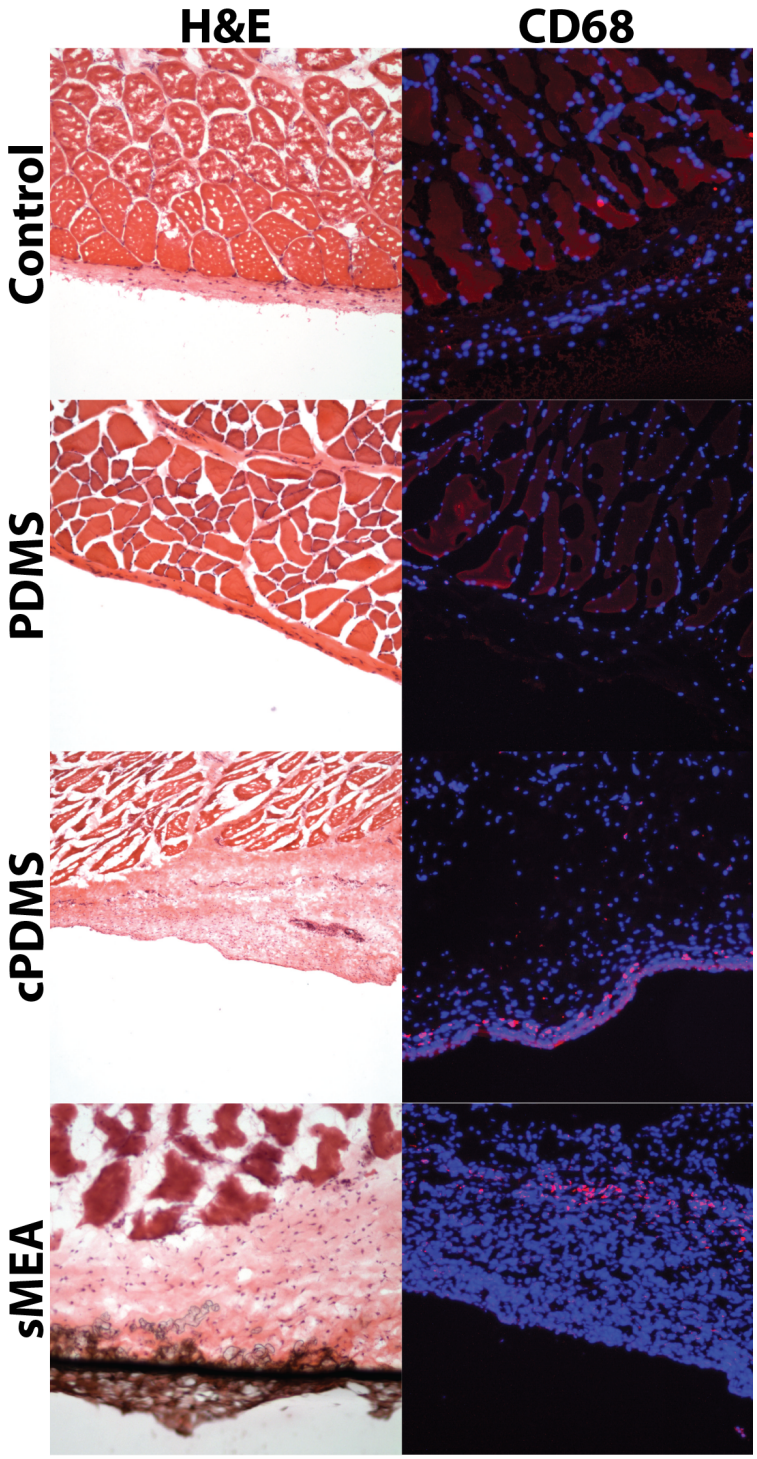

Figure 2.13: Examples of muscle sections that were dissected from all four implant groups and stained for tissue analysis. Muscle sections shown in the right column were stained by CD68 antibodies (red) and DAPI (blue), and were used to quantify the ratio of CD68+ cells to the total number of cells within a region of muscle. The left column provides examples of muscle tissue that were stained with hematoxylin and eosin (H&E), and were used to measure the thickness of the connective tissue (light pink) on the muscle surface that contacted, or would have contacted, an implant.

The photographs of the muscle sections were analyzed using an image-processing program (ImageJ [69]). Photographs of fluorescent cells were modified to increase the contrast of the cells, and effectively apply a cell-counter program. Within each image of H&E stained muscle, the thickness of the connective tissue was measured at three evenly distributed locations along the edge of the muscle.

2.3.5.4 Results

The objective of this study was to examine the long-term effects of an sMEA implanted on tissue to gain insight as to how the implant would affect a recipient's well-being and mobility, and how the recipient's immune response might affect the performance of the implant. To assess these attributes, the connective tissue and macrophages present after a 35-day implantation were measured. The biological responses induced by the surgeries and the different sMEA materials were isolated by dividing the rats into four groups: (i) received sham surgeries, (ii) received PDMS strip implants, (iii) received cPDMS strip implants, and (iv) received sMEA implants without connector cables. All implantations and surgeries were performed on the biceps femoris muscles of the rats.

At the conclusion of the 35-day study, the rats produced normal locomotive movements, failed to exhibit any signs of stress or pain, and had regrown their hair in the locations where the surgeries took place. Their muscles were sectioned and stained with a CD68 marker and an H&E stain to provide quantitative measurements of the presence of macrophages and connective tissue, respectively (Fig. 2.13). Within the center of the muscle tissue, no significant difference in the proportion of CD68+ cells to DAPI stained cells (n = 10 per implant group) was observed across all four implant groups (Fig. 2.14a). Differences in the CD68+:DAPI ratio were observed, however, between the implant groups in the outermost 750 μm of muscle tissue that contacted the implants (Fig. 2.14b). On average, the rats which received cPDMS and sMEA implants exhibited ~11.8 and ~9.6 times, respectively, the CD68+:DAPI cell ratio of the control group. No

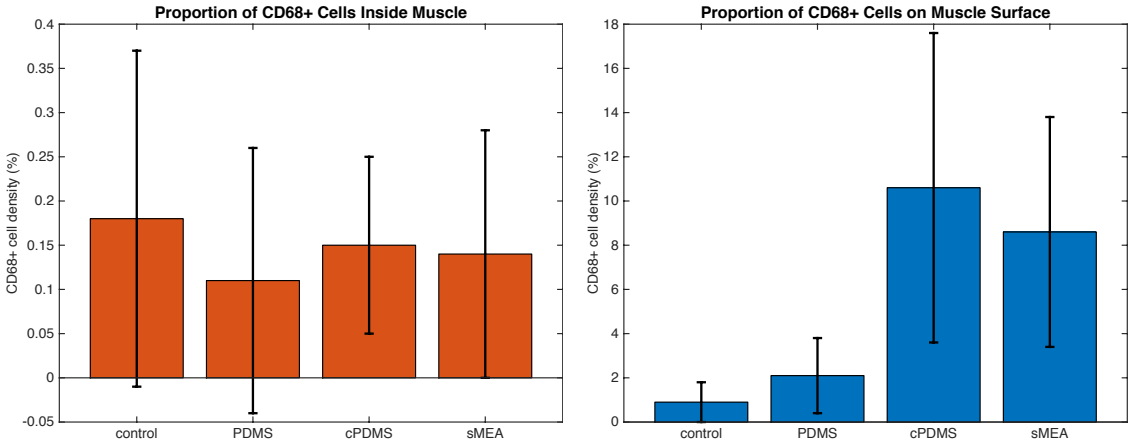

Figure 2.14: The average proportion of CD68+ cells to DAPI stained cells, observed within the (a) inner regions of the rat muscles, and (b) on the muscle surface that contacted the implant material. Cells that were fluorescently marked by CD68 were principally localized within the outer most 750 µm of the muscle. Muscles dissected from the control group were analyzed on the edge that would have contacted an implant. Error bars represent the 95% confidence interval.

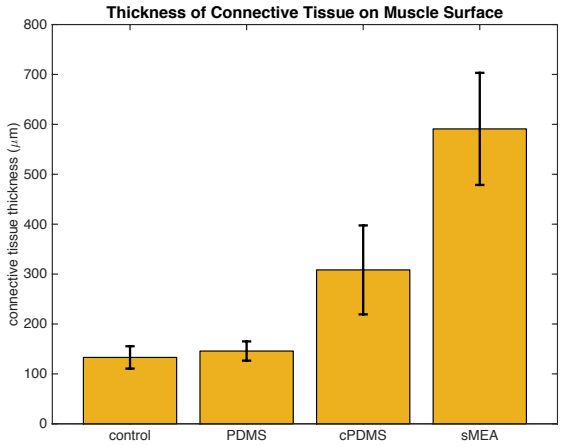

Figure 2.15: The average thickness of the connective tissue on the muscle surface that contacted the implant material. Muscles dissected from the control group were analyzed on the edge that would have contacted an implant. Error bars represent the 95% confidence interval.

difference in CD68+:DAPI cell ratio was observed in the edge muscle tissue between the control and the PDMS implant groups. The muscle sections given an H&E stain (n = 42-60 per implant group) revealed no significant difference in the thickness of the connective tissue on the muscle surface, between the control group and that which received the PDMS strip implants (Fig. 2.15). The cPDMS and sMEA implant groups,

however, were observed to have on average ~2.3 and ~4.4 times, respectively, the thickness of connective tissue on their muscle surface than the control group.

2.3.5.5 Discussion

We were particularly interested in the inflammation and the fibrosis induced by the long-term implantation of an sMEA device. Chronic inflammation of the muscle can cause pain [70], muscle weakness, and loss of muscle function [71] – reducing the overall benefit of an sMEA implant. Fibrosis can increase the electrical resistance between the excitable tissue of the muscle and the sMEA, thereby reducing the efficacy of the device to stimulate and measure EMG activity [72]. To acquire quantitative indicators of the inflammation and fibrosis incurred, the muscle sections were dyed for macrophages and connective tissue with a CD68 marker and an H&E stain, respectively; where macrophages are an immune cell present within the inflammatory process [73]. Although CD68 has been observed to stain fibroblasts in addition to macrophages and monocytes, the proportion of fibroblasts stained has been observed to be ~15% [74]. When our muscle sections were inspected by an expert in muscle immunology, the CD68+ cells were identified as macrophages [75].

Both the cPDMS and sMEA implants were observed to cause a significant increase in the proportion of macrophages and the thickness of connective tissue on the surface of the muscles, compared to the sham surgeries (i.e. the control group); while no significant difference was observed in such properties between the control group and the muscles which received PDMS implants. Within the center of the muscle, no significant difference was observed in the proportion of CD68+ cells present across all four test-groups of our biocompatibility analysis. Given these results, three materials may have caused the increase in macrophages and connective tissue thickness: the silver flakes in the cPDMS, the stainless-steel microneedle electrodes, and the polyimide sheets. Although stainless steel, implanted in skeletal muscle, increases the proportion of macrophages present in the tissue, such macrophages were observed to return to near

normal levels after 10 days [76]. Multiple research studies have identified polyimide to be biocompatible [77]–[79]. Thus, given that the cPDMS and sMEA implants contains similar amounts of silver flakes and they induced similar proportions of macrophages on the surface of the muscle, we attribute macrophage response to the silver flakes. Although the silver flakes likely caused the immune response of the rats to form connective tissue on the surface of the muscle, muscles that received sMEA implants were observed to have connective tissue, on average, 92% thicker than those that received cPDMS implants. We attribute this difference in fibrotic response to the initial muscle trauma caused by the implantation of the sMEA microneedles into the muscle. An increase in fibrous tissue was also observed by other research groups when implanting stainless steel into skeletal muscle [76] .

The macrophages are principally restricted to the outer-most 750 μm of the muscle tissue. If the spread of macrophages remains in this domain or reduces in magnitude, their presence should have minimal effect on the muscle's function. However, if they were spread into the center of the muscle tissue, or adversely impact the neuromuscular junction, then the inflammation would have serious consequences relating to the well-being and the mobility of the animal. Given, however, that the silver flakes in the cPDMS are the principal cause for the increase in macrophage count, inflammation can be reduced by substituting silver flakes with a more biocompatible conductive material, such as gold flakes, palladium flakes, or carbon nanotubes [80]. The connective tissue that developed as a result of the sMEA implantation can both improve and worsen the performance of the device. The connective tissue can serve as a wrapping to keep the device against the surface of the muscle, but it can also increase the impedance between the microneedle electrodes of the device and muscle fibers [72], thereby reducing the device's effectiveness. To fully evaluate how the performance of the device might change over time, the device would need to be implanted in rats electrically connected to a head-

plug, such that real-time EMG measurement and electrical stimulation may be performed over an extended period, and the device's electrical performance assessed.

2.3.6 Mechanical Stability of the sMEA on Moving Muscle

To assess the utility of this device for acute animal experiments, we tested the mechanical stability of the device by lengthening/shortening a muscle that received electrical stimulation from an sMEA. All experimental procedures within this study were conducted in accordance with the guidelines of the National Institutes of Health and the Georgia Tech Institutional Animal Care and Use Committee.

In total, five cat experiments were conducted to collect the results presented. In each experiment, one cat was anesthetized with isoflurane in an induction chamber, then tracheostomized to deliver controlled levels of the isoflurane. The carotid arteries were ligated to control bleeding during the decerebration, and the external jugular vein was cannulated for the delivery of fluids. A wide craniotomy was performed and the cerebral cortices removed. The brainstem was transected rostral to the anterior boundary of the superior colliculi, and all rostral brain tissue was removed. One or both limbs were fixed firmly to the experimental apparatus, by applying bone screws to the tibias and femurs, and by clamping the ankles. An sMEA was placed upon the surface of a lateral gastrocnemius (LG) muscle to stimulate the tissue to contract (Fig. 2.16), with all sixteen electrodes of the sMEAs configured for bipolar stimulation. Each cat was taken off anesthetic once the surgery had been completed, and was euthanized with Euthasol® (Virbac, Corp.) or potassium chloride after the experiment had been performed.

If the sMEA is to electrically interface with tissue, it must provide a reliable connection to the tissue to stimulate and measure its electrical muscle activity. One approach by which to analyze this device/tissue connection is to examine the smoothness of muscle contractions that are induced by sMEA electrical stimulation, as the length of the muscle is stretched and shortened. In our studies, the muscle was electrically

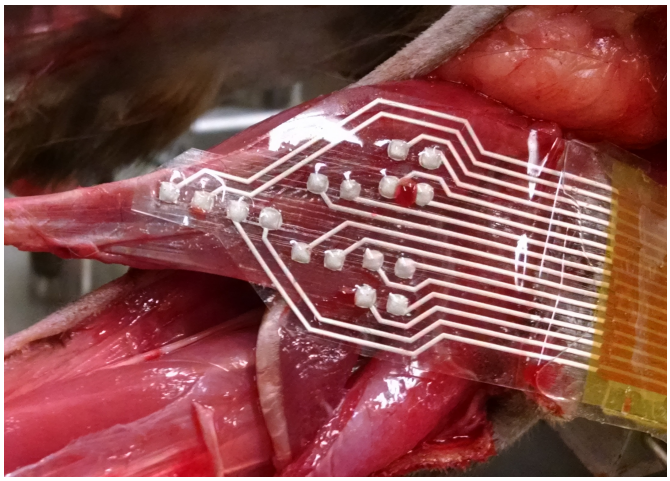

Figure 2.16: The sMEA was implanted in the lateral gastrocnemius (LG) muscle of felines to both measure their EMG activity and electrically stimulate the tissue to produce muscle contractions. To measure the EMG activity, the contralateral tibial nerve was electrically stimulated to recruit the crossed-extensor reflex and induce the LG muscle to contract.

stimulated at frequencies of 20, 40, or 80 Hz and stretched/released by displacements of 2 and 5 mm, at velocities of 7.2, 12.5, and 14.4 mm/s. These displacements and velocities were chosen to emulate the intermediate physiological activity range of a cat [39]. To stretch/release the muscle, as well as measure its contractile force, the tendon of the LG muscle was separated from its insertion and clamped to a force transducer and motor (Fig. 2.17).

Over the course of 160 trials during which the muscle was electrically stimulated and stretched/released, there were only two instances in which an unexpected jump in the muscle's contractile force was observed (Fig. 2.18). The remaining ~99% of trials produced smooth contractile forces before, during, and after the change in muscle length (Fig. 2.18).

2.3.7 Measurement of Multichannel EMG Activity

We assessed the ability of the sMEA to measure EMG activity by implanting it on LG muscles and recording the electrical activity produced during spontaneous and reflexive contractions. The latter induced by stimulating the contralateral tibial nerve with

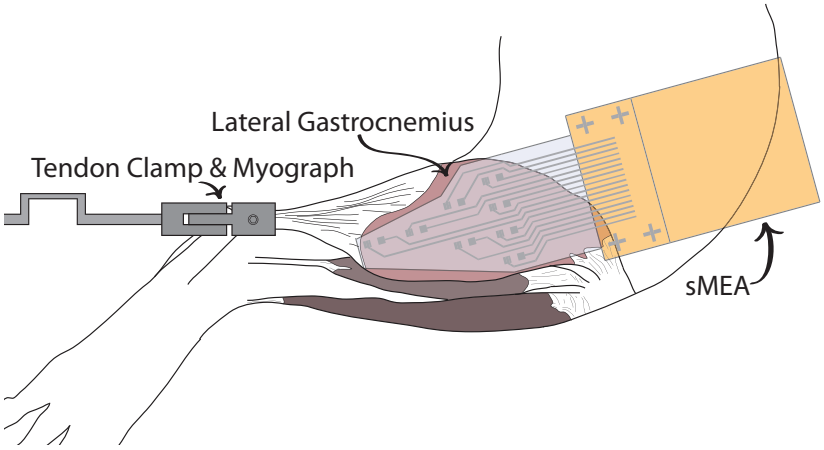

Figure 2.17: A diagram depicting the experimental setup used to electrically stimulate muscle and measure the produced contractile force. To assess the stability of the sMEA-muscle connection, the muscle length would be increased/decreased by 2 and 5 mm, at a constant velocity, while the sMEA electrically stimulated the muscle to produce a contraction. The smoothness of the resultant muscle contractions was analyzed to assess the stability of the device implantation.

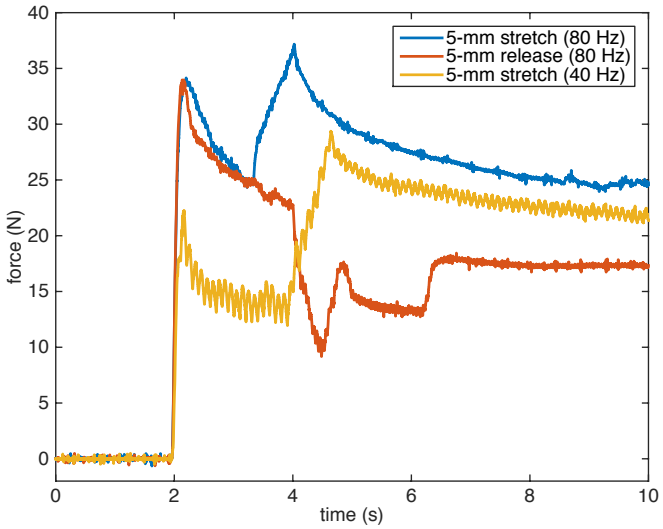

Figure 2.18: Three example trials of the contractile force produced by muscle when electrically stimulated with an sMEA, and the muscle length is stretched or shortened by 5 mm during the stimulation. The first rise in force is due to the initiation of electrical stimulation. After which, the muscle length was stretched (blue and yellow) or released (red). The stretched muscle produced a smooth force for the entirety of both trials, as observed in ~99% of our studies. The released muscle briefly dropped in contractile force at the 5 s mark, likely due to a loss of contact between the sMEA and the muscle tissue. This drop in force was observed in 2 of 160 trials.

a bipolar cuff electrode, to activate the crossed extensor reflex. When stimulating the tibial nerve, a uniphasic square wave was delivered with a pulse width of 100 μs, a

frequency of 40 Hz, and an amplitude between 0.3 and 5.0 V. A ground electrode was implanted in the popliteal fat pad, ipsilateral to the sMEA implantation site. EMG signals were recorded through the sMEA's bipolar electrodes, amplified by a factor of 1000, and digitized at a sampling rate of 3.0 kHz/channel before they were transmitted to a computer. Motion artifacts were removed post-recording with a 20 Hz high-pass Butterworth filter, the electromagnetic noise was removed post-recording with a 60 Hz notch Butterworth filter, and all stimulation artifacts were replaced with interpolated data points. One cat experiment was necessary to produce the EMG results presented.

Two properties of the measured EMG signals were analyzed, their signal-to-noise ratio (SNR) and their median frequency. The SNR provides a quantitative measure of the signal quality, and the median frequency indicates the frequency spectrum of which the signal is comprised. The SNR of the EMG signals were calculated via (2.1), where "signal" is a sample of the EMG activity and "noise" is a sample of the background electrical activity during which no muscle contractions were observed.

$$SNR = 10\log_{10}\left[\left(\frac{\mathrm{rms}(signal)}{\mathrm{rms}(noise)}\right)^2\right] \tag{2.1}$$

When the EMG signals measured through the electrodes of the sMEA were compared, they were observed to be visually unique with respect to the amplitude and timing of their compound motor unit action potentials (CMUAP) (Fig. 2.19). The SNRs and median frequencies of these EMG signals were measured and compared to those collected from intramuscular steel-wire electrodes implanted in feline LG muscles (Table 2.1).

TABLE 2.1
PROPERTIES OF EMG MEASURED VIA ELECTRODES

Electrode Type	SNR	FFT Median Frequency
sMEA	31.8 dB	271 Hz
Steel Wire	25.4 dB	267 Hz

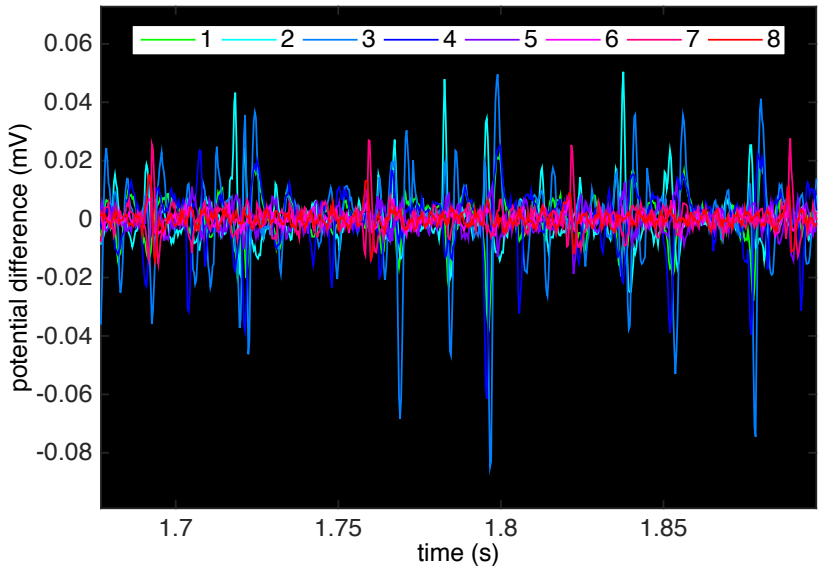

Figure 2.19: Eight EMG signals measured across the bipolar channels of the sMEA. Compound motor unit action potentials of various amplitudes and timing may be observed across the eight signals.

2.4 Discussion

The objective of our research was to develop a stretchable microneedle electrode array (sMEA) that can stimulate and measure the electrical activity of muscle at multiple fixed locations within the tissue, while conforming to the muscle's change in length and shape. To accomplish this objective, we fabricated an array of intramuscular electrodes composed of a PDMS substrate, conductive PDMS (cPDMS) traces, and penetrating electrodes; characterized the device's electrical and mechanical properties, and assessed its cytotoxicity; and applied the device to *in vivo* preparations to measure regional EMG activities and produce smooth and stable muscle contractions.

2.4.1 Scalability of the Fabrication Process

The sMEA fabrication process was developed with mass-manufacturing in mind, but various steps will require different levels of modifications to truly facilitate mass production. The molding process for the sMEA's cPDMS traces, for example, is already well suited for bulk production. The master molds are constructed using photolithography and ICP etching, from which numerous (e.g. 10-20) sMEAs may be produced. Although

the fabrication of the microneedle electrodes is automated via laser micromachining or photochemical milling, their substitution with commercially available large-area processes would make the fabrication more cost-effective. At present, the microneedles are incorporated into the sMEA device by hand, which is a slow and laborious process. This step, however, can be automated with a robotic pick-and-place system, which is standard in the chip-on-board industry.

2.4.2 Electrode Impedance

To assess the tissue–electrode impedance of the sMEA, the device was placed in a saline solution of similar ionic concentration to an *in vivo* environment, and the impedance spectra of the electrodes were measured. In this study, the sMEA electrodes exhibited low and relatively uniform impedances with an average impedance of ~7.6 ± 2.2 kΩ at a frequency of 1 kHz. The relatively small deviation of these electrode impedances facilitates the uniform measurement of EMG activity across the array, and indicates that our fabrication process yields traces of an acceptable impedance with a high degree of consistency. The DC measurements of trace resistance are on the order of 100 Ω; as expected, the majority of the impedance is attributable to the electrode–saline interface. To reduce the overall impedance, the microneedle electrodes can be electroplated with platinum black, which has been shown to decrease the tissue-electrode impedance by an order of magnitude [81], [82].

2.4.3 sMEA Encapsulation

It is necessary to robustly encapsulate sMEAs (i) to prevent the inner non-biocompatible components from contacting tissue, (ii) to insulate their conductive traces, and (iii) to ensure their mechanical integrity. We encapsulated the sMEA by encasing the substrate and polyimide sheet in PDMS, and by insulating the backside of the cPDMS

traces with PDMS. To assess the quality of this encapsulation, electrical, compatibility, and *in vivo* tests were performed.

We have demonstrated that the PDMS encapsulation effectively encases the silver flakes of the sMEA and protects biological matter from the cytotoxic effects of silver [83]. This was confirmed via the 28-day cytocompatibility study, in which cortical cells cultured with the sMEA's materials presented similar levels of health as those cultured with a polystyrene control. We verified that the traces were insulated from the external environment through the measurement of both the trace resistance and EMG activity. EMG measurements collected through the sMEA possessed a high SNR, and exhibited little in the form of low-frequency artifacts, which would have been introduced by the movement of tissue against adjacent uninsulated traces.

The sMEA was stored in an aqueous environment for 28 days to evaluate the durability of the device. Moisture can permeate PDMS [84], and in the process weaken the laminated bond between the PDMS substrate and the polyimide sheet, rendering the traces non-conductive. Additionally, moisture may corrode the cPDMS traces [85] and thereby increase their resistance [86]. After 28 days, the sMEA remained fully functional, and its electrodes experienced minimal change to their impedance (e.g. ~310 ± 230 Ω at 1 kHz). This result suggests that any corrosion or layer separation caused by PDMS moisture permeability is minimal over the first 28 days of implantation. A much longer study is necessary, however, to assess whether the permeability of PDMS may adversely affect the performance of the sMEA in a chronic setting. If the permeability of PDMS were to prove problematic, it could be remedied by passivating the PDMS/polyimide portion of the sMEA with a hermetic material, such as parylene [87]; or replacing the silver flakes used in the cPDMS with a less reactive biocompatible metal, such as gold, palladium, or carbon nanotubes [80].

2.4.4 Effects of Stretching on Trace Integrity

It is necessary to understand the effects of strain on an sMEA when stretched by muscle, and when stretched to the point of failure. Feline muscle–tendon units may change in length by ±25% while walking or galloping [39], [38]. To characterize the performance of the sMEA, the resistance of the device's traces were measured while the traces were repeatedly stretched to a 40% tensile strain, and were stretched beyond the limits of their operation.

We demonstrated that the traces of the sMEA were able to maintain a resistance below 10 kΩ up to a 63% tensile strain. This 10 kΩ resistance is comparable to the sMEA's electrode-to-saline impedance across the frequency range of 10-1000 Hz. Thus, the sMEA's electrodes/traces should operate effectively within muscle's physiological range of motion, with no more than half of the delivered power lost across the device during stretching. While the sMEA is under strain, it is also crucial for the microneedles of the sMEA to remain embedded within the device's cPDMS. Test traces produced with embedded microneedles broke at the cPDMS and microneedle junction, on average, between 56% and 61% tensile strain. One potential method by which to reduce the stress at the microneedle-trace junction and increase the sMEA's stretchability is to reduce the thickness of the PDMS substrate.

The conductance of cPDMS test strips is attributable to the direct contact between silver flakes (Fig. 2.20) and the effects of electron tunneling between these silver flakes, where the latter have been observed to play a greater role within conductive polymers [88]. Over the course of the loading and reversal of cPDMS test strips, the degree of contact between the silver flakes and the electron tunneling may be modified by both reversible and irreversible changes to the strips. To an extent, three reversible modifications to the cPDMS strips include the distance between the silver flakes, the clustering of the silver flakes, and the orientation of the silver flakes [88]. When the strips are loaded, the silver flakes will experience a loss of cohesion at their interface and will align themselves along the axis of strain, decreasing the surface area of silver-flake

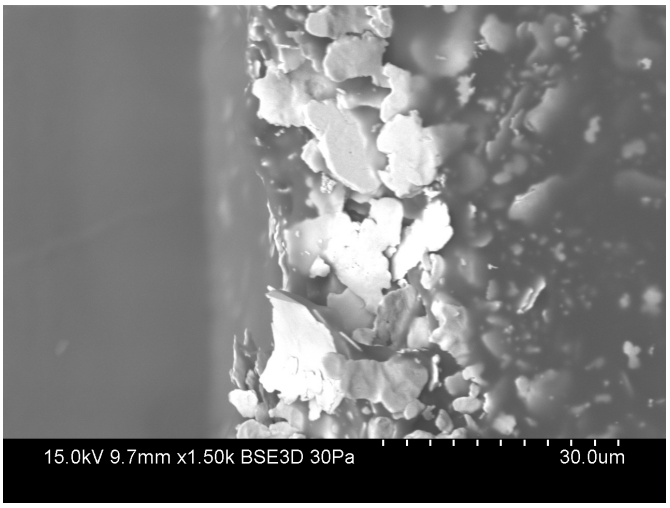

Figure 2.20: The cross section of a cPDMS test trace, captured with a scanning electron microscope. A clear border between PDMS and cPDMS can observed, with the silver flakes of the cPDMS touching.

contact and increasing the resistance. Concurrently, higher tensile strains increase the probability of silver flake cluster formations, causing a decrease in resistance [88]. When the strips undergo load reversal, these three factors will influence the strips' resistance in the opposite manner.

During the loading and load reversal of the cPDMS strips, the strips may also experience irreversible changes. For example, scissions may occur in the polymer chains and cross-links of the cPDMS material, preventing the cPDMS strips from returning to their original state and regaining their original resistance [89]–[91]. Buckling between a conductive polymer and its elastomer substrate has also been observed following an initial load, creating a tensile strain threshold below which there is little change in resistance [92], [93]. When the cPDMS test strips were loaded for the first time, their resistance rose steadily with increasing tensile strain, however, they were unable to return to their original resistance. Although variations in the resistance of the sMEA's cPDMS traces are undesirable, within the tensile strain domain of 40%, the resistance of sMEA traces is relatively well contained below 1 kΩ, and is minor compared to the resistance of the tissue/device interface.

2.4.5 Mechanical Stability

Our *in vivo* experiments demonstrated that the sMEA presented herein effectively activates excitable tissue, and maintains stable contact with moving tissue. When electrically stimulating moving muscle, there were two instances out of 160 trials during which a step change in the contractile force of the muscle was observed. Although these two jumps were undesirable, the device maintained stable contact for ~99% of the trials, indicating that the sMEA provides reliable contact with tissue and may be used to study/control moving muscle in acute *in vivo* laboratory studies. We hypothesize that these discontinuities were attributable to brief separations of the sMEA from the muscle tissue. To reduce the probability of such discontinuities, it is necessary improve the adhesion of the sMEA to muscle tissue. This could be achieved by applying fibrin glue between the sMEA and the muscle, or by suturing the sMEA to the muscle or surrounding tissue.

2.4.6 Fidelity of Recording and Stimulation

The sMEA measured the regional electrical activity of contracting muscle, producing eight channels of EMG activity that contained CMUAPs, which differed in their timing and amplitude. The EMG signals recorded through the sMEA and through traditional steel-wire electrodes were very similar in their SNR and median frequencies, with the sMEA producing EMG at a slightly higher SNR and with a broader frequency range (Table 2.1). These results indicate that the sMEA technology can provide EMG measurements of a similar quality to steel-wire electrodes, across multiple sites of excitable tissue.

The capability of sMEAs to facilitate a large number of intramuscular electrodes makes the technology particularly useful for high-resolution studies of compartmental muscle activation. At present, we are using an sMEA to measure the EMG activity of a single muscle that has multiple neuromuscular compartments, and are using this data to

examine how muscles are physiologically recruited. These neuromuscular compartments are composed of different proportions of muscle fiber types [18], so heterogeneity in the spatial EMG activity of the muscle may be observed when the muscle is recruited to produce different amounts of force, and/or when the muscle is recruited to perform different motor tasks [19]. Building on this research, we plan to use the sMEA technology to examine the synergistic recruitment of the neuromuscular compartments of multiple muscles.

During the mechanical stability assessment, all sixteen electrodes of the sMEA were used to electrically stimulate muscle to induce the tissue to produce smooth contractile forces (Fig. 2.18). By varying the frequency of the electrical signals delivered through the sMEA, we were able to modify the amplitude of these forces (Fig. 2.18). The sMEA's electrodes are 1.5-mm long, and as a consequence, it is difficult for the device to activate deep muscle tissue. To more fully activate muscle, we could wrap the sMEA around the entire surface of the muscle, build an sMEA with microneedle electrodes of various lengths to stimulate both superficial and deep muscle fibers, or implant an sMEA in the middle of muscle. Such strategies would all increase the invasiveness of the device and would need to be considered against the advantage of broader muscle activation.

2.5 Conclusion

We have presented an array of intramuscular electrodes that can stretch with muscle tissue and can provide an interface for the stimulation and measurement of muscle activity. An initial characterization of the stretchable microneedle electrode array (sMEA) demonstrated that the device can operate up to 56% tensile strain and withstand repeated stretching of up to 40% tensile strain. Our fabrication process yielded electrodes/traces of less than 1 kΩ resistance and of uniform impedance. These properties facilitate low-noise measurements of EMG activity uniformly across the sMEA, and the controlled delivery of charge to muscle tissue. The sMEA is cytocompatible for at least

28 DIV. When the sMEA was implanted in rats for a period of 35 days, it was observed to cause a significant increase in the macrophage count and the connective tissue on the edge of the muscle. The inflammatory macrophage response is likely attributable to the silver flakes of the cPDMS, and may be reduced by replacing the material with a more biocompatible conductor. We have demonstrated that the device measures EMG activity with a signal fidelity and frequency sensitivity similar to traditional steel-wire electrodes, and maintains a stable connection to moving tissue. The design of the device is scalable and utilizes electrode parallelism to provide high resolution, muscle stimulation and measurement, with a signal fidelity similar to, if not greater than, steel-wire electrodes. The multitude of minimally invasive microneedles embedded within the sMEA reduces both the difficulty and the damage incurred to tissue, associated with implanting multiple intramuscular electrodes.

In the future, we plan to implant the sMEA chronically to perform studies designed to further our understanding of how muscles and neuromuscular compartments are recruited. To further the capabilities of the sMEA technology, we intend to incorporate pre-amplification and multiplexing chips into the device packaging to improve the quality of its EMG measurements and increase the number of sites for muscle measurement/stimulation (e.g. Guo et al. [2]). Ultimately, this sMEA technology has the potential to advance the study of the neuromuscular system, to return greater mobility to the paralyzed, and to expand the capabilities of wearable technologies.

CHAPTER III

ELECTRICAL ACTIVATION OF MUSCLE VIA A STRETCHABLE MICRONEEDLE ELECTRODE ARRAY

We have developed a stretchable microneedle electrode array (sMEA) that can stimulate and measure the electrical activity of muscle with high spatial resolution and signal fidelity, and can conform to contracting muscle tissue. To characterize the capability of the neuroprosthetic device to electrically activate muscle, sMEAs were implanted on feline lateral gastrocnemius muscles, the muscles were stimulated by the sMEA under both isometric and non-isometric conditions, and the resultant contractile forces were measured. It was observed that the bipolar electrodes of the sMEA can selectively activate regions of muscle when inducing low force contractions (e.g. ~ 1 N per bipolar electrode), however, the spatial resolution would fall if the device were used to induce contractions of higher force (e.g. ~10 N per bipolar electrode). The rise times and the half-decay times of muscle twitches induced by each electrode of the sMEA varied based on where along the length of the muscle the stimulation was delivered. The rise times and half-decay times of muscle twitches induced by more distal electrodes were 16% and 22% longer, respectively, than those induced by more proximal electrodes. When the sMEA was used to spatially and temporally distribute charge across the surface of muscle, the induced contractions exhibited less fatigue and less ripple than muscle contractions that were induced by synchronous stimulation strategies. Lastly, it was observed that the stretch response of muscle activated by an sMEA was similar to that of an areflexive preparation. Through our characterization of the sMEA we demonstrated that the technology may be used to selectively activate regions of muscle tissue to produce contractions of differing temporal properties, and induce fused tetanic muscle contractions that are fatigue resistant. Advancements of this technology may facilitate the

study of how muscles and reflexes are recruited, and the return of a wider range in motor function to the paralyzed.

3.1 Introduction

Prosthetic technologies that electrically stimulate the neuromuscular system may be used for both clinical and scientific applications, such as returning motor function to the disabled, or examining the functionality of reflexes. For example, these prosthetic technologies have proven particularly effective at correcting foot drop within the hemiparetic, by stimulating the ankle dorsiflexor muscles during the swing phase of the gait cycles [94]. Other functional electrical stimulation (FES) systems have enabled the spinal cord injured to regain control over their paralyzed limbs, by electrically stimulating their paralyzed muscles based on the measured electromyographic (EMG) activity of their residual working muscles [28], [31]. This approach could also be used to investigate the role of force feedback in motor coordination, since the stimulation of muscle in proportion to its own activity would constitute an artificial positive force feedback loop.

Although electrically stimulating muscle can provide considerable utility, multiple attributes of electrically induced contractions can be improved. Stimulating muscle with conventional approaches, such as with individual steel-wire electrodes, will more greatly fatigue the tissue than physiologically recruiting muscle to produce the same contractile force. This difference in muscle fatigue is observed because electrical stimulation preferentially activates larger, more fatigable, muscle units and those more proximal to the electrode [25]; as opposed to recruiting the smaller, more fatigue resistant, motor units first and recruiting motor units distributed throughout the muscle/neuromuscular-compartment [16], [95]. If the frequency of electrical stimulation is too low, the muscle may exhibit unfused tetanus [96], and produce unacceptable oscillation in force. Additionally, if too few electrodes are used to activate a muscle, it

may not be possible to replicate that muscle's full range of physiological motion via electrical stimulation. Muscle can be composed of multiple neuromuscular compartments that are recruited differentially depending on the motor task performed [9], [13]. Although multiple transcutaneous electrodes may be applied to the skin to activate these neuromuscular compartments, the physical separation of transcutaneous electrodes from the muscle tissue reduces their spatial resolution and restricts their use to the most superficial muscles [97]. A more effective solution would be an array of intramuscular electrodes, designed to match the spatial resolution of the muscle's organization. Although it would be more difficult to recruit motor units in physiological order, a spatial array could potentially provide asynchronous activation, thereby decreasing fatigue and increasing the smoothness of the force output. Direct muscle stimulation is complicated, however, by the changing shape of the muscle during contraction.

We have developed a stretchable microneedle electrode array (sMEA) that can electrically interface with muscle across a large surface area and stretch with the muscle tissue. The sMEA's polydimethylsiloxane (PDMS) substrate and conductive PDMS traces enable the device to operate under high tensile strains (e.g. 63% along force-generating axis). The many intramuscular electrodes of the sMEA facilitate both the selective activation of muscle as well as the broad excitation of muscle units across the muscle's surface. Through the sMEA's electrodes multiple stimulation strategies may be implemented to regionally activate muscle, reduce the fatigue induced, or produce smooth force output while individual motor units undergo more physiological, unfused contractions [98]. For instance, sequential intramuscular electrical stimulation, in which stimuli are equally distributed in time and sequentially delivered across the electrodes, has been shown to cause less muscle fatigue than stimulation delivered via a single bipolar steel-wire electrode that induces the same initial contractile force [99]. Similar reductions in muscle fatigue were also observed when comparing the effects of sequential and synchronous stimulation delivered transcutaneously [100], epimysially [101], and

intrafascicularly [102]. Theoretically, through the sMEA, it may be possible to selectively activate neuromuscular compartments to reproduce physiological motion, induce less fatigue, and enable paralyzed individuals to regain motor function.

In the research presented, experiments were performed to demonstrate the utility of the sMEA to activate muscle more physiologically than achieved via conventional intramuscular electrodes. Individual bipolar electrodes of the sMEA were used to selectively activate regions of a compartmentalized muscle to induce muscle contractions of varying temporal properties. Electrical stimuli were delivered through sMEA, across the surface of muscle, to produce smooth contractions of limited fatigue. Additional studies were performed to assess whether muscle stimulated by an sMEA can reproduce the stretch response of physiologically recruited muscle. The results from these studies should provide insight into the full capabilities of the sMEA and how the device may be utilized in other technologies or studies.

3.2 Methods

To evaluate the capacity of the stretchable microneedle electrode array (sMEA) to stimulate muscle, a decerebrate cat model was developed that enabled the measurement of a muscle's contractile force when the muscle was recruited reflexively or activated via sMEA stimulation. This model afforded us to examine a variety of muscle performance properties when stimulated by an sMEA, both with regards to the forces generated and their reflexive responses. These experiments were performed on 8 animals, some of whom were also used for other reflex studies. All experimental procedures within this research were conducted in accordance with the guidelines of the National Institutes of Health and the Georgia Tech Institutional Animal Care and Use Committee.

3.2.1 Stretchable Microneedle Electrode Array

The stretchable microneedle electrode array (sMEA) used in this study is composed of a polydimethylsiloxane (PDMS) substrate, conductive PDMS traces, stainless steel arrow-head penetrating electrodes, and a polyimide sheet / flat-flexible connector cable (Fig. 2.1). The sMEA contains 16 paired microneedle electrodes, of 1.5 mm in height, with 2-mm spacing between the electrodes of each pair. The principal advantage of this technology is that it facilitates the implantation of many intramuscular electrodes to stimulate and measure the electrical activity of muscle with high spatial resolution and signal fidelity. The sMEA was designed to fit the dimensions of a feline lateral gastrocnemius (LG) muscle to facilitate the activation of its muscle units. The fabrication procedure and the characterization of this device will be published in another journal article.

3.2.2 Animal Preparation

To evaluate the ability of our sMEA to activate muscle tissue through electrical stimulation, the device was applied to feline lateral gastrocnemius (LG) muscles and the resultant muscle contractile forces were measured. Each cat was placed in an induction chamber and anesthetized with isoflurane. A tracheotomy was performed to allow for controlled ventilation. To manage the bleeding induced by the decerebration, the carotid arteries were looped with suture, and to deliver the cat fluids during the experiment, the external jugular vein was cannulated. To fix the limb positions of the cat, bone screws were inserted into the tibias and femurs, the bone screws were attached to a metal frame, and the ankles were clamped. The LG muscle of either leg was then dissected free from its tendinous insertion in order to measure contractile force and impose length changes. Following the leg surgery, the cerebral cortices and all brain tissue rostral to the anterior boundary of the superior colliculi were removed. Each cat was taken off anesthetic once the surgery had been completed.

The sMEA was implanted beneath the fascia, on the surface of the cat's LG muscle, and distally along the length of the muscle. The LG muscle was selected for this study because it is composed of four neuromuscular compartments that differ in their muscle fiber composition [18]. If the sMEA is capable of selectively activating these regions, differences in the muscle's contractile force properties (e.g. muscle twitch rise time, fatigue) should be observed when the muscle is stimulated by various sMEA electrodes. The sMEA was electrically connected to a multi-channel electrical signal generator (STG2008, Multi Channel Systems MCS GmbH) to control the electrical stimulation delivered across each bipolar electrode of the sMEA. A cuff electrode was wrapped around the tibial nerve contralateral to the sMEA implantation to enable the activation of the crossed-extensor reflex and the physiological recruitment of the LG muscle. The heads of the gastrocnemius muscle were separated to isolate the LG muscle from the medial gastrocnemius muscle. To measure the contractile force produced by the LG muscle, while held isometrically or stretched, the muscle's tendon was separated from its insertion and clamped to a force transducer and motor (Fig. 3.1). To assess the

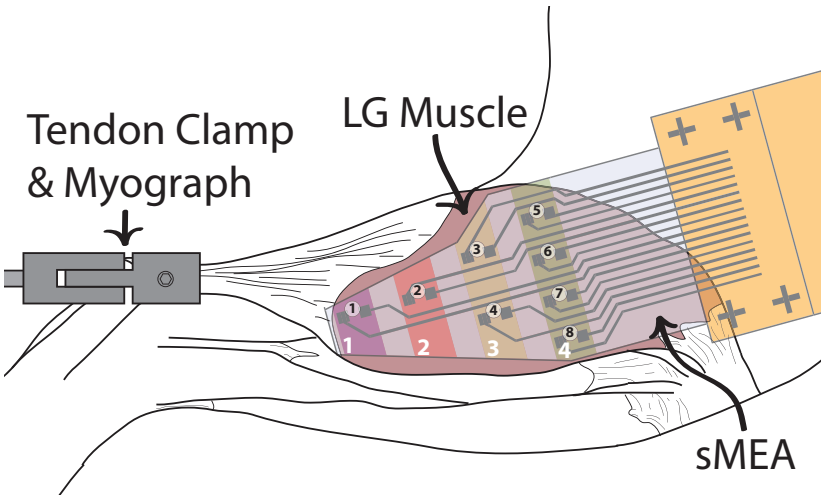

Figure 3.1: A diagram depicting the experimental setup used to electrically stimulate muscle and measure the produced contractile force. Electrical stimulation was delivered across the eight bipolar electrodes of the sMEA. The electrodes were grouped into rows 1-4, based on their distance along the muscle's length. The sMEA was placed on the LG muscle, as depicted here, in all of the experiments; with electrode 1 implanted most distally along the muscle's length, and electrodes 5-8 implanted most proximally.

stretch response of areflexive muscle activated by an sMEA near the end of the experiments, the LG muscle's innervating nerve was transected. Each cat was euthanized with Euthasol® (Virbac, Corp.) or potassium chloride after the experiment had been performed.

3.2.3 Electrical Stimulation and Stretching of Muscle

To investigate whether the stimulation of two electrode sites would result in linear summation of the individual forces, electrical stimuli were delivered across one or two of the sMEA's bipolar electrodes. These stimuli consisted of a brief train of four biphasic rectangular pulses, of 6.4 ms in width, and were delivered at a frequency of 40 Hz to achieve a brief, fused contraction. These brief contractions were also used to evaluate the rates of rise and fall of tension. The amplitudes of stimulation were varied between ± 1-8 V, to produce different magnitudes of contractile force. Between each stimulus, the muscle was provided 30 seconds to rest and recover.

To induce more prolonged muscle contractions to evaluate ripple and fatigue, the tissue was electrically stimulated by all electrodes of the sMEA in a synchronized or sequential manner (Fig. 3.2). Synchronized electrical stimulation would deliver rectangular biphasic pulses, at a set frequency, simultaneously across the electrodes. Sequential electrical stimulation, of the same frequency, would phasically shift the stimulus waveforms delivered across the electrodes, such that the stimulus pulses were evenly distributed in time. Both protocols delivered biphasic rectangular pulses, of 6.4 ms in width, ± 1-8 V in amplitude, and provided the muscle 5 minutes of rest between trials.

To evaluate the extent to which the sMEA can induce stable contractions during natural movements of the tissue, the muscle was stimulated while stretched from a length in which no slack was present in the tissue. To remove slack in the muscle, the tissue was stretched until ~2 N of tension was placed on the muscle. From this position, the muscle was stretched a displacement of 2 mm at a constant velocity of 12.5 mm/s, held at the 2-

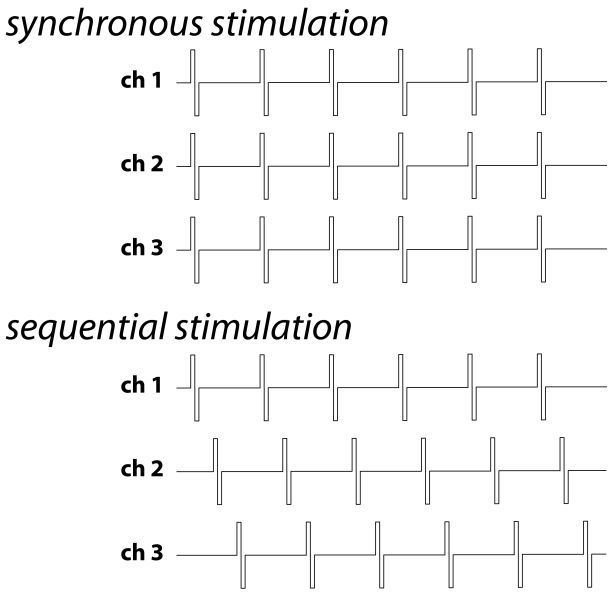

Figure 3.2: Illustrated above, are examples of sequential and synchronous electrical stimulation, delivered across three electrodes, at the same frequency.

mm displacement for 250 ms, and returned to its original length with the same constant velocity. Within a trial, the muscle was provided an 800-ms rest between stretches. Between trials, the muscle was provided a 5-minute rest. The velocity and the displacement of the stretch were selected because they are within the reported physiological range of the cat step cycle [39] and have been observed to elicit the stretch reflex [103]. The stretch response of muscle stimulated by an sMEA was compared to that of physiologically recruited muscle. To recruit the LG muscle, the tibial nerve contralateral to the sMEA's implantation was electrically stimulated to activate the crossed extensor reflex. The tibial nerve was stimulated with 100 μs monophasic rectangular pulses, at a frequency of 40 Hz, and an amplitude within the range of 1-20 V.

Four properties of the stretch response of muscle were analyzed (Fig. 3.3): the *baseline force*, the *dynamic force response*, the *initial stiffness*, and the *incremental stiffness*. The *baseline force* was calculated as the average force within the time domain of 90 – 50 ms before a stretch. The *dynamic force response* was defined as the difference between the peak force produced at the termination of the muscle stretch and the *baseline*

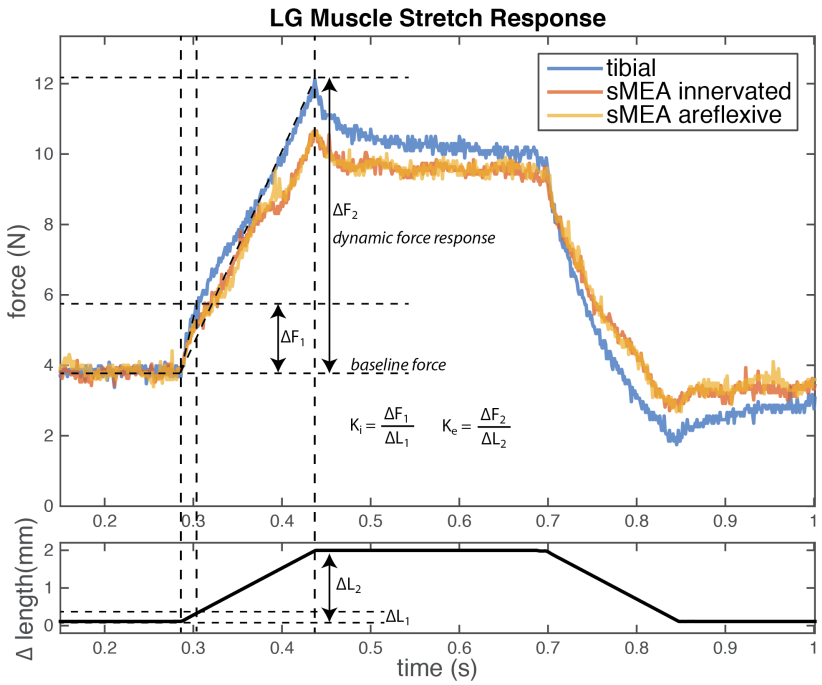

Figure 3.3: The stretch response of a physiologically recruited muscle (blue), an innervated muscle electrically stimulated by an sMEA (red), and an areflexive muscle electrically stimulated by an sMEA (yellow). The four properties of the stretch response that were analyzed are labeled within the figure.

force. The *initial stiffness* (K_i) was defined as the change in force divided by the change in muscle length during the first 2-11% of the 160 ms stretch, and was expressed in the units N/mm. The *incremental stiffness* (K_e) was defined as the change in force divided by the change in muscle length, during the first 2% -100% of the 160 ms stretch. The first 1% was ignored to avoid the period during which the motor accelerated to its programmed stretch velocity. The index K_e/K_i was plotted over the baseline force to assess the degree of muscle yielding that occurred in each of the preparations [104].

3.3 Results

We characterized the capabilities of the sMEA to electrically activate muscle through four studies that were performed with the following goals: (i) to assess the spatial resolution by which the device can selectively activate regions of tissue, (ii) to determine whether the sMEA may induce a muscle to produce contractile forces of varying

temporal properties, (iii) to examine how spatially/temporally distributed electrical stimulation may be used to reduce the fatigue and/or ripple of induced muscle contractions, and (iv) to compare the stretch response of muscle activated by an sMEA to that of physiologically recruited muscle.

3.3.1 Spatial Resolution

The goal of this study was to evaluate the sMEA's spatial resolution, with which the sMEA can selectively activate regions of muscle tissue. To perform this assessment, we stimulated feline LG muscle with individual bipolar electrodes of the sMEA and compared the sum of the force responses produced by two individual electrodes to that produced by stimulating the muscle with the two electrodes simultaneously. The electrical stimuli consisted of brief stimulus trains as described in the Methods section. If the regions of muscle activated by each bipolar electrode were completely independent, the force response produced by stimulating through two bipolar electrodes simultaneously would equal the algebraic sum of the force produced by each bipolar electrode individually, minus a small correction for common compliance [105]. The order by which individual bipolar electrodes and pairs of bipolar electrodes delivered stimuli was randomized to reduce order effects. Within each animal experiment, three trials were performed for each selection of electrodes and stimuli. This study was performed on five cats.

Figure 3.4, presents the results from our analysis of the spatial resolution by which the sMEA can activate muscle tissue. When individual sMEA bipolar electrodes induced fused twitches of less than 2 N, the force produced by the simultaneous stimulation of two electrodes differed from the algebraic summation of the forces produced by those two electrodes individually, by 11% of the twitch produced by the algebraic summation (Fig. 3.4a). In another experiment, when the bipolar electrodes stimulated muscle to produce fused twitches of greater force (e.g. ~10-20 N), this

difference in force increased to 40% of the twitch produced by the algebraic summation (Fig. 3.4b). In some trials, it was observed that stimulating through two electrodes simultaneously resulted in a greater contractile force than the sum of the forces produced by each bipolar electrode individually (Fig. 3.4a).

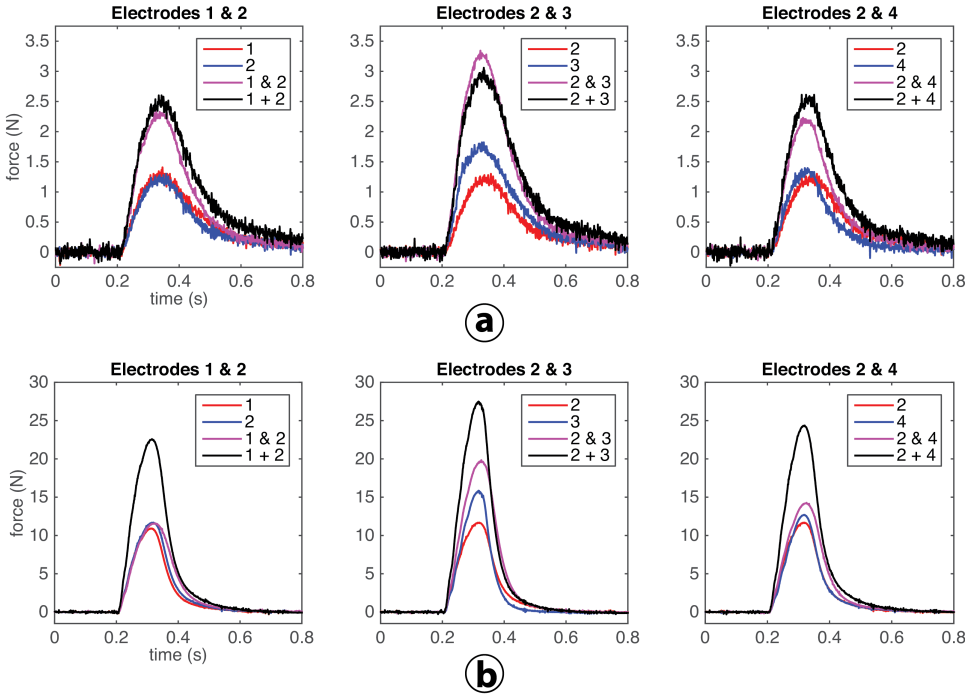

Figure 3.4: The average twitch forces (n = 3) induced by electrically stimulating the muscle with bipolar electrodes of the sMEA. Within each graph, "A" denotes the first electrode in the title, and "B" denotes the second electrode in the title. When the sMEA electrically stimulated muscle to produce (a) low force contractions, the twitch forces produced by stimulating with two electrodes simultaneously ("&" in pink) were equivalent to the summation of the twitch forces produced by stimulating with each electrode individually ("+" in black). When the larger twitch forces were induced (b), however, the difference between the induced twitches significantly increased.

3.3.2 Regional Force Profiles

The objective of this study was to test the hypothesis that the sMEA can induce muscle contractions of differing temporal properties by stimulating the muscle in different regions. This hypothesis is based on the observation that muscles can be composed of multiple neuromuscular compartments, which can differ in their muscle

fiber composition [18] and the torque that they exert on their tendon(s) [6], [7]; and that the force responses produced by different muscle fiber types may differ in their temporal properties [106]. To test this hypothesis, the force responses of the LG muscle to brief trains of stimulation delivered by individual sMEA bipolar electrodes, were compared. This was achieved by analyzing two parameters, namely, the time necessary for fused twitches to rise to their peak force, and decay from their peak to 50% of their peak force. The rise times and half-decay times of muscle twitches varied between cats, so to compare the effect of regional stimulation on the induced fused twitches, the rise-times and half-decay times were normalized by the maximum rise time or half-decay time within each trial. Each trial consisted of eight fused twitches, produced by each of the sMEA's bipolar electrodes. In general, the neuromuscular compartments of the feline LG muscle that contain more type II muscle fibers are positioned more proximally within the muscle [18]. To analyze the dependence of these two parameters on the location at which electrical stimulation was delivered along the length of the muscle, the parameters associated with each row of the sMEA were averaged together (Fig. 3.1). This study was performed on five cats, with three trials conducted in each cat, yielding a sample size of 15 per bipolar electrode. The data used in this study was collected through the sMEA spatial resolution study, in which low amplitudes of electrical stimulation were delivered to the muscle.

The temporal properties of the force responses, specifically their rise times and half-decay times, produced by individual sMEA electrodes differed based on the site at which electrical stimulation was delivered (Fig. 3.5). The shape of the fused twitches (Fig. 3.5) exhibited a significant dependence (95% C.I.) on the sMEA electrode row by which the twitches were electrically induced (Fig. 3.6). Specifically, the sMEA electrodes located more distally along the length of the LG muscle induced fused twitches of longer rise and half-decay times than sMEA electrodes located more proximally along the

muscle. For example, the most distal row produced normalized rise and half-decay times of 0.94±0.05

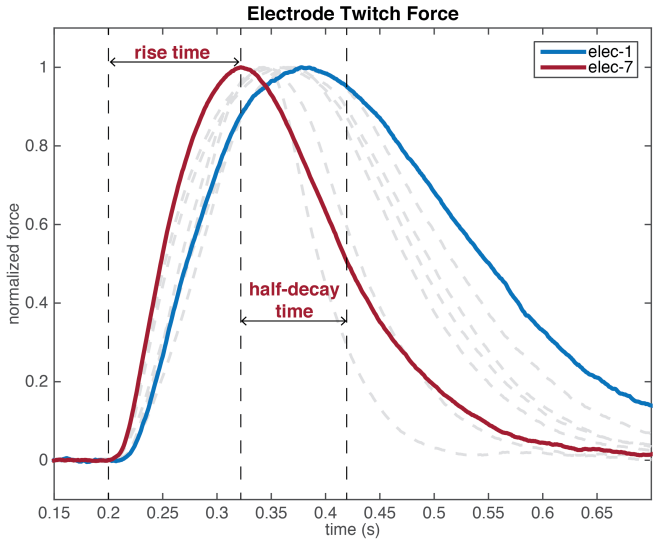

Figure 3.5: Each curve depicts a normalized, average twitch force, induced by stimulating the LG muscle with an individual bipolar electrode of the sMEA. These twitch forces greatly varied in their respective rise times and half-decay times.

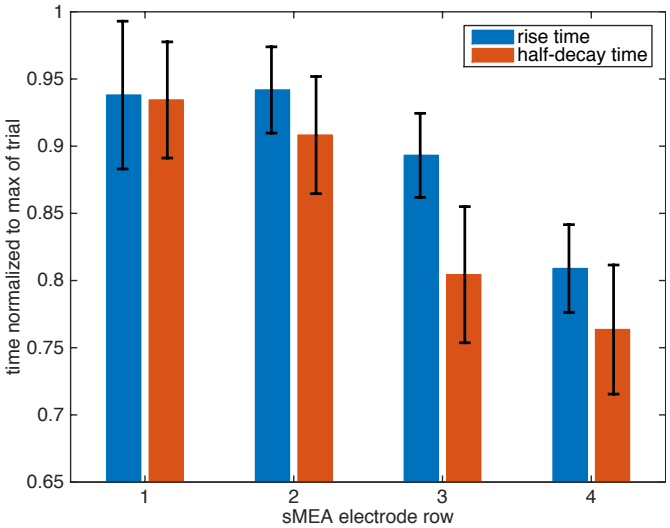

Figure 3.6: Presented above, are the rise times and half-decay times of the twitch forces induced by stimulating muscle with each bipolar electrode of the sMEA. The rise times and half-decay times were normalized to the maximum induced by any of the eight bipolar electrodes, within each trial. These normalized rise and half-decay times were averaged with those produced by the electrodes in the same row of the sMEA. The most proximal sMEA row (i.e. row 4) induced twitches of significantly shorter rise times and half decay-times than the most distal row (i.e. row 1). Error bars denote the 95% confidence interval.

(95% CI) and 0.93±0.04 (95% CI), respectively, whereas the most proximal row induced rise and half-decay times of 0.81±0.03 (95% CI) and 0.76±0.05 (95%), respectively. Thus, the most distal row produced fused twitches ~16% and ~22% longer in rise time and half-decay time, respectively, than the most proximal row.

3.3.3 Sequential v. Synchronous Electrical Stimulation

The objective of this study was to test the hypothesis that electrical stimuli delivered sequentially across the sMEA's eight bipolar electrodes, as opposed to synchronously, may reduce both the ripple and the fatigue of the induced muscle contractions. To test this hypothesis, the LG muscle was electrically activated via (i) 5-Hz stimuli delivered synchronously, (ii) 40-Hz stimuli delivered synchronously, and (iii) 5-Hz stimuli delivered sequentially. We were interested in the muscle fatigue and ripple induced by 40-Hz synchronous stimulation because the stimulus activates muscle the same number of times as 5-Hz stimulation interleaved across all 8 sMEA electrodes. The initial force responses, across the three protocols, were equilibrated by adjusting the voltage amplitude for each stimulus train. Each stimulus train was delivered for a period of 30 seconds.

Figure 3.7 illustrates the smoothness of the muscle contractions induced via the three stimulation protocols delivered across the sMEA's electrodes. In two of two animal preparations, the 5-Hz sequential and 40-Hz synchronous electrical stimuli produced muscle contractions, on average ~62% and ~78% less ripple than 5-Hz synchronous stimulation, respectively (Fig. 3.7 and Table 3.1). To compare the degree of contractile force ripple, the force oscillations were isolated by subtracting the 199-ms square sliding window average of the measured force, from the measured force. The ratio of the peak-to-peak of each trial's force oscillations, over the envelope of the contractile force's local maxima, were averaged with those produced by the same stimulation strategy.

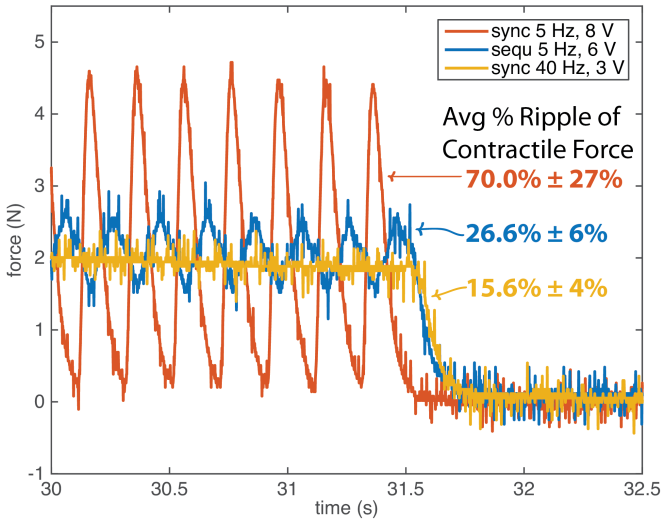

Figure 3.7: An example of the ripple in the contractile forces induced by stimulating muscle with synchronous and sequential stimulation. The stimulation amplitudes were varied, in an attempt to equilibrate the initial force of the contractions induced.

TABLE 3.1
PROPORTION OF RIPPLE IN CONTRACTILE FORCES

Electrical Stimulation	% Ripple
40-Hz Synchronized	15.6 ± 3%
5-Hz Synchronized	70.0 ± 21%
5-Hz Sequential	26.6 ± 5%

*range is 95% confidence interval

Over the 30-second stimulation trials, 5-Hz sequential and 5-Hz synchronous stimuli induced similar levels of muscle fatigue, with both retaining on average ~18% more of the initial contractile force than the muscle contractions produced by 40-Hz electrical stimulation (Fig. 3.8a). To quantify the muscle fatigue induced, the measured forces were smoothed with a 199-ms square sliding window average, and normalized to their initial peak force. Synchronous and sequential 5-Hz stimulation produced similar levels of muscle fatigue. To better compare the fatigue induced by the 5-Hz stimulation strategies to that induced by synchronous 40-Hz stimulation, the normalized and smoothed force trials produced by 40-Hz stimulation were subtracted from those

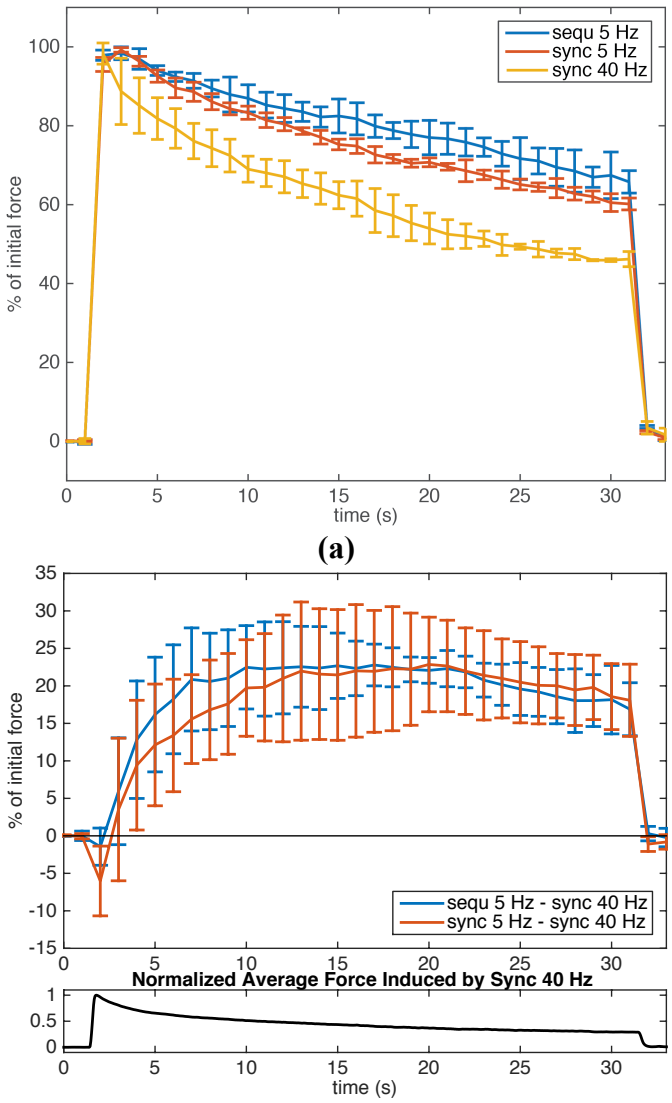

Figure 3.8: Muscle contractions produced by synchronous 40 Hz stimulation, observed significantly greater fatigue than those produced by synchronous 5 Hz and sequential 5 Hz stimuli. (a) Illustrates the average muscle fatigue induced by the three stimulation protocols, in a single cat. The error bars indicate the standard deviation. (b) The normalized force, produced by synchronous 40 Hz stimulation, was subtracted by those produced by synchronous 5 Hz, and sequential 5 Hz stimulation. After 30 seconds, both synchronous 5 Hz and sequential 5 Hz stimulation retained ~18% of their initial force, more than that retained by synchronous 40 Hz stimulation. This data was collected from two cats, and the error bars indicate the 95% confidence interval.

produced by the 5-Hz stimulation strategies. The average and the corresponding 95% confidence interval for these subtracted forces were calculated (Fig. 3.8b).

3.3.4 Stretch Response

The goal of this study was to determine whether the electrical stimulation of a muscle, through an sMEA, would facilitate the activation of the muscle's stretch reflex, if the muscle were lengthened. To test this hypothesis, the stretch response of three preparations was evaluated: (i) Muscle was recruited physiologically via the crossed extensor reflex; (ii) reflexive muscle was stimulated electrically by an sMEA; and (iii) denervated muscle was stimulated electrically by an sMEA. In both sMEA preparations, the electrical stimulation was delivered by two groups of four bipolar electrodes, with each group stimulating at 10-Hz sequentially.

In order to compare the stretch response of the three preparations, it was necessary to standardize the baseline forces at which the muscles were stretched. Stimulating the tibial nerve recruits the crossed extensor reflex and induces the contralateral LG muscle to produce a contractile force that slowly habituates, and provides a wide range of baseline forces with which the relationship between the dynamic force response and the baseline force may be constructed. To produce a similar range of baseline forces with sMEA stimulated muscle, the amplitude of electrical stimulation was varied. The LG muscle was stimulated for no more than 10 seconds at a time, by the sMEA, to avoid hysteresis caused by muscle fatigue. While induced to contract via tibial nerve or sMEA stimulation, the LG muscle was stretched and returned to its original length. Within all trials, the sMEA maintained stable contact with the moving muscle tissue. The stability of the sMEA during the stretching experiments was confirmed by comparing the stretch response of muscle activated by the sMEA to that of muscle recruited by the crossed extensor reflex (Fig. 3.9). Both types of muscle activation produced smooth stretch responses without discontinuities.

In all four cats used for this study, the dynamic stretch response of muscle activated by an sMEA was less than that of muscle physiologically recruited by the crossed extensor reflex (Fig. 3.10). Minimal difference in the dynamic stretch response of muscle was observed between the reflexive and the denervated preparations that were

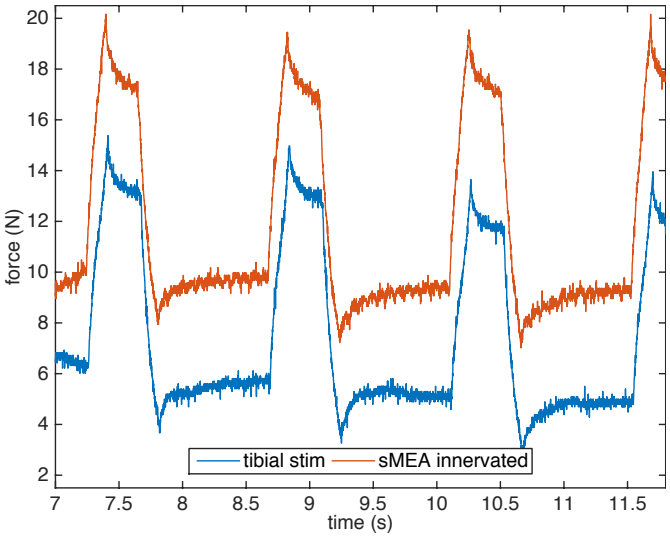

Figure 3.9: The stretch response of muscle stimulated by an sMEA was observed to be similarly smooth and stable to the stretch response of muscle physiologically recruited.

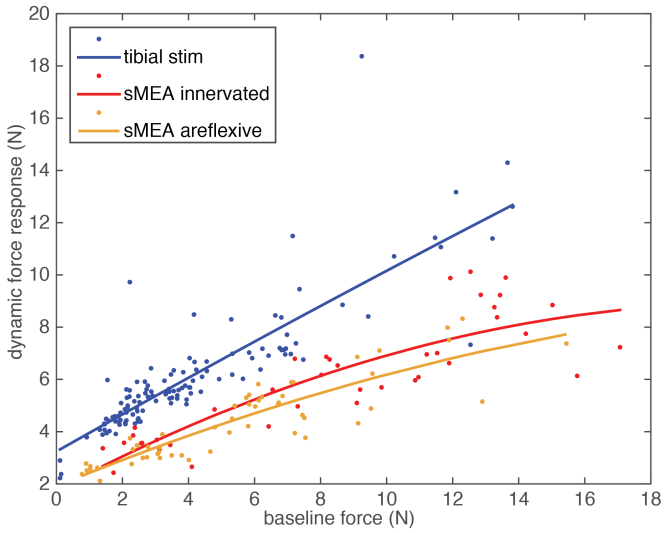

Figure 3.10: The dynamic force response of the feline LG muscle across a range of baseline forces, when physiologically recruited (blue), fully innervated and electrically stimulated by an sMEA (red), and areflexive and stimulated by an sMEA (yellow). The dynamic force response of a fully innervated muscle stimulated by an sMEA, closely matches that of an areflexive preparation.

electrically activated by an sMEA (Figs. 3.3 and 3.10). The incremental stiffness of physiologically recruited muscle was much greater than the initial stiffness when the baseline force was below 4 N, however, at larger baseline forces the index K_e/K_i converged at ~0.8 (Fig. 3.11). Comparatively, the index K_e/K_i of muscle activated by an

sMEA, principally remained below one across the full range of baseline forces tested, for both the reflexive and denervated muscle preparations.

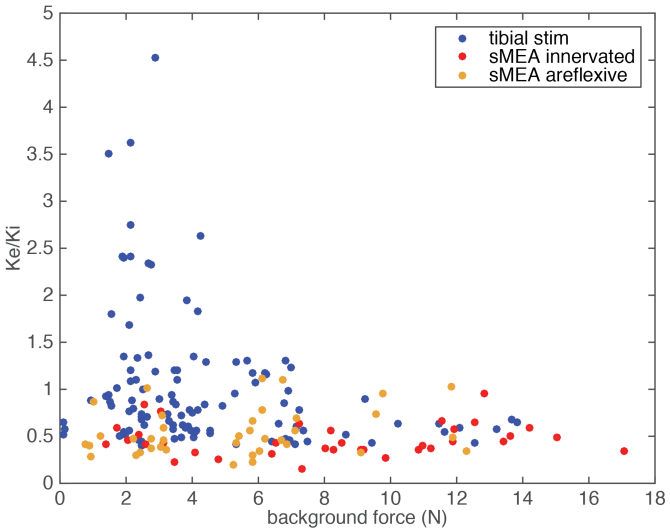

Figure 3.11: K_e/K_i plotted as a function of the baseline force, when the feline LG muscle was physiologically recruited (blue), fully innervated and stimulated by an sMEA (red), and areflexive and stimulated by an sMEA (yellow).

3.4 Discussion

We have developed a stretchable microneedle electrode array (sMEA) to stimulate and measure the electrical activity of muscle intramuscularly with high signal fidelity and high spatial resolution, to enable the compartmental activation of muscle tissue. The research presented herein experimentally demonstrates that the sMEA can selectively excite regions of muscle to produce fused twitches of differing temporal properties, can reduce the ripple and fatigue of muscle contractions induced by electrical stimulation, and can produce stable muscle contractions during muscle stretch.

3.4.1 Spatial Resolution

For the purpose of this spatial resolution study, we analyzed the force response of the LG muscle to brief trains of stimuli. When an individual bipolar electrode of the sMEA stimulates muscle, the region of tissue activated by the electrode expands as the

amplitude of stimulation is increased [25], [107]. When multiple bipolar electrodes stimulate simultaneously, the electric fields summate [108]. At low amplitudes of electrical stimulation, the summation of charge will not activate additional muscle units. Electrodes #1 and #2 of Figure 3.4a provide an example of this scenario, where the summation of forces produced by individual bipolar electrodes closely resembles that produced by the two electrodes stimulating simultaneously. As the amplitudes of stimulation are increased, however, the additional charge will excite muscle units that would not have been activated by either electrode individually [108]. This scenario was likely observed when electrodes #2 and #3 of the sMEA stimulated muscle to produce low contractile forces (Fig. 3.4a). As the amplitudes are increased further, the regions of muscle unit activation overlap, and the force produced by stimulating across electrodes simultaneously is less than the algebraic sum of that produced by each electrode individually (Fig. 3.4b). For example, when stimulating muscle to produce fused twitches of low force (e.g. ~2 N), the twitches produced by stimulating through two bipolar electrodes simultaneously, differed from the algebraic sum of the force responses produced by each bipolar electrode individually by 11%. This small difference in twitch force indicates that the device is capable of selectively activating muscle units when inducing low force contractions. When the muscle was electrically stimulated to produce higher contractile forces (e.g. ~15 N), however, this difference increased to 40% and the spatial resolution by which the device could activate distinct portions of muscle was decreased.

Although an array of electrodes facilitates the spatial activation of muscle, it preferentially activates superficial muscle units over those deeper in the tissue. As a result of the preferential activation of superficial muscle units and the amplitude effects discussed above, there is a tradeoff between the contractile force the sMEA can stimulate a muscle to produce, and the spatial selectivity by which the sMEA can activate tissue. Multiple strategies may be explored to increase the level of contractile force an sMEA

stimulated muscle can produce, while preserving the device's spatial resolution. The electrode length may be increased to facilitate the activation of deeper muscle tissue. The sMEA may be designed to wrap around the muscle, to provide the technology direct contact with a greater proportion of the muscle units. Alternatively, a subset of the sMEA's bipolar electrodes may be used to inhibit the excitation of muscle units [109] surrounding the desired region of muscle activation.

3.4.2 Regional Force Profiles

Through this study, we investigated how regional electrical stimulation of muscle, delivered by the sMEA, can influence the produced muscle contractions. The feline LG muscle contains four neuromuscular compartments that differ in their muscle fiber composition and the torque they exert on their tendon [7], [18]. Within this study, we focused on the differential temporal properties of the induced muscle contractions that may result from the heterogeneous muscle fiber composition of the tissue.

Individual bipolar electrodes of the sMEA were used to stimulate LG muscles and produce fused twitches. Across five cats, it was observed that the rise and half-decay times of these fused twitches were dependent on the location along the length of the muscle at which the muscle was stimulated. Specifically, electrodes placed more distally along the length of the LG muscle induced force responses with normalized rise and half-decay times, ~16% and ~22% longer, respectively, than those placed most proximally. Type I muscle fibers are known to produce muscle twitches of longer rise and half-decay times than type II muscle fibers [106], which suggests that the more distal electrodes of the sMEA activated a greater proportion of type I muscle fibers than the more proximal sMEA electrodes. A histochemical analysis of the muscle fiber composition of the LG muscle identified a similar tissue distribution – that more type I muscle fibers were located more distally within the muscle [18]. These results indicate that regional

electrical stimulation of muscle, delivered by an sMEA, may be used to produce contractile forces of varying properties.

Given the observed differentiation in the force responses produced by regionally stimulating muscle, the sMEA may be capable of producing muscle contractions of different torques or fatigue, if the device were applied to compartmentalized muscle that was heterogeneous in its muscle fiber composition or architecture. For example, type I muscle fibers are more resistant to fatigue than type II muscle fibers [110], thus if the sMEA were to preferentially activate the regions of muscle with a greater proportion of type I muscle fibers, less fatigue would be induced. If the neuromuscular compartment that contains more type I muscle fibers does not produce the appropriate torque for the desired motor action, however, this approach may not be suitable. To assess whether the sMEA is capable of reproducing the contractile activity of a physiologically recruited muscle, two sMEAs may be implanted in bilateral muscles that possess neuromuscular compartments. One sMEA would measure the EMG activity of a physiologically recruited muscle, while the other sMEA would stimulate the contralateral paralyzed muscle to produce the same force and/or torque. The deltoid muscle would be well suited for this experiment because it can produce a broad range of torque trajectories on its tendon depending on the neuromuscular compartments recruited [19], [111]. It is anticipated that at high contractile forces the sMEA may not be able to replicate the physiologically produced torques in the paralyzed muscle, due to a reduction in the device's spatial resolution.

3.4.3 Sequential v. Synchronous Electrical Stimulation

One of the challenges of artificially activating muscle via electrical stimulation, is to produce smooth contractions of little ripple while minimizing the fatigue induced. Typically, muscle ripple is reduced by increasing the frequency of the electrical stimulation [96], however, this will also increase muscle fatigue [112]. The sMEA has the

potential to produce smooth muscle contractions, while inducing less fatigue than an individual electrode, by distributing the electrical stimuli both temporally and spatially across the surface of a muscle.

Muscle contractions produced by 5-Hz sequential electrical stimulation contained less ripple than those produced by 5-Hz synchronous stimulation, and maintained a greater proportion of the initial contractile force as compared to those produced by 40-Hz synchronous stimulation. Thus, sequential electrical stimulation delivered through an sMEA facilitates fused tetanic contractions of high fatigue resistance. This technology may be used to extend the period by which paralyzed muscles can be electrically stimulated before appreciable fatigue is observed, and has direct applications to FES devices and studies of the neuromuscular system. If an sMEA were used to selectively activate regions of a muscle, fewer electrodes of the device could then be utilized to deliver sequential stimulation, and the stimulation strategy may be less effective at reducing fatigue. If the advantages of sequential stimulation are significantly reduced by the electrode limitation, it may be necessary to use an sMEA with a higher electrode density.

It was hypothesized that sequential electrical stimulation would induce less fatigue than synchronous stimulation, if the same frequency were delivered and the same contractile force were induced. Within the studies performed by Rack and Westbury [98], sequential stimulation, delivered across five groups of ventral root filaments innervating a muscle, produced a greater contractile force than synchronous stimulation. This difference in force magnitude was attributed to the comparatively stable contractions produced by muscle activated by sequential stimulation. The lower mean forces, associated with synchronous stimulation, result from the greater internal movement produced by this type of stimulation (28). Therefore, when stimulating the ventral root filaments, synchronous stimulation may require a greater amplitude than sequential stimulation to produce an equivalent force, and as a result induce greater fatigue. When

Rack et al. electrically stimulated ventral filaments, each muscle unit could only be excited by a single electrode. Thus, sequential and synchronous stimulation would excite all muscle units at the same frequency. When directly stimulating muscle through an sMEA, however, muscle units may be excited by multiple electrodes. As a result, sequential stimulation may activate some muscle units more frequently than synchronous stimulation, and cause greater muscle fatigue. The charge delivered by the sMEA's electrodes may also summate during synchronous stimulation, enabling the stimulation strategy to activate more muscle units than sequential stimulation, and reducing the difference between the muscle contractions produced by the two strategies. Both the activation of muscle units by multiple electrodes and charge summation diminish the disparity in the muscle fatigue induced by sequential and synchronous stimulation. Within this study, we did not observe a significant difference in the muscle fatigue caused by sequential and synchronous electrical stimulation delivered at the same frequency.

3.4.4 Stretch Response of Muscle

Within this study, we examined the degree to which muscle electrically stimulated by an sMEA, when stretched, reproduces the physiological stretch response of muscle. In particular, we compared two properties of the stretch responses, across a range of baseline forces: the dynamic force response and the ratio of the incremental stiffness over the initial stiffness (K_e/K_i).

Muscle electrically activated by an sMEA, exhibited greater yielding when stretched than physiologically recruited muscle (Figs. 3.10 and 3.11), and the stretch response proved independent of the muscle's innervation. The K_e/K_i indexes of sMEA activated muscle and physiologically recruited muscle matched that of reinnervated preparations and control preparations, respectively [104]. The resemblance of the stretch response of sMEA activated muscle to that of areflexive muscle, with intact innervation

from the spinal cord, likely results from the electrical stimulation of muscle bypassing the spinal cord and any effective regulation through autogenic reflexes, and not directly recruiting sensory afferents [113]. Neither are the gamma efferents likely to be activated by electrical stimulation, due to the small size [114] and sparse distribution [115] of the efferents. The resemblance in the stretch response also shows that the electrode array maintains electrical contact with moving muscle to produce smooth contractions and smooth stretch responses.

The stretch response of sMEA activated muscle can potentially be increased by modifying the electrical stimulation in real-time, based on the length of the muscle. Such a close-loop system could measure the muscle's length through sonomicrometry, via piezoelectric crystals implanted at either end of the muscle [116], [117]. The increase in electrical stimulation would be predetermined, based on the initial length, the change in length, and the contractile force of the muscle, to make the stretch response of sMEA activate muscle match that of the physiological stretch reflex. The development of this approach is currently ongoing in our research laboratory. In addition, this method can be used to selectively activate Golgi tendon organs and to investigate the function of inter-muscular pathways arising from these receptors.

3.5 Conclusion

We have demonstrated that the stretchable microneedle electrode array (sMEA) (i) can selectively activate regions of muscle via individual bipolar electrodes when inducing low contractile forces, (ii) can produce muscle contractions of differing temporal properties depending on the location at which electrical stimulation is delivered, (iii) can reduce the ripple and fatigue of induced muscle contractions by spatially and temporally distributing charge across the sMEA's electrodes, and (iv) can reliably activate muscle while the tissue is stretched, indicating that this technology can potentially be used during natural movements. The stretch response of muscle activated

by an sMEA is similar to that of an areflexive preparation. The use of force or length signals fed back to the stimulator could be used to realize reflex actions of various types and magnitudes.

Building upon this research, we intend to use the sMEA to study how muscle activation may excite or inhibit the recruitment of other muscles via reflexive mechanisms, and further characterize the capability of the device to replicate the contractile activity of physiologically recruited muscle, in paralyzed muscle, via regional stimulation of the tissue. If incorporated into FES systems, the sMEA may be used to both measure the regional electrical activity of residual or functioning muscle, and stimulate paralyzed muscle based on the measured EMG activity. Alternatively, the sMEA may be used to examine the stability of neuromuscular systems via artificial reflexes – in which the sMEA electrically stimulates muscle proportionally to the contractile force produced by that muscle or another. To extend the capabilities of the sMEA technology, we intend to incorporate multiplexing chips into the device packaging to increase the number of electrodes and the spatial resolution, by which the sMEA can activate muscle. Advancements of this technology may facilitate the study of the neuromuscular system, and lead to the return of a greater degree of motor function to the disabled.

CHAPTER IV

MEASUREMENT OF ELECTROMYOGRAPHIC ACTIVITY VIA A STRETCHABLE MICRONEEDLE ELECTRODE ARRAY

We developed a stretchable microneedle electrode array (sMEA) to stimulate and measure the regional electrical activity of muscle. We evaluated the capability of the device to measure the spatial and temporal dimensions of the electromyographic (EMG) activity of feline lateral gastrocnemius (LG) muscles while the muscles produced a wide range of contractile forces. Through analysis of the EMG and force measurements, we demonstrated that the eight EMG signals measured across the sMEA exhibited different periods of activation, correlations to muscle force, and frequency compositions. These regional differences in the EMG signals were consistent with the contractile properties of the muscle fibers known to compose those areas of the LG muscle. The eight EMG signals were observed to be very weakly correlated to each other, and a principal component analysis determined that a minimum of six and eight dimensions would be required to retain 95% and 99% of the variance, respectively. When the EMG signals were used to estimate contractile force, the median accuracy increased from 60.9% to 87.6%, when one and eight channels were used, respectively. This technology has the potential to both improve scientific investigations of the neuromuscular system, and expand the capabilities of clinically applied neuroprostheses.

4.1 Introduction

Neuroprostheses that measure the electrical activity of muscle have been used across a wide array of applications: to return mobility to the disabled, to control technology via muscle-computer interfaces, and to broaden our understanding of the neuromuscular system. Electrodes placed on the pectoral muscles have enabled amputee

individuals to manipulate robotic arms designed to replace their lost limbs [29]. This is achieved by using the EMG activity produced by their pectoral muscles as a control signal for the robotic arms. Muscle-computer interfaces are currently under development that would provide individuals the ability to control personal computing devices [118] and vehicles [119], [120], through the EMG activity produced by their muscles during contractions. In addition to using EMG activity as a means for control, it may also be utilized as a tool to study the tissue's function. Pathological EMG activity may be indicative of neuromuscular disorders [121]. Regional EMG activity can provide insight into how the neuromuscular compartments of a muscle are recruited [19].

Although neuroprosthetic technologies that measure EMG activity have considerable utility, they have been limited in their spatial resolution, signal fidelity, and/or interfacial area. These limitations are of significance because muscles can be composed of multiple neuromuscular compartments that may differ in their muscle fiber composition [18], the torque they exert on their tendon(s) [6], [7], and the conditions under which they are recruited [19]. Thus, to effectively measure the electrical activity of muscles requires the ability to measure the regional EMG activity of muscle, with high fidelity, across the entire tissue. Surface electrode arrays applied on the skin facilitate multi-site measurement of EMG activity, however, because the electrodes are separated from the muscle of interest by fat and skin, the technology is restricted to interfacing with the most superficial muscles, and as little as 36% of the EMG activity may be attributable to the muscle of interest [52]. Steel-wire intramuscular electrodes overcome the challenge of tissue filtering, however, they are better suited for sampling the EMG activity of a few muscles or neuromuscular compartments than from tens of sites within a single muscle.

Arrays of intramuscular electrodes have been developed to provide such capability, however, they too require tradeoffs; their substrates are typically composed of stiff materials (e.g. silicon [36] and parylene [1]) that can damage the tissue if implanted across too large of an interfacial area. Furthermore, if the intramuscular electrode array were implanted chronically, micro-vibrations between the device and the tissue could cause scar-tissue encapsulation, worsening the performance of the device [34].

We have developed a stretchable microneedle electrode array (sMEA) that can stimulate and measure the electrical activity of muscle, and conform to the surface of contracting muscle tissue. The device is composed of a polydimethylsiloxane (PDMS) substrate and contains conductive polydimethylsiloxane (cPDMS) traces, which enable the sMEA to operate up to tensile strains of ±63%. Embedded within the cPDMS traces are 16 microneedle electrodes. The microneedles were photochemically milled from biocompatible stainless steel, and designed with arrowhead tips to provide secure electrical contact with the muscle tissue. The many microneedle electrodes of the sMEA facilitate high spatial resolution and signal fidelity EMG measurements across the surface of the muscle, and the design of the sMEA is scalable to conform to the dimensions of any muscle. Through the EMG measurements collected via the microneedles, regional differences within the muscle may be discerned from the amplitude, timing, and frequency composition of the EMG signals.

To assess the capability of the sMEA to measure regional differences in the EMG activity of muscle, the device was used to measure the electrical activity of the feline lateral gastrocnemius (LG) muscle during both spontaneous and reflexively induced muscle contractions. The feline LG muscle was selected for our experiments because it is composed of four neuromuscular compartments that are separately innervated [18]. To

compare the EMG signals measured across the electrodes of the sMEA, their periods of activation, magnitude, and frequency compositions were analyzed and compared to the muscle's contractile force. The similarity of the EMG signals was quantified by calculating the correlation coefficients between signals, and the number of dimensions to which the EMG signals could be compressed. In order to demonstrate the value of sampling the EMG activity of a muscle from multiple locations, the EMG signals measured across the electrodes of the sMEA were used to estimate the contractile force of an isometrically held LG muscle. To provide physiological relevance to our quantification of EMG signals, the observed EMG properties were compared to the known composition and architecture of the LG muscle.

4.2 Methods

To assess the efficacy by which the sMEA can distinguish the regional EMG activity of muscle, each device was applied to a feline lateral gastrocnemius (LG) muscle and was used to measure the muscle's electrical activity during both spontaneous contractions and contractions elicited via contralateral tibial nerve stimulation. EMG signals measured through the sMEA, were compared by their time of activation, amplitude, frequency composition, and implantation site. All experimental procedures within this study were conducted in accordance with the guidelines of the National Institutes of Health and of the Georgia Tech Institutional Animal Care and Use Committee.

4.2.1 Stretchable Microneedle Electrode Array

The stretchable microneedle electrode array (sMEA) was fabricated with a polydimethylsiloxane (PDMS) substrate and conductive polydimethylsiloxane (cPDMS) traces (Fig. 2.1). These materials enable the device to stimulate and measure EMG activity, while conforming to contracting muscle. Sixteen arrowhead-microneedle

electrodes are embedded within the cPDMS traces of the sMEA, to provide an intramuscular interface by which to measure EMG activity. A bipolar electrode comprises two microneedles spaced by 2 mm. The bipolar electrodes of the sMEA have been shown to measure EMG activity with a signal-to-noise ratio similar to that provided by steel-wire intramuscular electrodes. The PDMS substrate of the sMEA was laminated and packaged with a polyimide strip, to electrically connect the sMEA to equipment for recording EMG signals. The electrode layout of the sMEA was designed to cover the surface of a feline LG muscle, so as to measure the EMG activity of the LG muscle's four neuromuscular compartments. Greater detail on the fabrication and characterization of the device will be published in another journal article.

4.2.2 Crosstalk Analysis

To effectively measure EMG activity across the surface of muscle, the sMEA must detect EMG activity with high spatial resolution and induce minimal crosstalk between its electrode's traces. The electrical crosstalk induced between traces of the sMEA was measured by applying an alternating current across a trace of the sMEA and measuring the potential difference induced across the adjacent bipolar electrode. One probe of a signal generator (33120A, Agilent Technologies) was hooked onto one of the sMEA's microneedles, and the other probe was placed on the microneedle's corresponding connector on the polyimide strip. A 4-V peak-to-peak sinusoid wave was applied across the two probes at frequencies of 100 Hz, 200 Hz, 300 Hz, and 1 kHz, to test the frequency range of intramuscular EMG measurements. To measure the signal induced in the sMEA bipolar electrode, the two probes of an oscilloscope (TDS 3014B, Tektronix, Inc.) were connected to the polyimide strip connectors corresponding to the sMEA bipolar electrode adjacent to the trace across which the alternating current was applied.

4.2.3 Animal Preparation

Two cats were used to obtain the EMG and force measurements presented herein. Each cat was anesthetized with isoflurane and tracheostomized to deliver controlled levels of the anesthetic. Each cat received a wide craniotomy, its cerebral cortices were removed, its brainstem was transected rostral to the anterior boundary of the superior colliculi, and all brain tissue rostral to the transection was removed. To ensure that the LG muscles were kept at a fixed length, the limb on which the sMEA was applied was fixed firmly to the experimental apparatus. This fixation was achieved by implanting bone screws into the tibias and femurs of the limb, and by clamping the ankles. An sMEA was implanted on the LG muscle of the fixed limb (Fig. 4.1), and placed as distally along the length of the muscle as possible. This placement was chosen to facilitate the measurement of the EMG activity produced by all four neuromuscular compartments of the LG muscle. A reference ground electrode was implanted in the popliteal fat pad, ipsilateral to the sMEA implantation, and a cuff electrode was wrapped around the tibial nerve, contralateral to the sMEA implantation. To measure the force produced by the LG muscle when contracting, its tendon was removed from its insertion and attached to a force transducer. Following completion of the surgery, each cat was taken off anesthetic. At the end of the experiment, each cat was euthanized with Euthasol® (Virbac, Corp.) or potassium chloride.

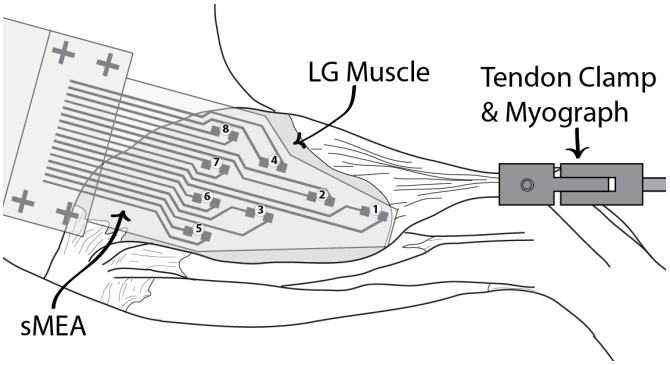

Figure 4.1: A diagram depicting the experimental setup used to measure the electromyographic activity and contractile force of the left lateral gastrocnemius (LG) muscle. In all experiments, the sMEA was placed on the LG muscle such that electrode 1 was implanted most distally along the muscle's length, and electrode 8 was implanted most medially/proximally.

The LG muscle was induced to contract by exciting the crossed extensor reflex through electrical stimulation of the contralateral tibial nerve. The tibial nerve was stimulated via the implanted bipolar cuff electrode, with a uniphasic square wave, with a pulse width of 100 μs, at a frequency of 40 Hz, and an amplitude between 0.3 V and 15.0 V. All 16 electrodes of the sMEAs were configured to measure EMG activity in a bipolar configuration, to provide eight bipolar electrodes. The EMG measurements collected by the sMEA were amplified by a factor of 1000, and digitized at a sampling rat of 3 kHz/channel. The force measurements were digitized at a sampling rate of 1 kHz/channel.

4.2.4 Electromyographic Signal Analysis

The EMG activity measured via the sMEA was analyzed in a numerical computing environment (MATLAB R2014b, MathWorks). Electromagnetic noise and motion artifacts were removed with a 55-65 Hz Butterworth notch-filter and a 20-Hz Butterworth high-pass filter, respectively. High frequency noise, unrelated to EMG activity, was attenuated with a 1-kHz Butterworth low-pass filter. Stimulation of the tibial nerve introduced 40-Hz spikes into the collected EMG measurements. These stimulation artifact spikes were replaced by piecewise-cubic interpolations, based on the surrounding EMG signal. Figure 4.2 provides examples of the filtered EMG signals, which possessed clear compound motor unit action potentials with different start times, durations, shapes, and amplitudes.

The envelopes of the EMG signals were used to analyze the overall magnitude of the EMG activity. To calculate the envelopes, the EMG signals were rectified, and then smoothed with a 4-Hz Butterworth low-pass filter. To determine the median frequency of an EMG signal, its power spectrum was calculated using a fast Fourier transform, and the frequency that divided the power spectrum into two equal parts was computed. The

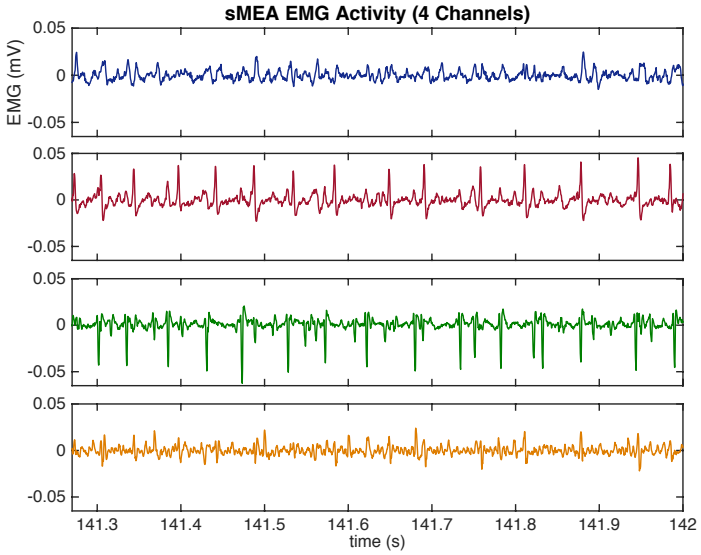

Figure 4.2: An example of the electromyographic activity measured through the sMEA during a muscle contraction.

sliding-window median frequency was calculated in the same manner, with the EMG signal sampled in 1-second windows, at 0.003-second increments. The sliding-window median frequency measurements were smoothed with a 0.03-second sliding window average. The median frequencies of EMG measurements collected from low-force muscle contractions were not used because their frequency compositions were distorted by that of the baseline EMG measurements.

4.2.5 Force Estimation

The envelopes of the measured EMG activity were used to estimate the contractile force of the LG muscle. For this study, the EMG envelopes were calculated in much the same way as described in the previous section, except the low-pass filter was given a 1-Hz cut off frequency, so that the frequency composition of the EMG envelopes would better match that of the contractile force. The force estimates (F_e) were calculated as a weighted sum of the EMG envelopes (X), following Equation 4.1. The weight matrix (β) was determined via linear least squares regression (Equation 4.2), which minimizes the sum of the square of the difference between the fit and the measured force (F_m). Within

Equation 4.2, N represents the number of samples and C represents the number of EMG channels. The percent error between the measured force and the estimated force was calculated as shown in Equation 4.3. A force estimate and its percent error were calculated for every number and combination of sMEA electrode channels, to determine the range of force estimation error produced by each number of EMG channels.

$$F_e = X\beta \tag{4.1}$$

$$\hat{\beta} = \arg\min_{\beta} \left(\sum_{i=1}^{N} \left| F_{m,i} - \sum_{j=1}^{C} X_{ij}\beta_j \right|^2 \right) \tag{4.2}$$

$$\text{Percent Error} = 100\% \times \sqrt{\frac{\sum_N (F_e - F_m)^2}{\sum_N {F_m}^2}} \tag{4.3}$$

4.3 Results

To evaluate the capacity of the sMEA to measure the regional EMG activity of muscle, the electrical crosstalk between traces of the sMEA was characterized and the EMG signals measured through the electrodes of the sMEA were analyzed. Specifically, the EMG signals were analyzed to determine the fewest channels necessary to retain the variance of the measured EMG activity; the timing of activation, magnitude, and frequency composition of the EMG signals were contrasted to distinguish differences in activity; and these properties of the EMG signals were compared to the known muscle fiber composition and architecture of the LG muscle.

4.3.1 Electrical Crosstalk

The objective of this study was to measure the electrical crosstalk induced in the EMG signals carried by the traces of the sMEA. The electrical crosstalk induced depends on the frequency composition of the signals carried by the aggressor traces as well as the distance of the aggressor traces with respect to the victim traces. Electromagnetic radiation decays with distance (r) by $1/r^2$ [122]. Thus, to determine the crosstalk contribution of any aggressor trace on the victim traces, the crosstalk induced by the most adjacent trace was multiplied by $1/(n+1)^2$, where n is the number of traces between the aggressor trace and the victim traces. To calculate the range of crosstalk induced within the traces of the device, electrical crosstalk was calculated for victim traces in the middle, and on the edge of the sMEA connector. Where the former is subject to the greatest crosstalk, and the latter subject to the least. In each case, 14 traces of the sMEA induced crosstalk into two traces connecting to a bipolar electrode of the sMEA. The crosstalk contribution of each of the 14 traces were summed and scaled according to the aforementioned relationship, to determine the total crosstalk incurred.

It was observed that a single trace induced crosstalk values of -36.5 dB, -33.0 dB, -31.1 dB, and -26.3 dB at frequencies of 100 Hz, 200 Hz, 300 Hz, and 1 kHz, respectively. Given these measurements, a bipolar electrode with traces in the middle of the sMEA connector would be subject to crosstalk values -26.9 dB, -23.4 dB, -21.5 dB and -16.7 dB at frequencies of 100 Hz, 200 Hz, 300 Hz, and 1 kHz, respectively. Bipolar electrodes with traces on the edge of the sMEA connector would be subject to crosstalk values of -32.5 dB, -29.0 dB, -27.1 dB, and -22.3 dB, respectively.

4.3.2 Quantification of EMG Signal Heterogeneity

The objective of this study was to evaluate the heterogeneity of the EMG signals measured across the sMEA's electrodes. To achieve this objective, the linear correlation between EMG signals was assessed, and the dimensionality of the EMG signals was estimated. Pearson correlation coefficients quantify the linear relationship between two

Gaussian variables, where a correlation coefficient near zero suggests that the two signals are uncorrelated [123]. If the two signals are uncorrelated, this suggests that they represent different sources of electrical activity within the muscle.

To gauge the degree by which the EMG activity can be grouped into signals of similar variation, principal component analysis (PCA) was applied to the eight EMG signals, to transform the data to an uncorrelated orthogonal basis set [124]. This basis set was then used to find the minimum number of principal component dimensions necessary to retain 95% or 99% of the variance of the EMG signals, where each dimension represents an uncorrelated EMG signal. The principal components of the EMG signals were calculated using FastICA (Helsinki University of Technology), a package developed for MATLAB that performs both independent component analysis and PCA [125].

The absolute values of the Pearson correlation coefficients between the EMG signals, measured across the electrodes of the sMEA, are illustrated in Figure 4.3a. The

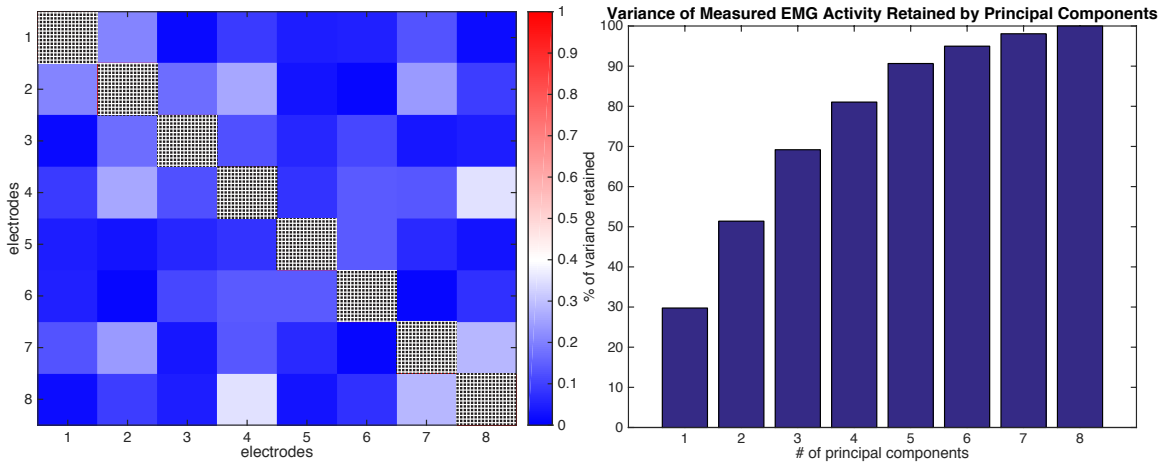

(a) **(b)**

Figure 4.3: The (a) Pearson correlation coefficients between the EMG signals measured through the sMEA, and (b) the variance retained by the principal components of the EMG signals.

absolute values of the coefficients were analyzed to focus on the strength of the correlations as opposed to their polarity. All correlation coefficients, between the EMG

signals, suggested the linear relationships between the EMG signals were very weak, with minimum, median, and maximum values of 0.011, 0.087, 0.353, respectively. A PCA of the ~8 minutes of filtered EMG signals determined that 95% of the measured variance could be retained by six dimensions and that 99% of the measured variance could be retained by eight dimensions (Fig 4.3b.). Each of the first six principal components produced by PCA, retained a significant proportion of the EMG signal variation, ranging from ~5% to ~30%.

4.3.3 Assessment of Differences in Regional EMG Activity

The objective of this study was to evaluate the capability of the sMEA to measure regional differences in EMG activity that result from the heterogeneous muscle fiber composition and architecture of the four neuromuscular compartments of the LG muscle. We measured the EMG activity and contractile force of feline LG muscle during both spontaneous and reflexively induced muscle contractions. To test our hypothesis that the spatial differences in muscle fiber composition can be detected through the EMG signals, we analyzed the EMG signals for differences in their periods of activation, dependencies on muscle force, and frequency compositions. Approximately eight minutes of EMG activity and force measurements were collected from each cat. Our analysis focused on comparing the EMG activity produced by the distal (e.g. electrodes 1 and 2) and medial/proximal (e.g. electrodes 7 and 8) regions of the LG muscle because they differ considerably in their muscle fiber composition. The distal region contains a greater proportion of the muscle's type I fibers, and the medial/proximal region comprises a greater proportion of the muscle's type II fibers [18].

We evaluated the quantitative differences between the EMG activity of the distal and proximal regions as a function of muscle force production. Figure 4.4a shows one example in which the force increased from ~12.4 N to ~21 N, during this trial the EMG activity on electrode 1 increased by ~26% while electrode 8 increased by ~85%, of their

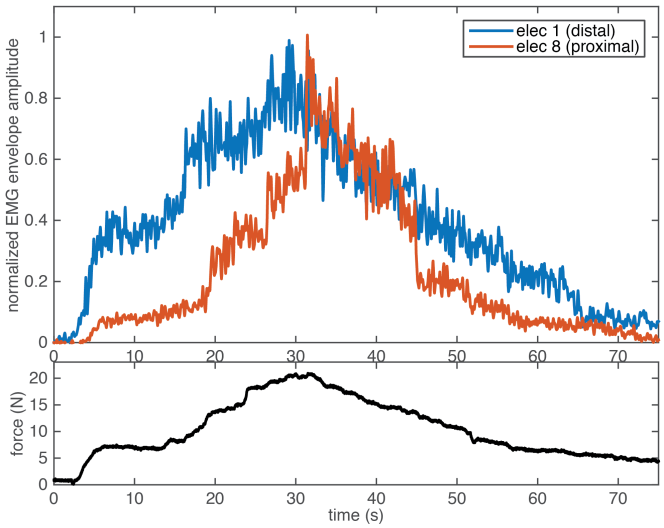

(a)

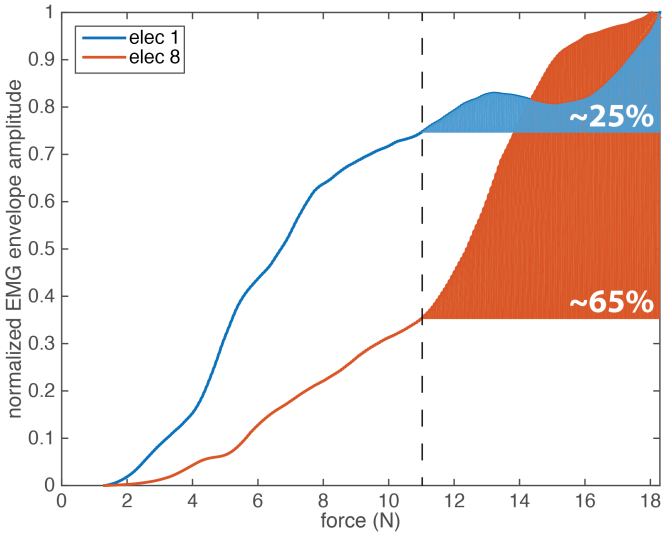

(b)

Figure 4.4: The EMG signals measured across the surface of the LG muscle, exhibited different dependencies on the muscle's contractile force. For example, (a) when the muscle produced a strong contraction, the EMG activity measured proximally along the muscle's length (electrode 8, red), increased significantly in amplitude when the contractile force rose above 10 N, whereas the EMG activity measured distally (electrode 1, blue) increased in most significantly in amplitude during weaker portions of the contraction. Approximately eight minutes of EMG signals and force measurements (seven trials) were aggregated to plot (b) the amplitude of the EMG envelopes as a function of contractile force. Within this aggregate data, the EMG activity measured distally increased in amplitude across a wide range of muscle contractions (e.g. > 5 N), whereas the EMG activity measured proximally increased in amplitude primarily only during strong contractions (e.g. > 11 N).

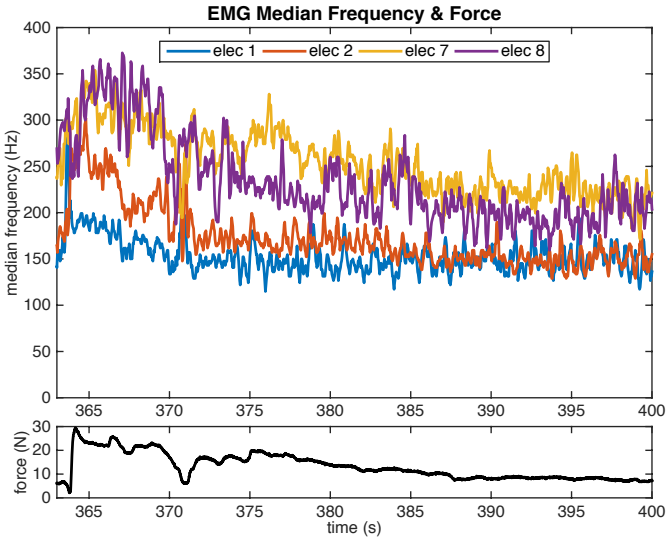

(a)

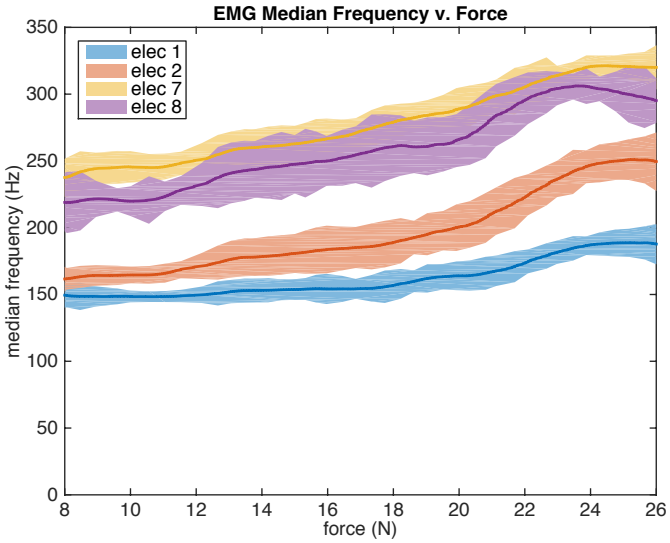

(b)

Figure 4.5: Within individual trials, (a) the EMG activity measured medially/proximally within the muscle (electrodes 7 and 8) was observed to have a significantly higher median frequency than the EMG activity measured distally (electrodes 1 and 2). Approximately five minutes of EMG signals and force measurements were aggregated to plot (b) the median frequency of the EMG signals as a function of contractile force. Within this aggregated data it was observed that the median frequency of the EMG signals increased almost monotonically with the muscle's contractile force.

respective maximal activities. Similar quantitative differences were observed across all trials when the aggregated EMG envelopes were plotted as a function of contractile force (Fig. 4.4b). The EMG envelopes measured across the more proximal regions of muscle exhibited a greater dependence on high-force muscle contractions (e.g. > 11 N) than that

measured more distally. For example, as the muscle's contractile force increased from 11 N to 18.3 N, the EMG envelope of electrode 1 increased by ~25% of its maximal amplitude, but the envelopes of electrodes 7 and 8 increased by ~49% and ~65% of their respective maximal amplitudes.

We also analyzed the frequency composition of the EMG signals, as related to the contractile force and electrode placement (Fig. 4.5a). Differences in the frequency composition of the EMG signals were observed between those recorded distally and proximally in which the more medial/proximal electrodes produced EMG signals on average ~52% higher in median frequency (i.e. ~90 Hz higher) than did the distal electrodes (Fig. 4.5b). We also observed that the median frequency of the EMG signals increased almost monotonically as a function of contractile force (Fig. 4.5b), for all electrodes.

4.3.4 Force Estimation Based on EMG Activity

The objective of this study was to determine how accurately contractile force produced by the muscle could be estimated from the EMG measurements. To achieve this objective, we calculated the least-squares fit of the EMG envelopes to the contractile force, using the EMG envelopes from every combination of the electrodes. We evaluated the least-squares fits based on the number of electrodes used, the electrode placement, and the percent error between the least-squares fits and the contractile force.

Figure 4.6a provides an example of the force estimates produced by fitting the EMG envelopes from a single proximal electrode and all eight electrodes of the sMEA, to the muscle's contractile force. Figure 4.6b illustrates the distribution of the percent error of the force estimate, calculated using a subset of the sMEA's EMG channels. We observed that as the number of EMG channels used was increased from one to eight, the median percent error fell from 39.1% to 12.4%, and the range of the percent error

decreased from 22.9% to 0%. The distribution of the percent error was approximately Gaussian around the median, with the 25 and 75 percentiles deviating from the median by

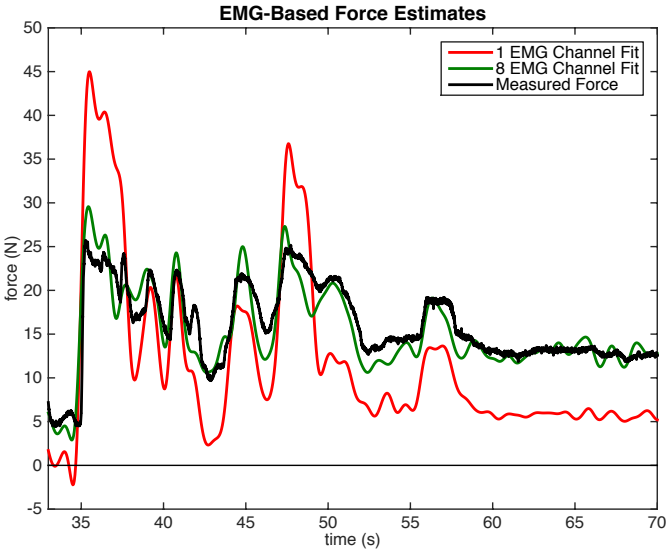

(a)

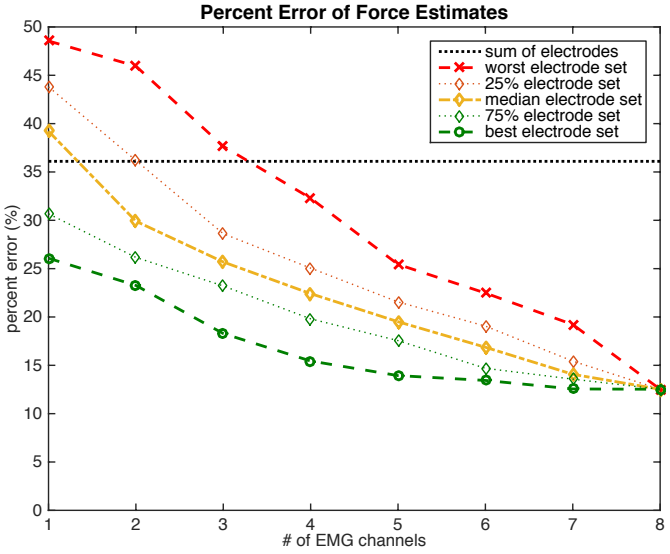

(b)

Figure 4.6: EMG-based force estimates were computed by least-squares fitting the EMG envelopes to the muscle's contractile force. (a) A least-squares fit based on the EMG activity measured from all eight sMEA electrodes (green line) was observed to provide a significantly better estimate of contractile force than a least-squares fit based on the EMG activity from a proximal electrode (electrode 7, red line). Force estimates were calculated using all possible numbers and combinations of EMG channels. (b) The percent error of these force estimates decreased as a function of the number of EMG channels used. The force estimate calculated based on the sum of all eight EMG channels (horizontal dotted line) was observed to yield a 36.1% error.

about ± 2-3%. When five or more electrodes were used to estimate the muscle's force, all combinations of electrodes provided a better estimate than the best-placed single electrode. The percent error of the force estimates given by the optimal selection of electrodes, plateaus at ~14% with five electrodes. We also summed the EMG envelopes form all electrodes of the sMEA to simulate the EMG envelope that might be measured by a single large electrode. We observed that this aggregate EMG envelope produced a force estimate with ~3% less error than the median single electrode. If two or more sMEA electrodes were used to estimate the muscle's force, the median consistently performed better than the aggregate electrode.

4.4 Discussion

The results of our experiments establish that the sMEA is capable of recording the electrical activity of muscle robustly. The measured EMG signals were linearly uncorrelated and demonstrated a high level of linear independence as per PCA. During muscle contractions, we observed significant differences among the EMG signals, based on both the electrode placement and the muscle's contractile force. Specifically, the distal EMG signals, when compared to the proximal signals, were more readily recruited, possessed lower median frequencies, and were less sensitive to changes in muscle force above 10 N.

4.4.1 Electrical Crosstalk

Electrical crosstalk is an important measure of the sMEA's performance because it limits the effective resolution by which the system can measure the EMG activity of muscle. Compared to the crosstalk introduced by neighboring muscles observed within surface EMG measurements, which may be as high as -3.9 dB [52], the electrical crosstalk between traces of the sMEA is minimal. The electrical crosstalk among the electrode channels of the sMEA was estimated between -27.1 dB and -21.5 dB at a

frequency of 300 Hz, in traces on the edge and in the center of the sMEA connector, respectively. At a frequency of 1 kHz, crosstalk of -16.7 dB was estimated to be induced in the traces in the center of the sMEA connector. Although this crosstalk is greater than desired, very little EMG activity is expected to be measured at such a high frequency – the majority of intramuscular EMG activity is contained below the frequency of 500 Hz [126]. These experiments demonstrate that EMG measurements collected through an sMEA reflect the EMG activity proximal to the electrodes.

Although electrical crosstalk was not a problem under the tested conditions, under other scenarios it may be necessary to mitigate the electrical crosstalk to better differentiate regional EMG activity. Such scenarios might occur if the sMEA were fabricated with a greater number of electrodes or a higher electrode density, which would increase electrical crosstalk between traces. To reduce the electrical crosstalk, the traces of both the sMEA and the polyimide connector could be shortened to decrease the duration of time the EMG signals are susceptible to electromagnetic interference. The spacing between traces may be increased to decrease the mutual inductance and capacitance between traces. Lastly, a PDMS-insulated ground plane may be vaporized onto the back of the sMEA to minimize the overlap of the electric fields produced by the traces, and hence the crosstalk [127].

4.4.2 Quantification of EMG Signal Heterogeneity

The heterogeneity among the EMG signals characterizes the sMEA's ability to differentially measure regional EMG activity across the surface of muscle. To quantify the similarity among the EMG signals, their Pearson's correlation coefficients were calculated to assess the linear correlation of the signals, and PCA was performed to evaluate the dimensionality of the signals. The PCA revealed that at minimum, six and eight dimensions would be required to retain 95% and 99% of the variance within the measured EMG signals, respectively (Fig. 4.3b). These data demonstrate that each

electrode measured distinct electrical activity within the muscle, and that the dimensionality of the resulting signals cannot be easily compressed. The absolute values of the Pearson correlation coefficients between the EMG channels were all less than 0.4 (Fig. 4.3a), with ~57% of the coefficients below 0.1, indicating that the channels were weakly linearly correlated.

We conclude from these analyses that the detection volumes of the electrodes were sufficiently small such that the electrodes could detect highly localized EMG activity. In order to further reduce the detection volumes of the microneedle electrodes, the sides of the microneedles could be insulated with parylene or polyimide, such that only the tips of the microneedles are exposed. If this were properly implemented, we could reduce the space between the electrodes while maintaining localized detection volumes.

4.4.3 Assessment of Differences in Regional EMG Activity

We measured regional differences in the EMG amplitude and frequency composition, consistent with the muscle's architecture and fiber composition. We observed ordered recruitment [16], in which the regions of the muscle with more type I muscle fibers were recruited earlier than the regions with more type II muscle fibers. This relationship between regional EMG activity and contractile force was found in both individual trials as well as in the aggregated data. In individual trials (Fig. 4.4a), the proximal regions of the muscle produced EMG activity of high amplitude only during strong contractions (e.g. 13 N), whereas the distal regions produced similar levels of EMG activity across a much wider range of muscle contractions. Similar relationships were observed when we evaluated the aggregate data from a large number of trials (Fig. 4.4b): the EMG envelopes measured across the more proximal electrodes increased in amplitude during higher-force contractions (e.g. > 10 N); whereas those measured across

the distal electrodes increased in amplitude across a wide range of contractions (e.g. > 5 N).

We observed that the frequency composition of the EMG signals corresponded to the muscle fiber composition and architecture of the LG muscle. The rate and magnitude of type II muscle fiber depolarization are greater than those of type I muscle fibers [106], [128]. Therefore, the electrical activity of type II muscle fibers should increase the high frequency component of EMG activity. In particular, the median frequency of a muscle's EMG activity is higher within muscles with a greater proportion of type II muscle fibers [128], [129]. Our experimental results are consistent with these studies: the distal regions of the LG muscle in which a greater proportion of the type I muscle fibers are localized [18], produced EMG activity with a lower median frequency than the proximal regions (Fig. 4.5).

4.4.4 Force Estimation Based on EMG Activity

Prior studies have used EMG activity to estimate the contractile force and torque produced by a muscle [130]–[132]. In order to estimate the muscle force from EMG activity, we measured EMG signals across all four of the LG muscle's neuromuscular compartments, expecting that these signals would represent different components of the muscle's force. These neuromuscular compartments differ in both their fiber composition [18] and the torque they apply to the tendon [7]. By combining the measurements of electrical activity from these compartments, we can provide an estimate of total muscle force for the isometric conditions under which we experimented.

We observed that an increase in the number of EMG channels improved the accuracy of the force estimates. As the number of EMG channels used to estimate the muscle's contractile force was increased from one to eight, the percent error in force estimation dropped significantly from 39.1% to 12.4%. In contrast, the sum of the eight channels, which provides an estimate of the activity measured across a single large

electrode, produced an estimation error of 36.1%. It may be possible to further reduce this error by including EMG measurements from other regions of the muscle, such as the deeper LG muscle tissue, which contains a greater proportion of type I muscle fibers than the surface.

The accuracy of the force estimates was dependent on the locations of the electrode implantations within the muscle. Figure 4.6a, shows an example in which the electrode that provided the force estimate was implanted in the LG_m/LG_2 neuromuscular compartments, both of which have high percentages of type II muscle fibers [18]. When the muscle was contracting at low levels of force, the EMG activity measured across the electrode was small; however, when the muscle produced bouts of strong contractions (e.g. 25 N), the EMG activity was significantly larger. This difference indicates that the electrode was placed in a region that was predominated by type II muscle fibers. Because it primarily measured the activity of type II fibers, this electrode yielded a poor estimate of contractile force, with a large error of 48.6%.

These analyses effectively demonstrate that the application of multiple electrodes provides valuable information for assessing the contractile activity of muscle. Stretchable microneedle electrode arrays could be combined with artificial neural networks [133] or physiological models of muscle [131] to produce more accurate estimates of a muscle's activity than the method presented, which would prove valuable for both studies of the neuromuscular system and clinical applications. Any estimate of contractile force based on EMG measurements, however, is confounded by the dependence of the muscle's contractile force on the length [134] and the velocity [135] of the muscle.

4.5 Conclusion

We developed a technology for implementing stretchable microneedle electrode arrays (sMEA) that facilitate high-fidelity electrical stimulation and measurement of excitable tissue. We demonstrated that the sMEA is capable of detecting differences in

the regional electrical activity of muscle, such as in the timing of activation, the level of recruitment, and the frequency composition of the EMG activity. Our experiments demonstrated that the frequency composition and amplitude of the EMG activity measured via an sMEA may be used to discern the muscle fiber composition and recruitment strategies of a muscle's neuromuscular compartments. We also showed that the use of multiple intramuscular electrodes of the sMEA can provide a more accurate estimate of muscle force than a single intramuscular electrode.

Both the invasiveness and the signal fidelity of the array can be enhanced/modified for specific applications. To better measure the activation of muscle using intramuscular measurements, electrodes of varying length could be incorporated into the intramuscular sMEA to better contact deeper muscle tissue. Conversely, the size, electrode count, and electrode density of the sMEA could be increased to more thoroughly investigate the dimensionality of a muscle's EMG activity. To facilitate the use of sMEAs in transcutaneous applications, for which the invasiveness of an intramuscular sMEA may be prohibitive, the microneedles could be designed to penetrate skin, provide higher signal fidelity than surface electrodes [136], and induce little to no pain [137]. Both intramuscular and transcutaneous sMEAs could also benefit from the incorporation of onboard electronics, such as pre-amplifiers and multiplexing chips, to increase the SNR and manage higher electrode counts.

The technology has the potential for a broad range of scientific and clinical applications. The resulting devices could be applied to scientific studies of the neuromuscular system, to examine the changes in the regional recruitment of muscle after a spinal cord injury, or to analyze muscle synergies at a compartmental level. Further advancements of the sMEA could enable the technology to be used in clinical applications, to measure the regional EMG activity of volitionally controlled muscle by which robotic limbs, functional electrical stimulation systems, or muscle-computer interfaces may better return mobility and independence to the disabled.

CHAPTER V

CONCLUSIONS AND FUTURE DIRECTIONS

We have presented the development of a stretchable microneedle electrode array (sMEA) and its application to muscle for the purpose of regional stimulation and measurement of EMG activity (i.e. chapters 2-5). The device is composed of a PDMS substrate and cPDMS traces, which enable the device to stretch and conform to contracting muscle tissue.

5.1 Summary

Chapter 2 presents the fabrication process and the characterization of our sMEA. We demonstrated that the device maintains electrical conductance up to a 56% tensile strain, or up to a 40% tensile strain, if repeatedly stretched. The fabrication process of the sMEA yields electrodes/traces of low and uniform impedance, which enables the device to measure EMG activity with a high signal-to-noise ratio uniformly, and control the charge delivered across the surface of the muscle. The device is cytocompatible for at least 28 DIV, and causes a localized inflammatory response on the surface of muscle, if implanted for 35-days *in vivo*. The signal fidelity and frequency composition of EMG activity measured through the sMEA are similar to those acquired through steel-wire intramuscular electrodes. The sMEA can reliably maintain electrical contact with muscle when the tissue is both stretched and relaxed. The device reduces both the difficulty and the damage incurred to tissue associated with implanting multiple intramuscular electrodes.

Within Chapter 3, we demonstrated that the bipolar electrodes of the sMEA can selectively activate muscle regions when inducing muscle contractions of low force, and that the temporal properties of the induced muscle contractions were dependent on the location at which the electrical stimulation was delivered. By spatially and temporally

distributing charge across the surface of muscle via the electrodes of sMEA, it was also possible to reduce the ripple and fatigue of the muscle contractions induced via electrical stimulation. It was observed that muscle activated by an sMEA would produce a stretch response similar to that of areflexive muscle.

Lastly in Chapter 4, we showed that the bipolar electrodes of the sMEA are effective at measuring the regional EMG activity of muscle, and that the measured EMG activity is relatively localized to the proximity of the respective electrodes. The respective force sensitivities and frequency compositions of the measured EMG signals were consistent with the properties of the muscle fibers known to compose the corresponding regions of muscle. It was observed that increasing the number of sMEA EMG channels used to predict a muscle's contractile force, significantly reduced the error of the force estimation, indicating that the sMEA provides valuable information with which a muscle's kinematic state can be gauged.

5.2 Future Directions – Scientific Studies

Scientific studies and research, to which the sMEA described herein may be more immediately applied, include the selective activation of excitable tissue, the study of reflexes mediated by the Golgi tendon organ, the stability of the neuromuscular system, and response of cells to physical stress. These applications should not be considered an exhaustive list.

Selective stimulation: The experiments presented within this dissertation explore the spatial distribution of charge within a muscle, however, the pulses of the electrical stimulation may also be modified to better control the activation of the tissue. A depolarizing pre-pulse (DPP) is the application of a protracted sub-threshold depolarizing square wave immediately before the excitatory pulse. These sub-threshold stimuli are theorized to cause a conformational change in the sodium ion channels of a nerve, such that the probability of the membrane channel pore opening in response to a supra-

threshold stimulus is reduced [109]. Through DPPs, the nerves proximal to an electrode may be inhibited. Thus, a greater degree of specificity of muscle activation may be obtained utilizing this strategy of electrical stimulation. For example, the electrodes that surround the excitatory electrodes may delver DPPs to reduce the spread of activation, and produce a more localized activation of muscle, which would be particularly useful for the selective activation of neuromuscular compartments.

Alternatively, quasitrapezoidal stimulus pulses may be delivered to the muscle instead of the square wave stimuli utilized in our research. Quasitrapezoidal stimuli have been observed to preferentially excite smaller axons [138], as opposed to larger axons, as is typically observed through square wave pulse electrical stimulation. This difference in axonal excitation may, theoretically, be used to activate muscle in a more physiological manner, activating the smaller axon type I motor units, before the larger axon type II motor units, to produce smoother contractions via electrical stimulation and induce less fatigue. Such stimulation may also be used to enable the sMEA to activate muscle spindle fibers, and facilitate the physiological stretch response of muscle electrically stimulated by an sMEA.

Study of Golgi tendon organ mediated reflexes: Muscle electrically activated by an sMEA was observed to produce stretch responses similar to areflexive preparations, principally due to the lack of activation of muscle spindle fibers or interneurons within the spinal cord. The inability of the sMEA to activate muscle spindle fibers may be utilized to explore the individual contribution of Golgi tendon organs to reflexes. The electrodes of the sMEA would better facilitate the activation of excitable tissue than an individual steel-wire electrode, and may be used to study the neuromuscular contribution to Golgi-tendon organ mediated reflexes.

Study the stability of the neuromuscular system: The sMEA may also be used to examine the stability of neuromuscular systems via artificial positive force-feedback reflexes. Positive force feedback has been observed in the extensor muscles regulating

stance and gait [139], [140]. An artificial positive force-feedback reflex may be constructed by using the sMEA to electrically stimulate a muscle proportionally to the contractile force produced by that muscle. It is hypothesized that the length-tension curve of muscle inherently limits the gain of positive force feedback and ensures neuromuscular stability. Artificial positive force-feedback reflexes may be used to assess this hypothesis and the stability of neuromuscular systems under different conditions and with different muscle groups. Stimulating muscle with an sMEA to produce these artificial reflexes would facilitate the production of smooth, fatigue-resistant contractions by the activated muscle.

Study of the cellular response to stress: The stretchability and cytocompatibility of the sMEA, makes the device well suited for the study of the cellular response of tissue to strain and stress. The research from which may be used to further our understanding of the mechanisms behind traumatic brain injuries, cardiomyopathies, and vascular disorders [63]. Such a system might attach the edges of the sMEA to motors in order to stretch or compress the cell cultures, while stimulating or measuring the electrical activity of the cell cultures. Stretchable electrode arrays are predominately fabricated with micro-patterned gold traces [61], [62], which can produce impedances greater than 850 kΩ as a result of strain [141]. The sMEA presented herein would provide a cytocompatible and low-impedance platform by which to conduct such cell stress experiments.

5.3 Future Directions – Clinical Applications

The ability of the sMEA to selectively activate and measure the regional activity of muscle gives promise that the device may be used in clinical applications to return or expand the motor function of individuals. Before the sMEA is utilized for such purposes, however, the design must be modified to improve its biocompatibility. Assuming this revision of the sMEA is achievable, the device may be used to improve the performance

of muscle-computer interfaces, functional electrical stimulation (FES) systems, and intracranial stimulation and measurement systems.

Muscle-computer interfaces: The many intramuscular electrodes of the sMEA enable the device to measure compartmental or regional EMG activity with a high SNR, with which considerable information may be acquired regarding the muscle's recruitment. Such information may be used to predict the muscle's state or manipulate electronic devices. As a muscle-computer interface (MCI), the sMEA may be used to deliver control over electrical equipment both attached to, and separate from, the body. Regional intramuscular EMG activity may provide patients the ability to move prosthetic robotic limbs with greater precision, speed, and range of motion than EMG activity measured through surface or steel-wire electrodes. Alternatively, as an MCI, the sMEA could be used as a conduit to operate external devices such as motorized vehicles [120], wheelchairs, personal electronic devices [118], or assistant robots.

Functional electrical stimulation (FES): If incorporated into FES systems, the sMEA may be used to both measure the regional electrical activity of residual or functioning muscle, and stimulate paralyzed muscle based on the measured EMG activity. The sMEA would enable the localized activation of paralyzed muscle and potentially provide the individual the ability to perform a greater range of motion, than would be achieved if each paralyzed muscle were stimulated with a single steel-wire electrode, such as in the Freehand system [28]. With multiple intramuscular electrodes implanted in each muscle, the tissue may be more fully activated to produce stronger contractions, and electrical charge may be spatially distributed to reduce the muscle fatigue induced. An FES system that used sMEAs to both stimulate and measure the electrical activity of muscle would be particularly useful in circumstances where it is beneficial for paralyzed muscle to copy or mirror the activity of functioning muscle, such as in unilateral vocal cord paralysis (UVCP). Through the application of sMEAs, the contractile activity of the thyroarytenoid and lateral cricoarytenoid muscles on the

paralyzed side of the vocal cord could be synchronized with their functioning counterparts, to return the ability to adduct the vocal cord to UVCP individuals.

Stimulation and measurement of cortical activity: The stretchability and conformability of the sMEA enable the device to be applied across a large interfacial area, which can be useful for the stimulation and measurement of electrical cortical activity. The electrode layout and density could be modified to optimally electrically interface with regions of a cortex's surface. Through such devices, the cortex may be electrically stimulated to reduce the symptoms of neurological disorders. Electrical stimulation of the motor cortex, for example, has proven particularly effective at providing pain relief to those suffering from trigeminal neuropathic pain and central pain syndromes [142]. Within medically intractable partial epileptic individuals, electrical stimulation delivered to the seizure foci via subdural cortical strip lead electrodes, significantly reduced the frequency of seizures experienced by these individuals [143]. Through the many electrodes of the sMEA, the spatial distribution of charge may be optimized to reduce the severity of pain, the frequency of seizures, or other neuropathic symptoms. Alternatively, the sMEA may be used as a brain-computer interface, to measure regional cortical activity by which prosthetic devices or external electrical equipment may be controlled.

5.4 Conclusions

We have developed a stretchable prosthesis that can conform to moving tissue and can be scaled to electrically interface across a large area of excitable tissue. The research presented herein describes how the device was fabricated, characterizes its mechanical and electrical properties, and demonstrates its capabilities to stimulate and measure the regional electrical activity of skeletal muscle. In its present form, the device may be utilized to analyze the operations and the stability of neuromuscular systems.

Advancements of this technology may ultimately be applied to return mobility to the paralyzed and reduce the severity of the symptoms of neurological disorders.

APPENDIX A

POLYDIMETHYLSILOXANE MICROSTENCILS MOLDED ON 3D-PRINTED TEMPLATES

Microstencils have been utilized in biomedical engineering to pattern cell cultures, to engineer tissues, and to pattern conductive materials in microelectronics for the measurement of bioelectric activity. However, fabricating these microstencils can be considerably time consuming, expensive, and cleanroom processing or laser micromachining intensive. We present microfabrication strategies for producing stencils rapidly and cost effectively, with minimal use of cleanroom facilities, ideal for prototyping or applications where microfabrication costs need to be conserved. The process utilizes 3D-printed templates as master structures from which polydimethylsiloxane (PDMS) microstencils are molded. The entire process, from concept to completed stencil, requires approximately one day, however, the majority of this time is budgeted for PDMS curing cycles, so it requires only ~1-2 person hours to complete. These microstencils were used to pattern metal traces ~160 – 1000 μm wide, on three commonly used BioMEMS substrate materials; to pattern rat cortical neuronal cell cultures with radii between ~300 μm and ~1000 μm; and to pattern organic materials. With the advancement of 3D printing technologies, we anticipate that our presented processes will improve in resolution and gain a greater cost advantage over traditional microstencilling methods.

A.1 Introduction

The Biomedical Engineering community is adopting a greater number of microfabrication technologies to construct BioMEMS devices for biological, medical, and chemical applications. Such applications include biosensors, diagnostic devices, drug delivery systems, pacemakers, therapeutic systems, and microfluidic devices [144], [145]. BioMEMS devices must be easily customized, biocompatible, mass manufacturable, and cost-effective to be utilized in such a wide range of applications. Microstencilling technology can play a key role in the microfabrication of BioMEMS devices because it can be used to pattern both biological and nonbiological materials repeatedly, rapidly, consistently, and cost-effectively. This makes microstencilling a versatile technological choice for the mass production of micro and nanoscale features.

Microstencils, or shadow masks, are typically thin layers of material (e.g. silicon, metals, glass, and polymers) that are micromachined to have patterned apertures for the controlled deposition of materials. Traditional stenciling technology is derived from the printed circuit board (PCB) industry where stencils are used for patterning PCB features, interconnects, solder pastes, and adhesives [146]. With advances in micro-electro-mechanical system (MEMS) technologies, microstencils have evolved to perform similar functions in the microsystems industry.

Microstencils have proven considerably useful for a wide variety of applications. For example, stencils can been utilized to engineer tissues [147]–[150], construct controlled networks of neurons [151], and study cell-cell interactions within co-cultures [147], [149], [150]. Stencils can be used to build cell-based biosensors, construct cell-based analogue systems to study the effects of chemicals on biological systems [152], or

pattern two-dimensional and/or three-dimensional cell cultures [147] or proteins [153], [154]. Of course, this technology can also be applied to construct devices with which to study biological tissues, through the patterning of microelectrodes, metal nanomechanical features, or nanoconductors [155]–[159]; by serving as replacement insulators for microelectrode arrays [160]; defining liquid alloy interconnects [161]; or producing complex 3D microfluidic chips [162].

To produce microstencils for so many applications, numerous strategies have been employed. More traditional stencils have been produced using inductively coupled plasma (ICP) silicon etching to construct rigid micro-scale [155], [159], [163], [164] and nano-scale stencils [156], principally for the purpose of patterning vaporized metal. Although such stencils have excellent spatial resolution they can take multiple days to produce and involve cleanroom processing such as resist coating, resist development, photolithography, and ICP etching. Although a cleanroom is not absolutely necessary to perform photolithography, a filtering of light and some level of particulate control are required to prevent the premature cross-linking of photoresist and to reduce the contamination of photoresist, respectively. Laser micromachining [153], [165], [166] was developed as a faster alternative process to ICP etching, in which stainless steel or polyimide stencils can be cut in less than 15 minutes [153], however, these stencils cannot be produced with as a fine resolution as they can be through ICP etching (e.g. 8.5 μm for laser micromachining [165] and 0.45 μm for ICP etching [156]), and the processing time scales linearly with the complexity of the desired design. Similarly, micro electrical discharge machining can produce metal stencils [167], however, they suffer from the same resolution and scalability challenges as laser micromachining.

Researchers have developed microactuated shadow masks to produce complex 3D structures in a single phase of vaporized metal deposition [158]; while other groups have endeavored to reduce the equipment and cost necessary to produce microstencils, utilizing photolithographic techniques to produce SU-8 [162] and polydimethylsiloxane (PDMS) stencils [147], [168]–[171]. Moldable PDMS microstencils have the added advantage of biocompatibility, and are also extendable to large-area manufacturing. The production of microstencils, however, can still be time consuming and expensive because of the use of photolithographic techniques and the requirement for specialized equipment such as lasers, mask aligners, and inductively coupled plasma-reactive ion etchers to cut/etch out patterns in metals, silicon wafers, and polymers.

PDMS, as a material, is ideal for producing microstencils for biological and BioMEMS applications such as cell culture scaffolds, engineered tissues, microelectrode arrays, genomic sequencing chips [172], microfluidic devices, and lab on a chip devices [149], [173], [174] because it is highly biocompatible [35], possesses a low surface energy [175], is micro-moldable and large area fabrication compatible. Thus, PDMS can be used with biological systems for prolonged periods of time without injurious effects, and can be easily applied to and removed from substrates.

More recently, templates produced via traditional photolithographic techniques have been substituted for those made by standard 3D printers, to mold PDMS microfluidic devices and reduce the time and cost necessary for device fabrication [176]. If such an approach were taken to create PDMS stencils, similar benefits could be obtained – making it ideal for applications that require rapid design revisions and for researchers with limited or no cleanroom access. Building upon this approach, we present

the use of 3D-printed templates to mold PDMS microstencils. We used this approach to pattern both metal traces/electrodes and cell cultures, to highlight its utility for both bioelectric and bioengineering applications. It should prove particularly useful to those in the biological/biomedical engineering communities because it facilitates the patterning of organic materials and removes the necessity for specialized equipment (e.g. mask aligners and lasers) and training for that equipment. For example, there are approximately 139 universities in the United States of America that have cleanroom resources [177], which comprise ~4.8% of 4-year universities [178]. Although the process cannot achieve the same resolution as photoresist molded templates [147], [168], [169], [171], often resolution below 200 μm is unnecessary for many biological applications. In addition, compared to photoresist molding methods, our process can be faster, cost effective, and easier to implement.

A.2 Materials and Methods

Our approach for producing PDMS microstencils for the patterning of materials may be broken down into three steps: (A) 3D printing and preparing a negative template; (B) molding a PDMS microstencil on the template; and (C) patterning materials with the microstencil. Figure A.1 illustrates the process flow of the steps involved. Within Step B, we adopted three different strategies to remove PDMS residue from the features of the 3D template; these strategies varied in their use of equipment, and are henceforth referred as our etched, sprayed, and clamped methods.

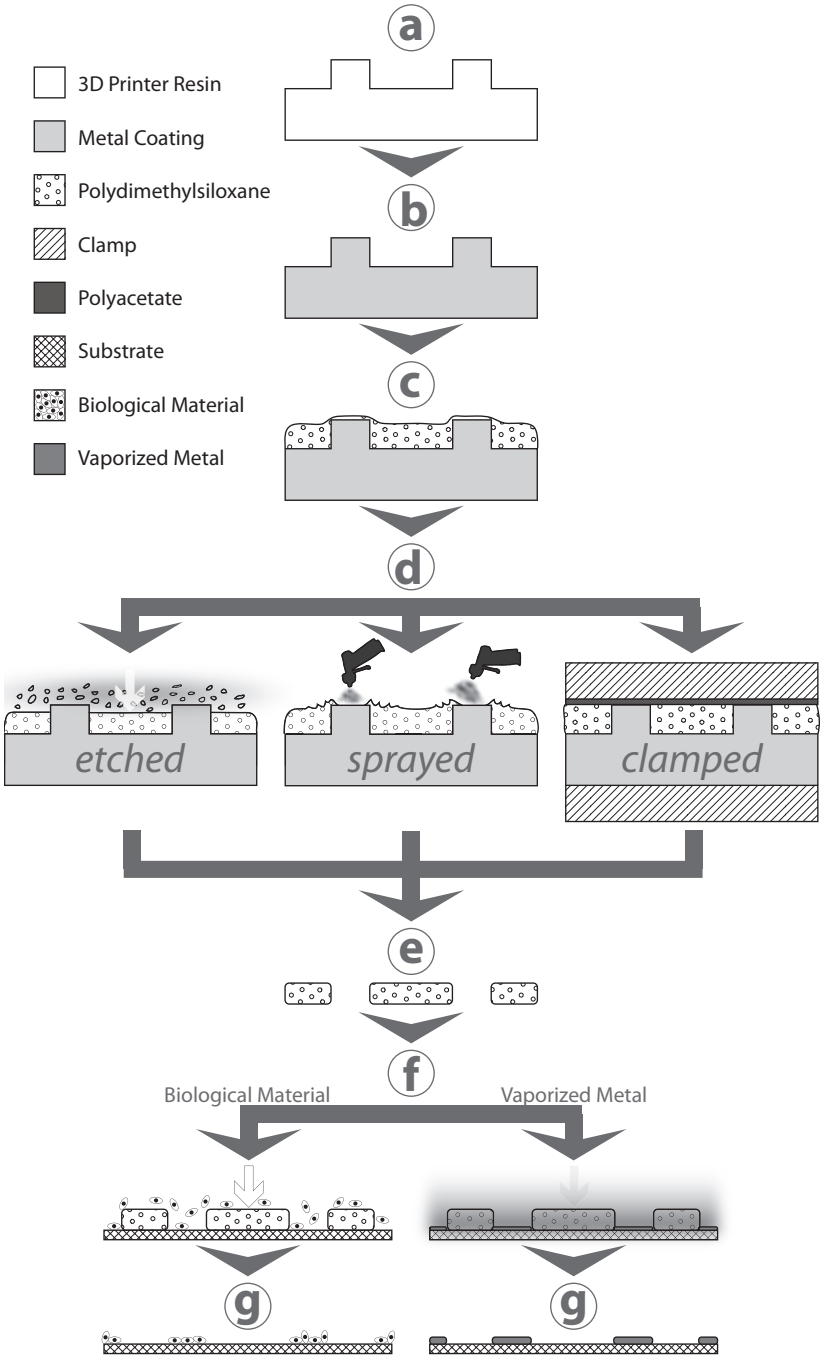

Figure A.1: An illustration of the process for patterning materials with template molded stencils. The (a) template is 3D printed to design and (b) coated in metal. (c) PDMS is cured on the template and any PDMS residue remaining on the template's features is removed (d) through either the etched, sprayed, or clamped strategies. The PDMS stencil is (e) demolded and applied to a substrate for (f) material patterning, after which the (g) stencil is removed to reveal the pattern.

A.2.1 3D Printing and Preparing a Negative Template

The 3D templates on which our PDMS stencils were molded, were drafted using a 3D computer-aided design software (SolidWorks 2012, Dassault Systèmes S.A.) with a 3-mm-thick base and 700-μm-tall features. This base thickness was experimentally determined to exhibit minimal warping during the 100 °C curing process, which follows at a later stage. If thicker or thinner stencils are desired, the features of the 3D template may be made taller or shorter, respectively. All of the 3D templates described in this paper, except for one, were printed with a glossy finish to produce stencils with smooth edges. The remaining template was printed with a matte finish to produce stencils with sharp corners. All of the templates (Fig. A.1a) were printed using an Eden 250 (Objet Geometries Ltd.) that was loaded with Transparent FullCure 720 and Support FullCure 705 (Objet Geometries Ltd.) materials. These printer materials inhibit the polymerization of PDMS [179], so to prevent PDMS from contacting the printer materials, a ~400 Å thick layer of gold was deposited on the mold (Fig. A.1b), using a sputter coater (Hummer VI, Anatech USA). The "vertical" features produced by the Eden 250 printer were slightly curved, as such, the sputter coater was able to cover the entire surface of the 3D template with gold. Before PDMS was cast, a mold release spray (SLIDE® Knock Out) was spray coated uniformly on the metalized 3D template for ~3 seconds, to allow for easy demolding.

A.2.2 Fabricating the PDMS Stencil

PDMS was prepared for molding on a template by mixing Sylgard 184 (Dow Corning) base and curing agent at a 10:1 weight ratio. The PDMS composite was subjected to a vacuum chamber for 30 minutes to remove air bubbles.

The etched and sprayed methods: PDMS was spin-coated onto the 3D template at 400 rpm, for 90 seconds, with a ramp time of 4.7 seconds, to produce a PDMS layer ~170 μm thick. The PDMS layer was cured at 100 °C for 45 minutes in an oven (Fig. A.1c). Our etched method (Fig. A.1d) removes PDMS residue remaining on the 3D template's features through the use of a reactive ion etcher (RIE) (790® RIE, Plasma-Therm) at a power of 300 W for 40 minutes with gas flow rates of 10 standard cubic centimeters (sccm) per minute for O2 and 40 sccm for SF6 [180]. A bench-top plasma system could be substituted for the RIE. The sprayed method (Fig. A.1d) removes PDMS residue by gently spraying nitrogen gas on the 3D template's features before curing the PDMS [168] – and this method does not require etching.

Following the removal of PDMS residue, the template was placed in a bath of hexane (Sigma-Aldrich) that causes the PDMS stencil to swell [181] and detach from the template. The detached PDMS stencil was then placed in a bath of 70% ethanol to return the PDMS to its original dimensions (Fig. A.1e).

The clamped method: Alternatively, stencils may be produced without a spin coater, a reactive-ion etcher, or hexane. To achieve this, we clamped uncured PDMS (Fig. A.1d) between a matte finish 3D template and a layer of polyacetate supported by a metal plate [182]. PDMS was cured in this arrangement at 60 °C for 24 hours, after which the stencils were demolded from the template (Fig. A.1e).

A.2.3 Patterning Materials with the Microstencil

We used our microstencils to pattern both microelectrodes and cortical cell cultures to highlight their utility for both device fabrication and biomedical applications.

Patterning metal: We patterned metal traces on glass, polycarbonate (PC), and PDMS substrates to evaluate the use of our etched stencils on commonly used BioMEMS substrates with a wide range of melting points, coefficients of thermal expansion, and Young's moduli. In an effort to determine the resolution of our process and equipment, these stencils were fabricated with apertures for five traces, designed to be 1000, 500, 250, 125, and 62.5 μm in width.

Each PDMS stencil was briefly soaked in a bath of 70% ethanol before it was placed on a substrate material (glass, PC, and PDMS). The ethanol was given five hours to evaporate and bond the two surfaces [183] after which, polyimide tape was applied to further secure the stencil to the substrate. This ethanol bonding technique ensured that the stencil mask and the substrate were bonded temporarily and minimized the "run off" between the stencil mask and the substrate. Vaporized chromium (300 Å at 1 Å s-1) and gold (3000 Å at 1 Å s-1) were deposited on the stencil and substrate using (Fig. A.1f) an electron-beam evaporator (a bench-top sputterer may be substituted). The polyimide tape and stencil were removed from the substrate to reveal patterned metal traces (Fig. A.1g).

The adhesion of the deposited metal to the substrates was assessed through a Scotch™ tape adhesion test. This test was performed by placing pressure-sensitive tape across the deposited metal/substrate and removing the tape by pulling it orthogonally to the substrate.

Patterning cell cultures: We designed and produced PDMS stencils for the patterning of cortical-cell cultures using our clamped and sprayed methods. These two stencil fabrication strategies require the least amount of equipment, and thus should be more useful to the bioengineering community that lacks microfabrication expertise. A

total of four types of 3D-printed templates were produced, as presented in Table A.I. Template i was printed with a matte finish and used with the sprayed process, while templates ii – iv were printed with a glossy finish and used with the clamped process. The column radii of 250 μm and 1000 μm, were selected to produce stencils that could confine cortical cell cultures to the field of view of two electrodes on a standard microelectrode array or to an entire microelectrode array, respectively. With such confined cell cultures, the activity of an entire culture could be measured during electrical stimulation or passive recording. The 10-mm long wall was designed to produce a channel within the stencil through which axons could grow and connect the two cortical cultures patterned at either end.

TABLE A.1
DIMENSIONS OF 3D-PRINTED TEMPLATES

Stencil	Column Radius	Column Height	Special Feature
*i**	250 μm	400 μm	
ii	250 μm	200 μm	inter-column spacing (500 – 4000 μm)
iii	1000 μm	400 μm	
iv	1000 μm	400 μm	10-mm long, 400-μm tall bridge

* design *i* was produced with a matte finish, while designs *ii – iv* were printed with a glossy finish

To pattern cell cultures, embryonic day 18 rat cortical neurons were enzymatically and mechanically dissociated [184]. Cortices were digested with papain for 30-60 minutes, strained (40 μm strainer) to remove clumps and centrifuged for 6 minutes to remove cellular debris. Neurons were resuspended in culture medium [185] and diluted to 2500 cells/μL. Before using the PDMS stencils to pattern cells, the stencils and petri-dishes were sterilized by soaking them in 70% ethanol for 15 minutes followed by an eight-hour UV exposure. Each stencil was then positioned atop a petri-dish using a drop of ethanol and allowed to dry. The petri-dishes and stencils were treated with 30 seconds of oxygen plasma and polyethylenimine (PEI) to hydrophilize their surfaces, followed by

three water washes and 30 minutes of drying. Laminin (0.02 mg/mL; Sigma-Aldrich L2020) was applied to the petri-dish for 20 minutes, after which the laminin was removed and ~30,000 neurons were plated atop the petri-dish (Fig. A.1f). Each stencil was lifted off after an hour (Fig. A.1g) to give the neurons time to adhere to the surface, and the petri-dishes were gently flooded with culture medium. Cultures were incubated at 35 °C in 5% carbon dioxide and 95% relative humidity. The culture medium was fully replaced on the first day in vitro (DIV) and then once every four DIV afterwards.

A.3 Results and Discussion

We evaluated the efficacy of our fabrication processes by characterizing the PDMS stencils and the designs they produced. We patterned metal traces/electrodes (Fig. A.2) to demonstrate that the microstencils could be used to fabricate devices with which to

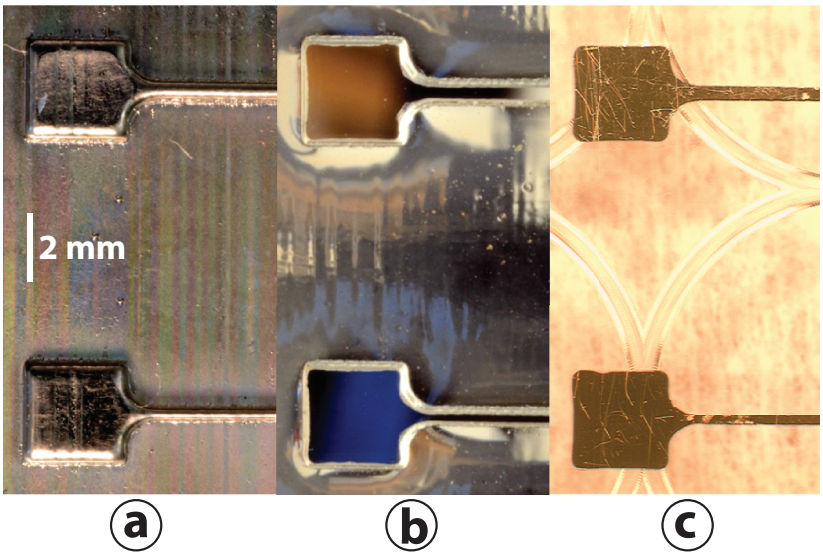

Figure A.2: Three stages of the process for patterning materials with stencils molded on 3D printed templates. (a) Metal coated 3D printed template, (b) PDMS micro-stencil molded from template, and (c) micro-stencil patterned metal traces.

measure bioelectric activity (e.g. microelectrode arrays). Conversely, we confined the plating of biological material, in this case cortical cell cultures, to show that the microstencils could also be used for tissue engineering, gene sequencing, and cell-cell interaction studies.

A.3.1 Patterning Vaporized Metal

The error in the aperture width accuracy of the PDMS stencils used to pattern metal traces, exhibited an observable dependence on the designed aperture widths (Fig. A.3). We observed that the widths of the microstencil apertures, designed to be 500 μm and 1000 μm, were on average narrower than intended, while the remainder of the designed apertures were on average wider than intended. We attribute this error to the resolution of the 3D printer. Although the 3D printer used in this study is described as possessing a resolution of 42 μm, 84 μm, and 16 μm for the x, y, and z axes, respectively, it did not print rectangular pillars of equal height, but rather rounded pillars that varied in height and curvature (Fig. A.4). If we assume that the etching process removes a uniform amount of PDMS from the top of the stencils, and that this produces 250-μm-wide apertures accurately, we would expect the same aforementioned trend in aperture width error.

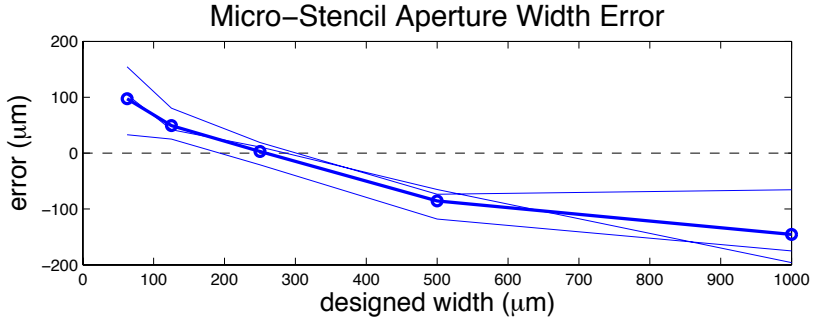

Figure A.3: The deviation of micro-stencil aperture widths from those designed, with the average of three micro-stencils in bold.

Although our stenciling method effectively patterned vaporized metal on glass, PC, and PDMS (Fig. A.5), we observed a dependence of the widths of the metal traces on the patterned substrate material (Fig. A.6). The widths of the stencil apertures were, at a

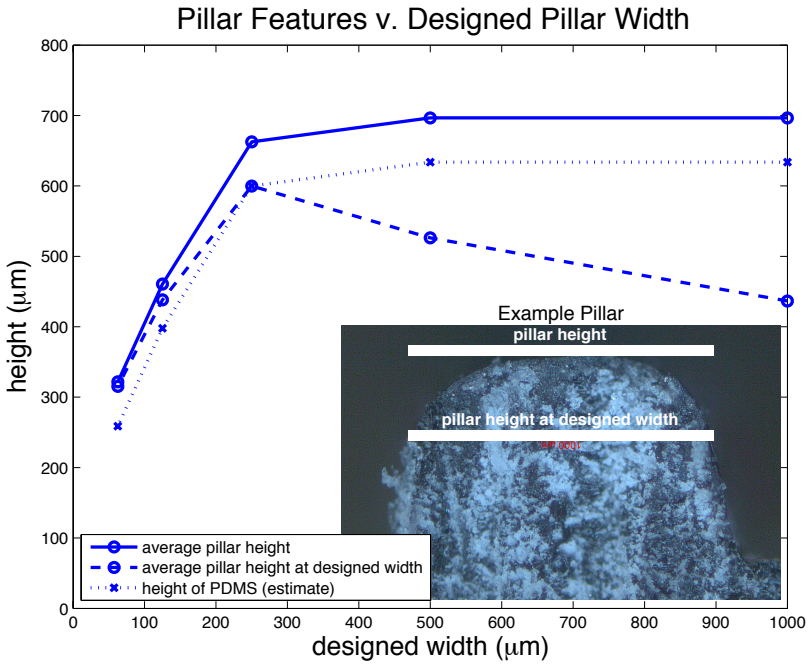

Figure A.4: The average pillar height across the designed pillar widths (n = 3 templates) and the average heights at which the pillar width equaled the designed width.

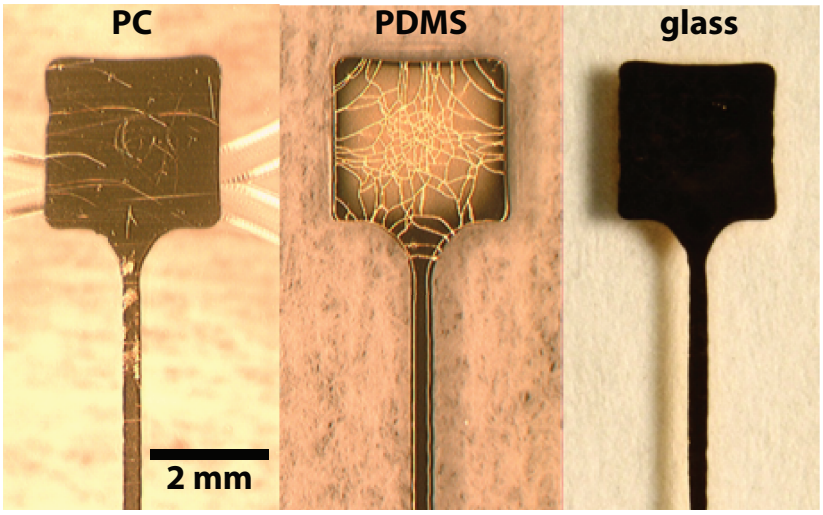

Figure A.5: Metal traces patterned on polycarbonate (PC), PDMS, and glass.

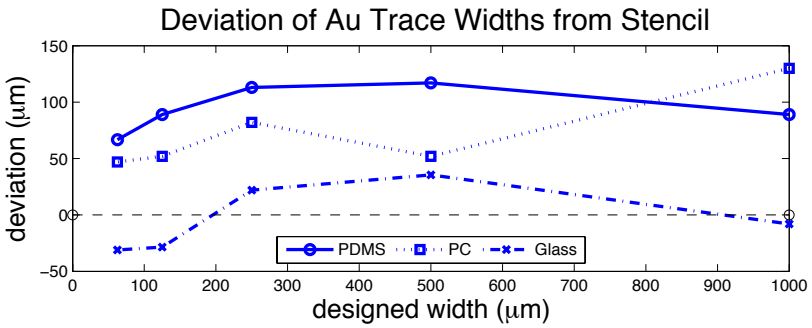

Figure A.6: The difference between the widths of the metal traces patterned on PC, PDMS, and glass, and the widths of their respective stencil apertures.

minimum, 47 μm and 66 μm narrower than the metal traces they patterned on PC and PDMS respectively, but the stencil apertures deviated at most by 36 μm from the metal traces patterned on glass. In theory, this trend should be reversed: The stencil apertures should most closely match the traces patterned on PDMS, and differ most greatly from those patterned on glass. This is because the CVC E-Beam Evaporator creates a high temperature environment (e.g. 150 °C) that should cause both the substrate and stencil to expand according to their coefficients of thermal expansion (αPDMS = 310 μm·m-1·K-1 [179], αglass = 9.2 μm·m-1·K-1 [186], αPC = 32.4 - 68.4 μm·m-1·K-1 [187]). We believe two factors contributed to this observed disparity. First, the PDMS substrate was cured on a glass slide, and this bond between the PDMS substrate and glass inhibited the lateral expansion of the PDMS substrate. Second, it was experimentally observed that ethanol evaporation bonding allows PDMS stencils to bond more securely to glass than to PDMS or PC. Thus, the PDMS stencil might form a larger air-gap with respect to the substrate on PDMS or PC than on glass, leading to "metal run-off" during deposition. Conversely, although there may have been differences in the bond strength between the PDMS stencils and the different substrate materials, the PDMS micro-stencils adhered securely to the substrates in all of the metallization trials – this was confirmed through

both optical and physical inspections. This strong bonding is largely attributed to the ethanol evaporation process. Thus, there is considerable doubt the e-beam evaporator affected the bond between the two materials. To pattern metal traces with widths closer to those intended, it should be possible to account for these aforementioned differences in the template design.

The Scotch™ tape test was performed ten times on the metal traces deposited on PC and glass, and no metal was observed to have been removed from these traces. However, when this test was performed on the metal traces deposited on PDMS, ~90% of the metal was removed during the first trial. We believe that PDMS performed poorly in this test because it has a low surface energy [175], resulting in poor adhesion of metal to PDMS.

We measured the resistance of the patterned metal traces (Fig. A.7) and observed the expected inverse relationship between their width and resistance. Traces patterned on

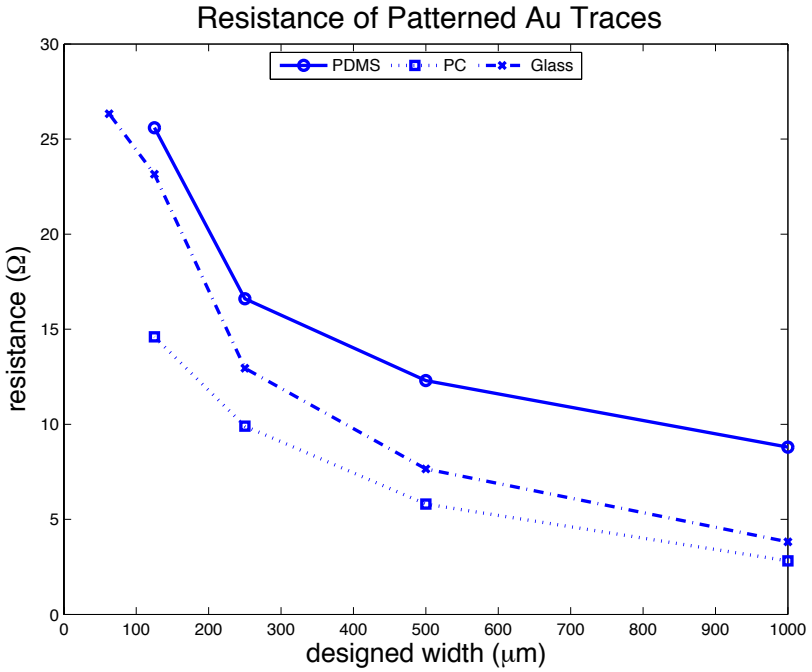

Figure A.7: The measured resistance across the 20-mm length of each of the patterned Au traces.

polycarbonate and glass had resistance ranges of 2.8 – 14.6 Ω and 3.8 – 26.3 Ω, respectively. Traces patterned on PDMS had the highest resistance with a range of 8.8 – 25.6 Ω, likely due to the low surface energy of the substrate material. Two traces, designed to be 62.5 µm wide, contained discontinuities, so we were unable to measure their resistance.

A.3.2 Patterning Cell Cultures

Both the sprayed and the clamped methods successfully produced PDMS stencils for patterning cell cultures (Figs. A.8 and A.9). Stencils of design i and ii, as described in

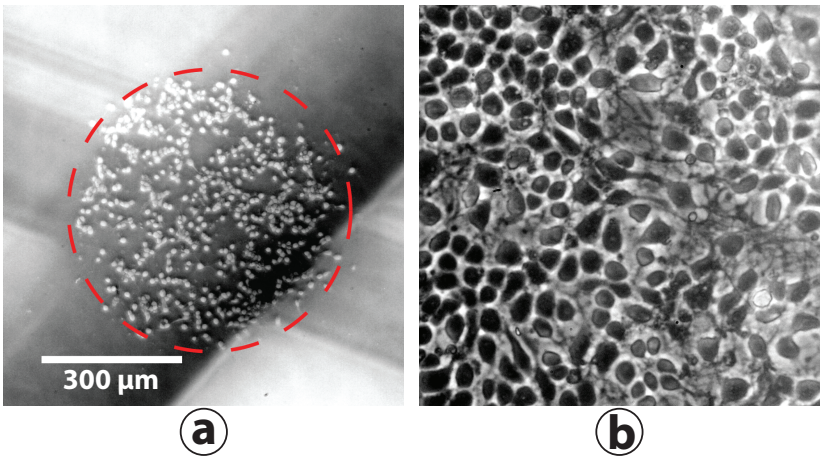

Figure A.8: Cortical neurons patterned using a sprayed stencil with an aperture radius of a ~300 um. (a) The cell culture, following stencil removal, on Day 0. After four days (b) extensive neurite growth was observed.

Section IIC, contained apertures, on average, 234-µm (n = 22 randomly sampled from 384 apertures) and 609-µm wide (n = 3), respectively, even though the templates for both methods were designed to have 500-µm-wide columns. This difference resulted from applying a glossy finish on the clamped template and a matte finish on the other. The glossy finish smoothed the surface and softened the edges of the template, thereby reducing the top surface area of the columns. In both methods, the size of the circular

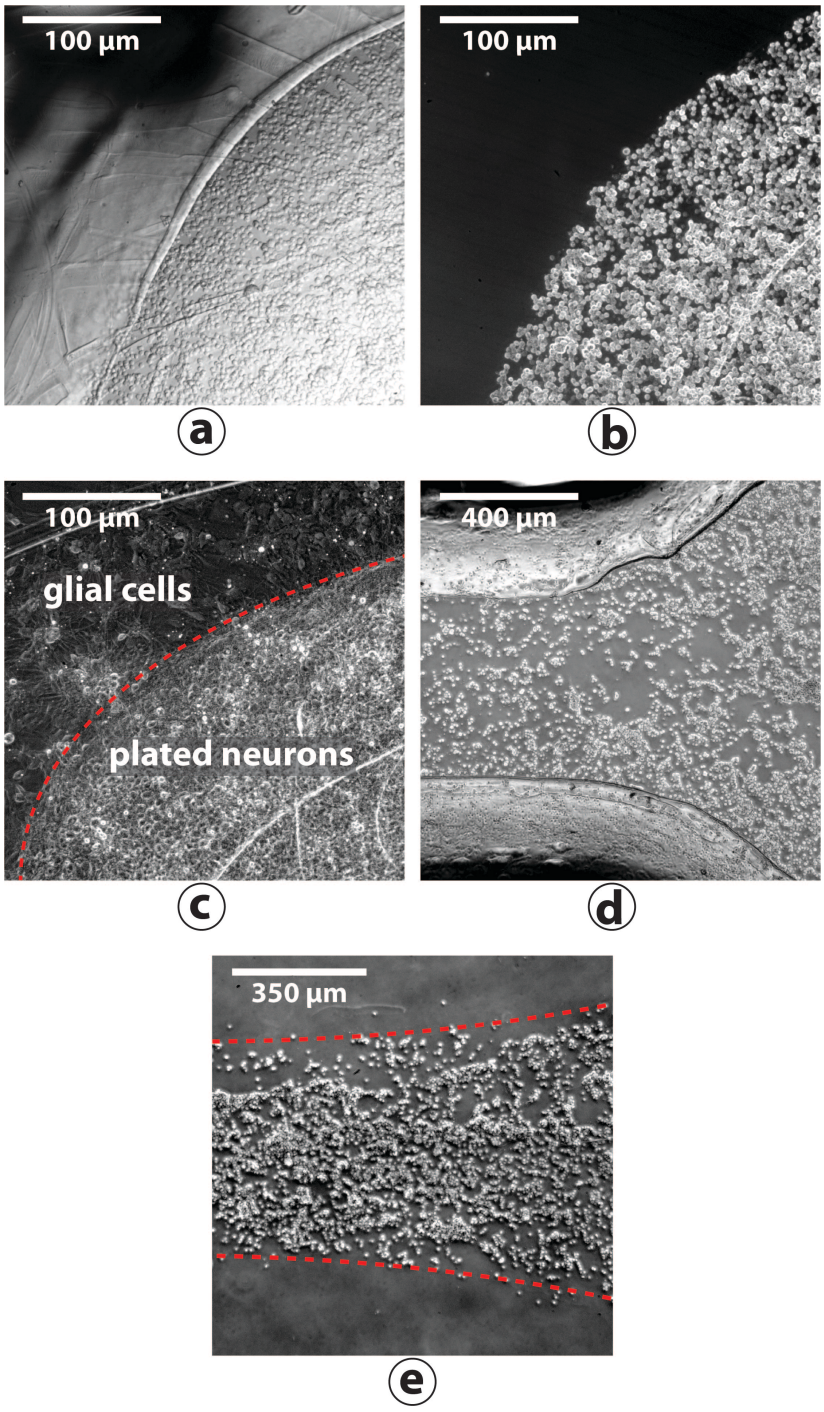

Figure A.9: Cortical neurons patterned using clamped stencils. A cell culture, patterned using a stencil with an aperture radius of ~1000 um, on Day 0 (a) with the stencil and (b) following stencil removal. By Day 7, (c) glial cells had greatly proliferated beyond the bounds of the plated neurons, however, the neurons themselves were observed to maintain their original position. Cortical cell cultures (d) before and (e) after stencil removal, patterned with a stencil of a more complex shape - a 10-mm long channel with circular apertures at either end.

apertures may be corrected by changing the widths of the template columns to compensate for process variabilities.

When using the sprayed and clamped stencils to plate cortical cell cultures, ~99% of the cells and the biomolecular coatings were localized and evenly distributed within the circular aperture areas. Stencils formed via the clamped process possessed flat bottoms formed by the polyacetate sheets, which enabled the stencils to form tight seals with the surface to be patterned and cultures with especially clear boundaries (Figs. A.9a, A.9b, A.9d, and A.9e). All of the stencils proved cytocompatible and after four days, extensive neurite outgrowth was observed throughout the cultures (Figs. A.8b). After seven days, glial cells had greatly proliferated beyond the bounds of the cell cultures (Fig. A.9c), however, the neurons largely maintained their original placement. In all trials, cell viability was equivalently high compared to control cultures and we observed little cell migration. These findings were determined via optical microscopy and highlight the effectiveness of our stencil method for plating and growing spatially confined neuronal cultures. These results demonstrate that the stencil fabrication processes described herein provide an easy and effective means by which to pattern organic materials with features of a wide size range (e.g. 500 μm – 2000 μm).

A.3.3 The Utility of Multiple Microstencil Fabrication Strategies

The approach for producing microstencils, presented herein, provides an alternative to the more traditional methods of laser cutting, inductively-coupled plasma (ICP) reactive-ion etching, and photoresist (e.g. SU-8) molding. Table II presents the required resources and the capabilities of these traditional methods. Our 3D template molding process can be completed at half of the cost of laser etching PDMS or one sixth

of the cost of molding PDMS with photoresist. Thus, 3D-template-molded stencils are ideal for prototyping and low budget applications. Template-molded stencils are also very suitable for controlling the spread of cell cultures because of their ability to adhere to glass surfaces, unlike silicon-wafer ICP-etched stencils, which are more useful for patterning vaporized metal. Although laser-etched-PDMS stencils can be produced with features as small as 8.4 μm, for many BioMEMS applications this resolution is unnecessary. Additionally, the etching process damages PDMS, reducing the reusability of the stencils.

Of the three strategies for fabricating microstencils presented, the etched method produces stencils that (1) most closely resemble their intended design, (2) possess the smoothest edges, and (3) can be produced to contain both large and small apertures. These three properties of etched stencils make them particularly suitable for patterning vaporized metal because they can produce features across the greatest range of resolution with the least variability. The etched method, however, relies on cleanroom equipment more than the other two techniques, thus if simple patterns need to be stenciled (e.g. circles of 300 μm in radius, or rectangles and pyramids similar in size) it may be best to use the clamped method because it is the most cost effective and simplest to implement. However, the apertures produced through the clamped process, have the greatest variance from the intended design. Thus, if a spin coater is available, it may be preferable to utilize the sprayed method when producing microstencils of small apertures or for the patterning of cell cultures. Table II compares the complexity, resolution, cost, and time required to produce a stencil through the etched, sprayed, and clamped strategies. It additionally compares these strategies to more traditional stencil microfabrication methods.

The etched process was observed to cause a slight deformation in one of the eight 3D templates used in the etching process. This occurred when PDMS residue was removed from the top of the 3D-template's features with a reactive-ion etcher. This slight deformation, however, was confined to a small region of the template's edge and thus did not affect the features of the template nor the apertures of the molded PDMS stencils (Fig. A.10).

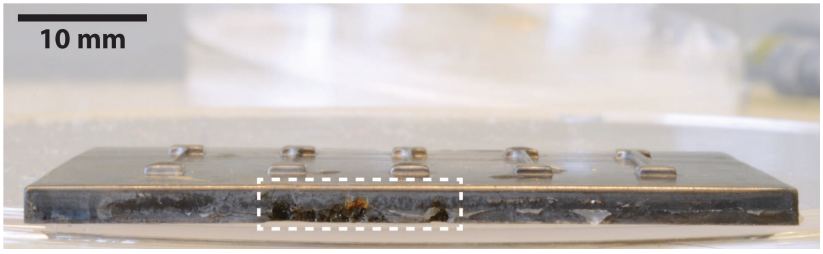

Figure A.10: Side view of the only 3D-printed template that was moderately ablated by the PDMS etching process. The area encapsulated by the white dotted line shows the full extent of the template's deformation, which did not affect the template's features nor the molded stencil. The light material partially attached to the template is cured PDMS.

Molding PDMS stencils on 3D-printed templates is considerably less expensive than producing stencils through more traditional methodologies. Although template molded stencils are limited in their spatial resolution, both their precision and affordability should improve with the advancement of 3D printer technologies. A 3D direct laser writer has already been developed that is capable of 100-nm resolution [188]. Such a 3D printer could enable this technology to produce nanometer-scale stencils.

A.4 Conclusions

We have described three processes to produce PDMS microstencils rapidly and cost-effectively with minimal usage of cleanroom-based tools. We have also demonstrated their application for patterning metal traces on multiple biocompatible substrates (e.g. PDMS, PC, and glass) as well as for patterning cell cultures and other

organic materials (e.g. PEI and laminin). These processes provide four main advantages over existing methodologies: (i) they facilitate the design and fabrication of microstencils rapidly, providing a quick turnaround for design changes; (ii) they are cost-effective; (iii) they minimize cleanroom processing; and (iv) they provide microstencils compatible with biologically-friendly materials. Thus, our processes are ideal for patterning projects that require rapid design revisions or BioMEMS applications such as tissue engineering, cell/protein patterning, electrode array patterning, and lab-on-a-chip devices. Future extensions of this work will include patterning other features, such as insulation and bimolecular coatings, on other substrates such as hydrogels, polymers, and collagen.

REFERENCES

[1] R. Wang, Z. Wei, W. Wang, and Z. Li, "Flexible microneedle electrode array based-on parylene substrate," in *16th International Conference on Miniaturized Systems for Chemistry and Life Sciences*, Okinawa, Japan, 2012, pp. 1249–1251.

[2] L. Guo, G. S. Guvanasen, X. Liu, C. Tuthill, T. R. Nichols, and S. P. DeWeerth, "A PDMS-Based Integrated Stretchable Microelectrode Array (isMEA) for Neural and Muscular Surface Interfacing," *IEEE Trans. Biomed. Circuits Syst.*, vol. 7, no. 1, pp. 1–10, Feb. 2013.

[3] B. G. Lapatki, J. P. van Dijk, I. E. Jonas, M. J. Zwarts, and D. F. Stegeman, "A thin, flexible multielectrode grid for high-density surface EMG," *J. Appl. Physiol.*, vol. 96, no. 1, pp. 327–336, Jan. 2004.

[4] Z. Lertmanorat, F. W. Montague, and D. M. Durand, "A Flat Interface Nerve Electrode With Integrated Multiplexer," *IEEE Trans. Neural Syst. Rehabil. Eng. Publ. IEEE Eng. Med. Biol. Soc.*, vol. 17, no. 2, pp. 176–182, Apr. 2009.

[5] V. S. Polikov, P. A. Tresco, and W. M. Reichert, "Response of brain tissue to chronically implanted neural electrodes," *J. Neurosci. Methods*, vol. 148, no. 1, pp. 1–18, Oct. 2005.

[6] A. W. English, D. I. Carrasco, and C. G. Widmer, "Torques Produced by Different Compartments of the Rabbit Masseter Muscle," *J. Appl. Biomech.*, vol. 15, no. 4, pp. 348 – 360, 1999.

[7] D. I. Carrasco, J. Lawrence 3rd, and A. W. English, "Neuromuscular compartments of cat lateral gastrocnemius produce different torques about the ankle joint," *Motor Control*, vol. 3, no. 4, pp. 436–446, Oct. 1999.

[8] A. Holtermann, K. Roeleveld, P. J. Mork, C. Grönlund, J. S. Karlsson, L. L. Andersen, H. B. Olsen, M. K. Zebis, G. Sjøgaard, and K. Søgaard, "Selective activation of neuromuscular compartments within the human trapezius muscle," *J. Electromyogr. Kinesiol.*, vol. 19, no. 5, pp. 896–902, Oct. 2009.

[9] A. W. English, S. L. Wolf, and R. L. Segal, "Compartmentalization of muscles and their motor nuclei: the partitioning hypothesis," *Phys. Ther.*, vol. 73, no. 12, pp. 857–867, Dec. 1993.

[10] A. W. English, “An electromyographic analysis of compartments in cat lateral gastrocnemius muscle during unrestrained locomotion,” *J. Neurophysiol.*, vol. 52, no. 1, pp. 114–125, Jul. 1984.

[11] J. A. Hoffer, N. Sugano, G. E. Loeb, W. B. Marks, M. J. O’Donovan, and C. A. Pratt, “Cat hindlimb motoneurons during locomotion. II. Normal activity patterns,” *J. Neurophysiol.*, vol. 57, no. 2, pp. 530–553, Feb. 1987.

[12] D. A. Hong, D. M. Corcos, and G. L. Gottlieb, “Task dependent patterns of muscle activation at the shoulder and elbow for unconstrained arm movements,” *J. Neurophysiol.*, vol. 71, no. 3, pp. 1261–1265, Mar. 1994.

[13] K. Watanabe, M. Kouzaki, and T. Moritani, “Task-dependent spatial distribution of neural activation pattern in human rectus femoris muscle,” *J. Electromyogr. Kinesiol. Off. J. Int. Soc. Electrophysiol. Kinesiol.*, vol. 22, no. 2, pp. 251–258, Apr. 2012.

[14] C. A. Buneo, J. F. Soechting, and M. Flanders, “Postural Dependence of Muscle Actions: Implications for Neural Control,” *J. Neurosci.*, vol. 17, no. 6, pp. 2128–2142, Mar. 1997.

[15] U. Herrmann and M. Flanders, “Directional tuning of single motor units,” *J. Neurosci. Off. J. Soc. Neurosci.*, vol. 18, no. 20, pp. 8402–8416, Oct. 1998.

[16] E. Henneman, G. Somjen, and D. O. Carpenter, “Functional Significance of Cell Size in Spinal Motoneurons,” *J. Neurophysiol.*, vol. 28, no. 3, pp. 560–580, May 1965.

[17] W. Letbetter, “Influence of Intramuscular Nerve Branching on Motor Unit Organization in Medial Gastrocnemius Muscle,” *Anat. Rec.*, vol. 178, no. 2, pp. 402–402, 1974.

[18] A. W. English and W. D. Letbetter, “A histochemical analysis of identified compartments of cat lateral gastrocnemius muscle,” *Anat. Rec.*, vol. 204, no. 2, pp. 123–130, Oct. 1982.

[19] J. B. Wickham and J. M. M. Brown, “Muscles within muscles: the neuromotor control of intra-muscular segments,” *Eur. J. Appl. Physiol.*, vol. 78, no. 3, pp. 219–225, Jul. 1998.

[20] “CDC - NIOSH Publications and Products - Selected Topics in Surface Electromyography for Use in the Occupational Setting: Expert Perspective (91-100).” [Online]. Available: http://www.cdc.gov/niosh/docs/91-100/. [Accessed: 09-Feb-2014].

[21] S. Andreassen and L. Arendt-Nielsen, “Muscle fibre conduction velocity in motor units of the human anterior tibial muscle: a new size principle parameter.,” *J. Physiol.*, vol. 391, pp. 561–571, Oct. 1987.

[22] C. H. Hakansson, “Conduction Velocity and Amplitude of the Action Potential as Related to Circumference in the Isolated Fibre of Frog Muscle,” *Acta Physiol. Scand.*, vol. 37, no. 1, pp. 14–34, 1956.

[23] W. F. Brown, C. F. Bolton, and M. J. Aminoff, *Neuromuscular function and disease: basic, clinical, and electrodiagnostic aspects*, vol. 1. Saunders, 2002.

[24] J. T. Mortimer, “Motor Prostheses,” in *Comprehensive Physiology*, R. Terjung, Ed. Hoboken, NJ, USA: John Wiley & Sons, Inc., 1981.

[25] M. Knaflitz, R. Merletti, and C. J. D. Luca, “Inference of motor unit recruitment order in voluntary and electrically elicited contractions,” *J. Appl. Physiol.*, vol. 68, no. 4, pp. 1657–1667, Apr. 1990.

[26] D. R. McNeal, “Analysis of a Model for Excitation of Myelinated Nerve,” *IEEE Trans. Biomed. Eng.*, vol. BME-23, no. 4, pp. 329–337, 1976.

[27] W. T. Liberson, H. J. Holmquest, D. Scot, and M. Dow, “Functional electrotherapy: stimulation of the peroneal nerve synchronized with the swing phase of the gait of hemiplegic patients,” *Arch. Phys. Med. Rehabil.*, vol. 42, pp. 101–105, Feb. 1961.

[28] K. L. Kilgore, H. A. Hoyen, A. M. Bryden, R. L. Hart, M. W. Keith, and P. H. Peckham, “An implanted upper-extremity neuroprosthesis using myoelectric control,” *J. Hand Surg.*, vol. 33, no. 4, pp. 539–550, Apr. 2008.

[29] A. E. Schultz and T. A. Kuiken, “Neural Interfaces for Control of Upper Limb Prostheses: The State of the Art and Future Possibilities,” *PM&R*, vol. 3, no. 1, pp. 55–67, Jan. 2011.

[30] P. Zhou, M. Lowery, J. A Dewald, and T. Kuiken, "Towards Improved Myoelectric Prosthesis Control: High Density Surface EMG Recording After Targeted Muscle Reinnervation," *Conf. Proc. Annu. Int. Conf. IEEE Eng. Med. Biol. Soc. IEEE Eng. Med. Biol. Soc. Conf.*, vol. 4, pp. 4064–4067, 2005.

[31] P. H. Peckham and J. S. Knutson, "Functional electrical stimulation for neuromuscular applications," *Annu. Rev. Biomed. Eng.*, vol. 7, pp. 327–360, 2005.

[32] D. C. Rodger, A. J. Fong, W. Li, H. Ameri, A. K. Ahuja, C. Gutierrez, I. Lavrov, H. Zhong, P. R. Menon, E. Meng, J. W. Burdick, R. R. Roy, V. R. Edgerton, J. D. Weiland, M. S. Humayun, and Y.-C. Tai, "Flexible parylene-based multielectrode array technology for high-density neural stimulation and recording," *Sens. Actuators B Chem.*, vol. 132, no. 2, pp. 449–460, Jun. 2008.

[33] S.-H. Cho, H. M. Lu, L. Cauller, M. I. Romero-Ortega, J.-B. Lee, and G. A. Hughes, "Biocompatible SU-8-Based Microprobes for Recording Neural Spike Signals From Regenerated Peripheral Nerve Fibers," *IEEE Sens. J.*, vol. 8, no. 11, pp. 1830–1836, Nov. 2008.

[34] N. A. Kotov, J. O. Winter, I. P. Clements, E. Jan, B. P. Timko, S. Campidelli, S. Pathak, A. Mazzatenta, C. M. Lieber, M. Prato, R. V. Bellamkonda, G. A. Silva, N. W. S. Kam, F. Patolsky, and L. Ballerini, "Nanomaterials for Neural Interfaces," *Adv. Mater.*, vol. 21, no. 40, pp. 3970–4004, Jul. 2009.

[35] M. C. Bélanger and Y. Marois, "Hemocompatibility, biocompatibility, inflammatory and in vivo studies of primary reference materials low-density polyethylene and polydimethylsiloxane: a review," *J. Biomed. Mater. Res.*, vol. 58, no. 5, pp. 467–477, 2001.

[36] Q. Bai and K. D. Wise, "Single-unit neural recording with active microelectrode arrays," *IEEE Trans. Biomed. Eng.*, vol. 48, no. 8, pp. 911–920, Aug. 2001.

[37] L. Guo and S. P. DeWeerth, "An Effective Lift-Off Method for Patterning High-Density Gold Interconnects on an Elastomeric Substrate," *Small*, vol. 6, no. 24, pp. 2847–2852, Dec. 2010.

[38] R. J. Gregor, D. W. Smith, and B. I. Prilutsky, "Mechanics of slope walking in the cat: quantification of muscle load, length change, and ankle extensor EMG patterns," *J. Neurophysiol.*, vol. 95, no. 3, pp. 1397–1409, Mar. 2006.

[39] G. E. Goslow, R. M. Reinking, and D. G. Stuart, “The cat step cycle: hind limb joint angles and muscle lengths during unrestrained locomotion,” *J. Morphol.*, vol. 141, no. 1, pp. 1–41, Sep. 1973.

[40] A. Larmagnac, P. Musienko, J. Vörös, and G. Courtine, “Skin-Like PDMS-Based Multi-electrode Array for Epidural Electrical Stimulation to Promote Locomotion in Paralyzed Rats,” in *5th European Conference of the International Federation for Medical and Biological Engineering*, Á. Jobbágy, Ed. Springer Berlin Heidelberg, 2012, pp. 1180–1181.

[41] J. Vörös, G. Courtine, A. Larmagnac, and P. Musienko, “PDMS-based stretchable multi-electrode and chemotrode array for epidural and subdural neuronal recording, electrical stimulation and drug delivery,” WO2011157714 A1, 22-Dec-2011.

[42] S. Bentin, T. Allison, A. Puce, E. Perez, and G. McCarthy, “Electrophysiological Studies of Face Perception in Humans,” *J. Cogn. Neurosci.*, vol. 8, no. 6, pp. 551–565, Nov. 1996.

[43] A. d’ Avella, P. Saltiel, and E. Bizzi, “Combinations of muscle synergies in the construction of a natural motor behavior,” *Nat. Neurosci.*, vol. 6, no. 3, pp. 300–308, Mar. 2003.

[44] J. M. DeSantana, D. M. Walsh, C. Vance, B. A. Rakel, and K. A. Sluka, “Effectiveness of Transcutaneous Electrical Nerve Stimulation for Treatment of Hyperalgesia and Pain,” *Curr. Rheumatol. Rep.*, vol. 10, no. 6, pp. 492–499, Dec. 2008.

[45] M. Brunner, M. Olschewski, A. Geibel, C. Bode, and M. Zehender, “Long-term survival after pacemaker implantation,” *Eur. Heart J.*, vol. 25, no. 1, pp. 88–95, Jan. 2004.

[46] P. Limousin, P. Krack, P. Pollak, A. Benazzouz, C. Ardouin, D. Hoffmann, and A.-L. Benabid, “Electrical Stimulation of the Subthalamic Nucleus in Advanced Parkinson’s Disease,” *N. Engl. J. Med.*, vol. 339, no. 16, pp. 1105–1111, Oct. 1998.

[47] A. Bohdjalian, B. Ludvik, B. Guerci, L. Bresler, E. Renard, D. Nocca, E. Karnieli, A. Assalia, R. Prager, and G. Prager, “Improvement in glycemic control by gastric electrical stimulation (TANTALUS) in overweight subjects with type 2 diabetes,” *Surg. Endosc.*, vol. 23, no. 9, pp. 1955–1960, Sep. 2009.

[48] R. Fisher, V. Salanova, T. Witt, R. Worth, T. Henry, R. Gross, K. Oommen, I. Osorio, J. Nazzaro, D. Labar, M. Kaplitt, M. Sperling, E. Sandok, J. Neal, A. Handforth, J. Stern, A. DeSalles, S. Chung, A. Shetter, D. Bergen, R. Bakay, J. Henderson, J. French, G. Baltuch, W. Rosenfeld, A. Youkilis, W. Marks, P. Garcia, N. Barbaro, N. Fountain, C. Bazil, R. Goodman, G. McKhann, K. Babu Krishnamurthy, S. Papavassiliou, C. Epstein, J. Pollard, L. Tonder, J. Grebin, R. Coffey, N. Graves, and the SANTE Study Group, "Electrical stimulation of the anterior nucleus of thalamus for treatment of refractory epilepsy," *Epilepsia*, vol. 51, no. 5, pp. 899–908, May 2010.

[49] H. S. Mayberg, A. M. Lozano, V. Voon, H. E. McNeely, D. Seminowicz, C. Hamani, J. M. Schwalb, and S. H. Kennedy, "Deep Brain Stimulation for Treatment-Resistant Depression," *Neuron*, vol. 45, no. 5, pp. 651–660, Mar. 2005.

[50] N. J. Rijkhoff, H. Wijkstra, P. E. Van Kerrebroeck, and F. M. Debruyne, "Urinary bladder control by electrical stimulation: Review of electrical stimulation techniques in spinal cord injury," *Neurourol. Urodyn.*, vol. 16, no. 1, pp. 39–53, Jan. 1997.

[51] G. Rau and C. Disselhorst-Klug, "Principles of high-spatial-resolution surface EMG (HSR-EMG): single motor unit detection and application in the diagnosis of neuromuscular disorders," *J. Electromyogr. Kinesiol.*, vol. 7, no. 4, pp. 233–239, Dec. 1997.

[52] J. Perry, C. S. Easterday, and D. J. Antonelli, "Surface versus intramuscular electrodes for electromyography of superficial and deep muscles," *Phys. Ther.*, vol. 61, no. 1, pp. 7–15, Jan. 1981.

[53] C. J. De Luca and R. Merletti, "Surface myoelectric signal cross-talk among muscles of the leg," *Electroencephalogr. Clin. Neurophysiol.*, vol. 69, no. 6, pp. 568–575, Jun. 1988.

[54] K. S. Türker and T. S. Miles, "Cross-talk from other muscles can contaminate EMG signals in reflex studies of the human leg," *Neurosci. Lett.*, vol. 111, no. 1–2, pp. 164–9, Mar. 1990.

[55] R. Merletti and D. Farina, "Analysis of intramuscular electromyogram signals," *Philos. Trans. R. Soc. Lond. Math. Phys. Eng. Sci.*, vol. 367, no. 1887, pp. 357–368, Jan. 2009.

[56] W. J. Kraemer and K. Häkkinen, *Handbook of Sports Medicine and Science, Strength Training for Sport*. Hoboken, NJ: John Wiley & Sons, 2008.

[57] R. Greger and U. Windhorst, *Comprehensive Human Physiology: From Cellular Mechanisms to Integration*. Berlin, Germany: Springer Science & Business Media, 2013.

[58] K. W. Meacham, R. J. Giuly, L. Guo, S. Hochman, and S. P. DeWeerth, "A lithographically-patterned, elastic multi-electrode array for surface stimulation of the spinal cord," *Biomed. Microdevices*, vol. 10, no. 2, pp. 259–269, Oct. 2007.

[59] I. R. Minev, P. Musienko, A. Hirsch, Q. Barraud, N. Wenger, E. M. Moraud, J. Gandar, M. Capogrosso, T. Milekovic, L. Asboth, R. F. Torres, N. Vachicouras, Q. Liu, N. Pavlova, S. Duis, A. Larmagnac, J. Vörös, S. Micera, Z. Suo, G. Courtine, and S. P. Lacour, "Biomaterials. Electronic dura mater for long-term multimodal neural interfaces," *Science*, vol. 347, no. 6218, pp. 159–163, Jan. 2015.

[60] Y. Xia and G. M. Whitesides, "Soft Lithography," *Angew. Chem. Int. Ed.*, vol. 37, no. 5, pp. 550–575, Mar. 1998.

[61] M. Maghribi, J. Hamilton, D. Polla, K. Rose, T. Wilson, and P. Krulevitch, "Stretchable micro-electrode array [for retinal prosthesis]," in *Microtechnologies in Medicine amp; Biology 2nd Annual International IEEE-EMB Special Topic Conference on*, Madison, WI, 2002, pp. 80–83.

[62] C. Tsay, S. P. Lacour, S. Wagner, and B. Morrison, "Architecture, Fabrication, and Properties of Stretchable Micro-Electrode Arrays," in *IEEE Sensors 2005*, Irvine, CA, 2005, pp. 1169–1172.

[63] P. Wei, R. Taylor, Z. Ding, C. Chung, O. J. Abilez, G. Higgs, B. L. Pruitt, and B. Ziaie, "Stretchable microelectrode array using room-temperature liquid alloy interconnects," *J. Micromechanics Microengineering*, vol. 21, no. 5, p. 054015, May 2011.

[64] M. D. Dickey, R. C. Chiechi, R. J. Larsen, E. A. Weiss, D. A. Weitz, and G. M. Whitesides, "Eutectic Gallium-Indium (EGaIn): A Liquid Metal Alloy for the Formation of Stable Structures in Microchannels at Room Temperature," *Adv. Funct. Mater.*, vol. 18, no. 7, pp. 1097–1104, 2008.

[65] J. C. Agar, K. J. Lin, R. Zhang, J. Durden, K.-S. Moon, and C. P. Wong, "Novel PDMS(silicone)-in-PDMS(silicone): Low cost flexible electronics without metallization," in *Electronic Components and Technology Conference (ECTC), 2010 Proceedings 60th*, Las Vegas, NV, 2010, pp. 1226–1230.

[66] M. B. I. Raez, M. S. Hussain, and F. Mohd-Yasin, “Techniques of EMG signal analysis: detection, processing, classification and applications,” *Biol. Proced. Online*, vol. 8, pp. 11–35, Mar. 2006.

[67] S. P. Crouch, R. Kozlowski, K. J. Slater, and J. Fletcher, “The use of ATP bioluminescence as a measure of cell proliferation and cytotoxicity,” *J. Immunol. Methods*, vol. 160, no. 1, pp. 81–88, Mar. 1993.

[68] N. Mokarram, A. Merchant, V. Mukhatyar, G. Patel, and R. V. Bellamkonda, “Effect of modulating macrophage phenotype on peripheral nerve repair,” *Biomaterials*, vol. 33, no. 34, pp. 8793–8801, Dec. 2012.

[69] M. D. Abramoff, P. J. Magalhães, and S. J. Ram, “Image processing with ImageJ,” *Biophotonics Int.*, vol. 11, no. 7, pp. 36–42, 2004.

[70] S. Mense, “The pathogenesis of muscle pain,” *Curr. Pain Headache Rep.*, vol. 7, no. 6, pp. 419–425, Nov. 2003.

[71] I. Loell and I. E. Lundberg, “Can muscle regeneration fail in chronic inflammation: a weakness in inflammatory myopathies?,” *J. Intern. Med.*, vol. 269, no. 3, pp. 243–257, Mar. 2011.

[72] D. Miklavčič, N. Pavšelj, and F. X. Hart, “Electric Properties of Tissues,” in *Wiley Encyclopedia of Biomedical Engineering*, John Wiley & Sons, Inc., 2006.

[73] T. A. Butterfield, T. M. Best, and M. A. Merrick, “The Dual Roles of Neutrophils and Macrophages in Inflammation: A Critical Balance Between Tissue Damage and Repair,” *J. Athl. Train.*, vol. 41, no. 4, pp. 457–465, 2006.

[74] M. Massani, T. Stecca, L. Fabris, E. Caratozzolo, C. Ruffolo, A. Furlanetto, S. Morton, M. Cadamuro, M. Strazzabosco, and N. Bassi, “Isolation and characterization of biliary epithelial and stromal cells from resected human cholangiocarcinoma: a novel in vitro model to study tumor-stroma interactions,” *Oncol. Rep.*, vol. 30, no. 3, pp. 1143–1148, Sep. 2013.

[75] T. J. Koh, “Question Regarding Presence of Macrophages in Muscle,” 02-Sep-2015.

[76] J. McGeachie, E. Smith, P. Roberts, and M. Grounds, “Reaction of skeletal muscle to small implants of titanium or stainless steel: a quantitative histological and autoradiographic study,” *Biomaterials*, vol. 13, no. 8, pp. 562–568, 1992.

[77] R. R. Richardson, J. A. Miller, and W. M. Reichert, “Polyimides as biomaterials: preliminary biocompatibility testing,” *Biomaterials*, vol. 14, no. 8, pp. 627–635, Jul. 1993.

[78] J.-M. Seo, S. J. Kim, H. Chung, E. T. Kim, H. G. Yu, and Y. S. Yu, “Biocompatibility of polyimide microelectrode array for retinal stimulation,” *Mater. Sci. Eng. C*, vol. 24, no. 1–2, pp. 185–189, Jan. 2004.

[79] P. J. Rousche, D. S. Pellinen, J. Pivin, D.P., J. C. Williams, R. J. Vetter, and D. R. kirke, “Flexible polyimide-based intracortical electrode arrays with bioactive capability,” *IEEE Trans. Biomed. Eng.*, vol. 48, no. 3, pp. 361–371, Mar. 2001.

[80] D. A. X. Nayagam, R. A. Williams, J. Chen, K. A. Magee, J. Irwin, J. Tan, P. Innis, R. T. Leung, S. Finch, C. E. Williams, G. M. Clark, and G. G. Wallace, “Biocompatibility of Immobilized Aligned Carbon Nanotubes,” *Small*, vol. 7, no. 8, pp. 1035–1042, Apr. 2011.

[81] S. Rajaraman, S.-O. Choi, R. H. Shafer, J. D. Ross, J. Vukasinovic, Y. Choi, S. P. DeWeerth, A. Glezer, and M. G. Allen, “Microfabrication technologies for a coupled three-dimensional microelectrode, microfluidic array,” *J. Micromechanics Microengineering*, vol. 17, no. 1, p. 163, Jan. 2007.

[82] S. A. Desai, J. D. Rolston, L. Guo, and S. M. Potter, “Improving Impedance of Implantable Microwire Multi-Electrode Arrays by Ultrasonic Electroplating of Durable Platinum Black,” *Front. Neuroengineering*, vol. 3, May 2010.

[83] N. Miura and Y. Shinohara, “Cytotoxic effect and apoptosis induction by silver nanoparticles in HeLa cells,” *Biochem. Biophys. Res. Commun.*, vol. 390, no. 3, pp. 733–737, Dec. 2009.

[84] T. C. Merkel, V. I. Bondar, K. Nagai, B. D. Freeman, and I. Pinnau, “Gas sorption, diffusion, and permeation in poly(dimethylsiloxane),” *J. Polym. Sci. Part B Polym. Phys.*, vol. 38, no. 3, pp. 415–434, Feb. 2000.

[85] C. Heintz, G. Riepe, L. Birken, E. Kaiser, N. Chakfé, M. Morlock, G. Delling, and H. Imig, "Corroded Nitinol Wires in Explanted Aortic Endografts: An Important Mechanism of Failure?," *J. Endovasc. Ther.*, vol. 8, no. 3, pp. 248–253, Jun. 2001.

[86] D. Roller and W. R. Scott, "Detecting and Measuring Corrosion: Using Electrical Resistance Techniques," *Anti-Corros. Methods Mater.*, vol. 8, no. 3, pp. 71–76, Mar. 1961.

[87] Hsu, J.-M., "Characterization of parylene-C film as an encapsulation material for neural interface devices," in *4M 2007, Third International Conference on Multi-Material Micro Manufacture*, 2007, p. 4.

[88] A. B. Oskouyi, U. Sundararaj, and P. Mertiny, "Tunneling Conductivity and Piezoresistivity of Composites Containing Randomly Dispersed Conductive Nano-Platelets," *Materials*, vol. 7, no. 4, pp. 2501–2521, Mar. 2014.

[89] S. M. Clarke, F. Elias, and E. M. Terentjev, "Ageing of natural rubber under stress," *Eur. Phys. J. E*, vol. 2, no. 4, pp. 335–341, Aug. 2000.

[90] S. Wang, P. Wang, and T. Ding, "Resistive viscoelasticity of silicone rubber/carbon black composite," *Polym. Compos.*, vol. 32, no. 1, pp. 29–35, Jan. 2011.

[91] C.-X. Liu and J.-W. Choi, "Analyzing resistance response of embedded PDMS and carbon nanotubes composite under tensile strain," *Microelectron. Eng.*, vol. 117, pp. 1–7, Apr. 2014.

[92] F. Xu and Y. Zhu, "Highly Conductive and Stretchable Silver Nanowire Conductors," *Adv. Mater.*, vol. 24, no. 37, pp. 5117–5122, Sep. 2012.

[93] Y. Zhu and F. Xu, "Buckling of Aligned Carbon Nanotubes as Stretchable Conductors: A New Manufacturing Strategy," *Adv. Mater.*, vol. 24, no. 8, pp. 1073–1077, Feb. 2012.

[94] T. M. Kesar, R. Perumal, A. Jancosko, D. S. Reisman, K. S. Rudolph, J. S. Higginson, and S. A. Binder-Macleod, "Novel Patterns of Functional Electrical Stimulation Have an Immediate Effect on Dorsiflexor Muscle Function During Gait for People Poststroke," *Phys. Ther.*, vol. 90, no. 1, pp. 55–66, Jan. 2010.

[95] S. Bodine-Fowler, A. Garfinkel, R. R. Roy, and V. R. Edgerton, "Spatial distribution of muscle fibers within the territory of a motor unit," *Muscle Nerve*, vol. 13, no. 12, pp. 1133–1145, Dec. 1990.

[96] R. Parasuraman and M. Rizzo, *Neuroergonomics: The Brain at Work*. Oxford University Press, 2006.

[97] B. M. Doucet, A. Lam, and L. Griffin, "Neuromuscular Electrical Stimulation for Skeletal Muscle Function," *Yale J. Biol. Med.*, vol. 85, no. 2, pp. 201–215, Jun. 2012.

[98] P. M. H. Rack and D. R. Westbury, "The effects of length and stimulus rate on tension in the isometric cat soleus muscle," *J. Physiol.*, vol. 204, no. 2, pp. 443–460, Oct. 1969.

[99] E. D. Zonnevijlle, N. N. Somia, R. W. Stremel, C. J. Maldonado, P. M. Werker, M. Kon, and J. H. Barker, "Sequential segmental neuromuscular stimulation: an effective approach to enhance fatigue resistance," *Plast. Reconstr. Surg.*, vol. 105, no. 2, pp. 667–673, Feb. 2000.

[100] D. G. Sayenko, R. Nguyen, M. R. Popovic, and K. Masani, "Reducing muscle fatigue during transcutaneous neuromuscular electrical stimulation by spatially and sequentially distributing electrical stimulation sources," *Eur. J. Appl. Physiol.*, vol. 114, no. 4, pp. 793–804, 2014.

[101] A. C. Hughes, L. Guo, and S. P. Deweerth, "Interleaved multichannel epimysial stimulation for eliciting smooth contraction of muscle with reduced fatigue," *Conf. Proc. Annu. Int. Conf. IEEE Eng. Med. Biol. Soc. IEEE Eng. Med. Biol. Soc. Conf.*, vol. 2010, pp. 6226–6229, 2010.

[102] D. McDonnall, G. A. Clark, and R. A. Normann, "Interleaved, multisite electrical stimulation of cat sciatic nerve produces fatigue-resistant, ripple-free motor responses," *IEEE Trans. Neural Syst. Rehabil. Eng.*, vol. 12, no. 2, pp. 208–215, Jun. 2004.

[103] T. R. Nichols and J. C. Houk, "Improvement in linearity and regulation of stiffness that results from actions of stretch reflex," *J. Neurophysiol.*, vol. 39, no. 1, pp. 119–142, Jan. 1976.

[104] C. M. J. I. Huyghues-Despointes, T. C. Cope, and T. R. Nichols, “Intrinsic properties and reflex compensation in reinnervated triceps surae muscles of the cat: effect of activation level,” *J. Neurophysiol.*, vol. 90, no. 3, pp. 1537–1546, Sep. 2003.

[105] J. C. Houk, J. J. Singer, and M. R. Goldman, “Evaluation of Length and Force Feedback to Soleus Muscles of Decerebrate Cats,” *J. Neurophysiol.*, vol. 33, no. 6, pp. 784–811, 1970.

[106] W. Wallinga-De Jonge, F. L. Gielen, P. Wirtz, P. De Jong, and J. Broenink, “The different intracellular action potentials of fast and slow muscle fibres,” *Electroencephalogr. Clin. Neurophysiol.*, vol. 60, no. 6, pp. 539–547, Jun. 1985.

[107] P. A. Grandjean and J. T. Mortimer, “Recruitment properties of monopolar and bipolar epimysial electrodes,” *Ann. Biomed. Eng.*, vol. 14, no. 1, pp. 53–66, 1986.

[108] R. G. H. Wilke, G. K. Moghadam, N. H. Lovell, G. J. Suaning, and S. Dokos, “Electric crosstalk impairs spatial resolution of multi-electrode arrays in retinal implants,” *J. Neural Eng.*, vol. 8, no. 4, p. 046016, Aug. 2011.

[109] W. M. Grill and J. T. Mortimer, “Stimulus waveforms for selective neural stimulation,” *IEEE Eng. Med. Biol. Mag.*, vol. 14, no. 4, pp. 375–385, Jul. 1995.

[110] R. L. Lieber, *Skeletal Muscle Structure, Function, and Plasticity*. Lippincott Williams & Wilkins, 2002.

[111] D. C. Ackland, P. Pak, M. Richardson, and M. G. Pandy, “Moment arms of the muscles crossing the anatomical shoulder,” *J. Anat.*, vol. 213, no. 4, pp. 383–390, Oct. 2008.

[112] B. Dreibati, C. Lavet, A. Pinti, and G. Poumarat, “Influence of electrical stimulation frequency on skeletal muscle force and fatigue,” *Ann. Phys. Rehabil. Med.*, vol. 53, no. 4, pp. 266–277, May 2010.

[113] M. A. Lyle, A. M. Cloutier, and T. R. Nichols, “Mapping intermuscular force dependent reflex pathways selectively using intramuscular stimulation in the decerebrate cat,” presented at the 45th Annual Meeting of the Society for Neuroscience, Chicago, IL, 2015.

[114] L. Lundy-Ekman, *Neuroscience: Fundamentals for Rehabilitation*. Elsevier Health Sciences, 2013.

[115] N. K. Chin, M. Cope, and M. Pang, "Number and distribution of spindle capsules in seven hindlimb muscles of the cat," presented at the Symposium on Muscle Receptors, Hong Kong, 1961, pp. 241–248.

[116] S. Newman, J. Road, F. Bellemare, J. P. Clozel, C. M. Lavigne, and A. Grassino, "Respiratory muscle length measured by sonomicrometry," *J. Appl. Physiol.*, vol. 56, no. 3, pp. 753–764, Mar. 1984.

[117] D. J. Coughlin, L. Valdes, and L. C. Rome, "Muscle length changes during swimming in scup: sonomicrometry verifies the anatomical high-speed cine technique.," *J. Exp. Biol.*, vol. 199, no. 2, pp. 459–463, Feb. 1996.

[118] S. Vernon and S. S. Joshi, "Brain-Muscle-Computer Interface: Mobile-Phone Prototype Development and Testing," *IEEE Trans. Inf. Technol. Biomed.*, vol. 15, no. 4, pp. 531–538, Jul. 2011.

[119] R. N. Khushaba, S. Kodagoda, D. Liu, and G. Dissanayake, "Muscle computer interfaces for driver distraction reduction," *Comput. Methods Programs Biomed.*, vol. 110, no. 2, pp. 137–149, May 2013.

[120] J. Gomez-Gil, I. San-Jose-Gonzalez, L. F. Nicolas-Alonso, and S. Alonso-Garcia, "Steering a Tractor by Means of an EMG-Based Human-Machine Interface," *Sensors*, vol. 11, no. 7, pp. 7110–7126, Jul. 2011.

[121] A. Subasi, "Classification of EMG signals using PSO optimized SVM for diagnosis of neuromuscular disorders," *Comput. Biol. Med.*, vol. 43, no. 5, pp. 576–586, Jun. 2013.

[122] M. A. Heald and J. B. Marion, *Classical Electromagnetic Radiation*. Mineola, New York: Dover Publications, 2012.

[123] S. Dowdy and S. Wearden, *Statistics for Research (Wiley Series in Probability and Statistics - Applied Probability and Statistics Section)*. New York: John Wiley & Sons Inc, 1983.

[124] H. Hotelling, “Analysis of a complex of statistical variables into principal components,” *J. Educ. Psychol.*, vol. 24, no. 6, pp. 417–441, Sep. 1933.

[125] H. Gävert, J. Hurri, J. Särelä, and A. Hyvärinen, *FastICA*. Helsinki University of Technology, 2005.

[126] G. J. Beneck, L. L. Baker, and K. Kulig, “Spectral analysis of EMG using intramuscular electrodes reveals non-linear fatigability characteristics in persons with chronic low back pain,” *J. Electromyogr. Kinesiol.*, vol. 23, no. 1, pp. 70–77, Feb. 2013.

[127] D. E. Bockelman and W. R. Eisenstadt, “Direct measurement of crosstalk between integrated differential circuits,” *IEEE Trans. Microw. Theory Tech.*, vol. 48, no. 8, pp. 1410–1413, Aug. 2000.

[128] E. J. Kupa, S. H. Roy, S. C. Kandarian, and C. J. De Luca, “Effects of muscle fiber type and size on EMG median frequency and conduction velocity,” *J. Appl. Physiol. Bethesda Md 1985*, vol. 79, no. 1, pp. 23–32, Jul. 1995.

[129] B. Gerdle, K. Henriksson-Larsén, R. Lorentzon, and M. L. Wretling, “Dependence of the mean power frequency of the electromyogram on muscle force and fibre type,” *Acta Physiol. Scand.*, vol. 142, no. 4, pp. 457–465, Aug. 1991.

[130] D. Staudenmann, I. Kingma, D. F. Stegeman, and J. H. van Dieën, “Towards optimal multi-channel EMG electrode configurations in muscle force estimation: a high density EMG study,” *J. Electromyogr. Kinesiol.*, vol. 15, no. 1, pp. 1–11, Feb. 2005.

[131] D. G. Lloyd and T. F. Besier, “An EMG-driven musculoskeletal model to estimate muscle forces and knee joint moments in vivo,” *J. Biomech.*, vol. 36, no. 6, pp. 765–776, Jun. 2003.

[132] T. S. Buchanan, M. J. Moniz, J. P. A. Dewald, and W. Z. Rymer, “Estimation of muscle forces about the wrist joint during isometric tasks using an EMG coefficient method,” *J. Biomech.*, vol. 26, no. 4–5, pp. 547–560, Apr. 1993.

[133] U. J. Naeem, A. A. Abdullah, and C. Xiong, “Estimating human arm’s muscle force using Artificial Neural Network,” in *2012 IEEE International Symposium on Medical Measurements and Applications Proceedings (MeMeA)*, 2012, pp. 1–6.

[134] A. M. Gordon, A. F. Huxley, and F. J. Julian, "The variation in isometric tension with sarcomere length in vertebrate muscle fibres," *J. Physiol.*, vol. 184, no. 1, pp. 170–192, May 1966.

[135] K. A. Edman, "Double-hyperbolic force-velocity relation in frog muscle fibres.," *J. Physiol.*, vol. 404, pp. 301–321, Oct. 1988.

[136] S. Rajaraman, J. A. Bragg, J. D. Ross, and M. G. Allen, "Micromachined three-dimensional electrode arrays for transcutaneous nerve tracking," *J. Micromechanics Microengineering*, vol. 21, no. 8, p. 085014, 2011.

[137] S. P. Sullivan, D. G. Koutsonanos, M. del Pilar Martin, J. W. Lee, V. Zarnitsyn, S.-O. Choi, N. Murthy, R. W. Compans, I. Skountzou, and M. R. Prausnitz, "Dissolving polymer microneedle patches for influenza vaccination," *Nat. Med.*, vol. 16, no. 8, pp. 915–920, Aug. 2010.

[138] Z.-P. Fang and J. T. Mortimer, "Selective activation of small motor axons by quasitrapezoidal current pulses," *IEEE Trans. Biomed. Eng.*, vol. 38, no. 2, pp. 168–174, Feb. 1991.

[139] A. Prochazka, D. Gillard, and D. J. Bennett, "Positive force feedback control of muscles," *J. Neurophysiol.*, vol. 77, no. 6, pp. 3226–3236, Jun. 1997.

[140] V. Dietz, A. Gollhofer, M. Kleiber, and M. Trippel, "Regulation of bipedal stance: dependency on 'load' receptors," *Exp. Brain Res.*, vol. 89, no. 1, pp. 229–231, 1992.

[141] S. P. Lacour, C. Tsay, S. Wagner, Z. Yu, and B. Morrison, "Stretchable micro-electrode arrays for dynamic neuronal recording of in vitro mechanically injured brain," in *IEEE Sensors 2005*, Irvine, CA, 2005, p. 4 pp.–.

[142] R. Levy, T. R. Deer, and J. Henderson, "Intracranial neurostimulation for pain control: a review," *Pain Physician*, vol. 13, no. 2, pp. 157–165, Apr. 2010.

[143] M. J. Morrell and RNS System in Epilepsy Study Group, "Responsive cortical stimulation for the treatment of medically intractable partial epilepsy," *Neurology*, vol. 77, no. 13, pp. 1295–1304, Sep. 2011.

[144] A. C. R. Grayson, R. S. Shawgo, A. M. Johnson, N. T. Flynn, Y. Li, M. J. Cima, and R. Langer, "A BioMEMS review: MEMS technology for physiologically integrated devices," *Proc. IEEE*, vol. 92, no. 1, pp. 6–21, 2004.

[145] R. Bashir, "BioMEMS: state-of-the-art in detection, opportunities and prospects," *Adv. Drug Deliv. Rev.*, vol. 56, no. 11, pp. 1565–1586, Sep. 2004.

[146] D. Rajkumar, T. Nguty, and N. N. Ekere, "Optimising process parameters for flip chip stencil printing using Taguchi's method," in *Electronics Manufacturing Technology Symposium, 2000. Twenty-Sixth IEEE/CPMT International*, 2000, pp. 382–388.

[147] C. H. Cho, J. Park, A. W. Tilles, F. Berthiaume, M. Toner, and M. L. Yarmush, "Layered patterning of hepatocytes in co-culture systems using microfabricated stencils," *BioTechniques*, vol. 48, no. 1, pp. 47–52, Jan. 2010.

[148] G. Vozzi, C. J. Flaim, F. Bianchi, A. Ahluwalia, and S. Bhatia, "Microfabricated PLGA scaffolds: a comparative study for application to tissue engineering," *Mater. Sci. Eng. C*, vol. 20, no. 1–2, pp. 43–47, May 2002.

[149] D. Wright, B. Rajalingam, S. Selvarasah, M. R. Dokmeci, and A. Khademhosseini, "Generation of static and dynamic patterned co-cultures using microfabricated parylene-C stencils," *Lab. Chip*, vol. 7, no. 10, p. 1272, 2007.

[150] S. Jinno, H.-C. Moeller, C.-L. Chen, B. Rajalingam, B. G. Chung, M. R. Dokmeci, and A. Khademhosseini, "Microfabricated multilayer parylene-C stencils for the generation of patterned dynamic co-cultures," *J. Biomed. Mater. Res. A*, vol. 86A, no. 1, pp. 278–288, 2008.

[151] R. Sorkin, T. Gabay, P. Blinder, D. Baranes, E. Ben-Jacob, and Y. Hanein, "Compact self-wiring in cultured neural networks," *J. Neural Eng.*, vol. 3, no. 2, p. 95, Jun. 2006.

[152] T. H. Park and M. L. Shuler, "Integration of Cell Culture and Microfabrication Technology," *Biotechnol. Prog.*, vol. 19, no. 2, pp. 243–253, 2003.

[153] K. S. Ellison, D. B. Chrisey, and D. M. Thompson, "Laser-machining of elastomeric microstencils," *J. Optoelectron. Adv. Mater.*, vol. 12, no. 3, pp. 659–662.

[154] R. Pal, K. E. Sung, and M. A. Burns, "Microstencils for the Patterning of Nontraditional Materials," *Langmuir*, vol. 22, no. 12, pp. 5392–5397, Jun. 2006.

[155] M. Graff, S. K. Mohanty, E. Moss, and A. Bruno Frazier, "Microstenciling: a generic technology for microscale patterning of vapor deposited materials," *J. Microelectromechanical Syst.*, vol. 13, no. 6, pp. 956–962, 2004.

[156] J. S. Lee, W. B. Park, C. W. Park, and G. M. Kim, "Fabrication of nanostencil using size reduction of micro-aperture by additional deposition," in *Microprocesses and Nanotechnology, 2007 Digest of papers*, 2007, pp. 190–191.

[157] F. Vroegindeweij, E. A. Speets, J. a. J. Steen, J. Brugger, and D. H. A. Blank, "Exploring microstencils for sub-micron patterning using pulsed laser deposition," *Appl. Phys. A*, vol. 79, no. 4–6, pp. 743–745, Sep. 2004.

[158] C. G. Courcimault and M. G. Allen, "Reconfigurable shadow mask technology: a microsystem for metal nanoline deposition," *Nanotechnology*, vol. 15, no. 10, pp. S528–S533, Oct. 2004.

[159] E. A. Speets, P. te Riele, M. a. F. van den Boogaart, L. M. Doeswijk, B. J. Ravoo, G. Rijnders, J. Brugger, D. N. Reinhoudt, and D. H. A. Blank, "Formation of Metal Nano- and Micropatterns on Self-Assembled Monolayers by Pulsed Laser Deposition Through Nanostencils and Electroless Deposition," *Adv. Funct. Mater.*, vol. 16, no. 10, pp. 1337–1342, 2006.

[160] Y. Nam, K. Musick, and B. C. Wheeler, "Application of a PDMS microstencil as a replaceable insulator toward a single-use planar microelectrode array," *Biomed. Microdevices*, vol. 8, no. 4, pp. 375–381, Dec. 2006.

[161] S. H. Jeong, A. Hagman, K. Hjort, M. Jobs, J. Sundqvist, and Z. Wu, "Liquid alloy printing of microfluidic stretchable electronics," *Lab. Chip*, vol. 12, no. 22, pp. 4657–4664, Oct. 2012.

[162] Y. Zheng, W. Dai, D. Ryan, and H. Wu, "Fabrication of freestanding, microperforated membranes and their applications in microfluidics," *Biomicrofluidics*, vol. 4, no. 3, p. 36504, 2010.

[163] L. M. D. Nao Takano, "Fabrication of metallic patterns by microstencil lithography on polymer surfaces suitable as microelectrodes in integrated microfluidic systems," *J. Micromechanics Microengineering*, vol. 16, no. 8, 2006.

[164] S. Selvarasah, S. H. Chao, C.-L. Chen, S. Sridhar, A. Busnaina, A. Khademhosseini, and M. R. Dokmeci, "A reusable high aspect ratio parylene-C shadow mask technology for diverse micropatterning applications," *Sens. Actuators Phys.*, vol. 145–146, pp. 306–315, Jul. 2008.

[165] W. Longsine-Parker and A. Han, "Laser stenciling: a low-cost high-resolution CO2 laser micromachining method," *J. Micromechanics Microengineering*, vol. 22, no. 1, p. 015006, Jan. 2012.

[166] J. E. Cotter, G. Yao, and B. Eggleston, "Laser-formed stencils for printed silicon solar cells," in *Conference Record of the Thirty-first IEEE Photovoltaic Specialists Conference, 2005*, 2005, pp. 1169–1172.

[167] S. M. Yi, S. H. Jin, J. D. Lee, and C. N. Chu, "Fabrication of a high-aspect-ratio stainless steel shadow mask and its application to pentacene thin-film transistors," *J. Micromechanics Microengineering*, vol. 15, no. 2, p. 263, Feb. 2005.

[168] J. H. Choi, H. Lee, H. K. Jin, J. Bae, and G. M. Kim, "Micropatterning of neural stem cells and Purkinje neurons using a polydimethylsiloxane (PDMS) stencil," *Lab. Chip*, vol. 12, no. 23, pp. 5045–5050, Dec. 2012.

[169] H. Wang, A. Chakraborty, and C. Luo, "Fabrication of Au micropatterns on vertical Si sidewalls using flexible PDMS shadow masks," *J. Micromechanics Microengineering*, vol. 20, no. 12, p. 127001, Dec. 2010.

[170] P. Jothimuthu, A. Carroll, A. A. S. Bhagat, G. Lin, J. E. Mark, and I. Papautsky, "Photodefinable PDMS thin films for microfabrication applications," *J. Micromechanics Microengineering*, vol. 19, no. 4, p. 045024, Apr. 2009.

[171] R. J. Jackman, D. C. Duffy, O. Cherniavskaya, and G. M. Whitesides, "Using Elastomeric Membranes as Dry Resists and for Dry Lift-Off," *Langmuir*, vol. 15, no. 8, pp. 2973–2984, Apr. 1999.

[172] Q. Xiang, B. Xu, R. Fu, and D. Li, "Real Time PCR on Disposable PDMS Chip with a Miniaturized Thermal Cycler," *Biomed. Microdevices*, vol. 7, no. 4, pp. 273–279, Dec. 2005.

[173] A. A. S. Bhagat, P. Jothimuthu, and I. Papautsky, "Photodefinable polydimethylsiloxane (PDMS) for rapid lab-on-a-chip prototyping," *Lab. Chip*, vol. 7, no. 9, p. 1192, 2007.

[174] H.-I. Wu, G.-H. Cheng, Y.-Y. Wong, C.-M. Lin, W. Fang, W.-Y. Chow, and Y.-C. Chang, "A lab-on-a-chip platform for studying the subcellular functional proteome of neuronal axons," *Lab. Chip*, vol. 10, no. 5, p. 647, 2010.

[175] S.-H. Hur, D.-Y. Khang, C. Kocabas, and J. A. Rogers, "Nanotransfer printing by use of noncovalent surface forces: Applications to thin-film transistors that use single-walled carbon nanotube networks and semiconducting polymers," *Appl. Phys. Lett.*, vol. 85, no. 23, pp. 5730–5732, Dec. 2004.

[176] J. C. McDonald, M. L. Chabinyc, S. J. Metallo, J. R. Anderson, A. D. Stroock, and G. M. Whitesides, "Prototyping of microfluidic devices in poly(dimethylsiloxane) using solid-object printing," *Anal. Chem.*, vol. 74, no. 7, pp. 1537–1545, Apr. 2002.

[177] "University Cleanrooms List." Brigham Young University, 2009.

[178] Thomas D. Snyder and Sally A. Dillow, "Digest of Education Statistics, 2012," 31-Dec-2013. [Online]. Available: https://nces.ed.gov/pubsearch/pubsinfo.asp?pubid=2014015. [Accessed: 09-May-2014].

[179] "Product Information – Sylgard® 184 Silicone Elastomer." Dow Corning Corp., Midland, MI, 2007.

[180] G. Bjørnsen and J. Roots, "Plasma etching of polydimethylsiloxane: Effects from process gas composition and dc self-bias voltage," *J. Vac. Sci. Technol. B*, vol. 29, no. 1, p. 011001, Jan. 2011.

[181] E. S. Tarleton, J. P. Robinson, S. J. Smith, and J. J. W. Na, "New experimental measurements of solvent induced swelling in nanofiltration membranes," *J. Membr. Sci.*, vol. 261, no. 1–2, pp. 129–135, 2005.

[182] J. Park, C. H. Cho, N. Parashurama, Y. Li, F. Berthiaume, M. Toner, A. W. Tilles, and M. L. Yarmush, "Microfabrication-based modulation of embryonic stem cell differentiation," *Lab. Chip*, vol. 7, no. 8, pp. 1018–1028, Aug. 2007.

[183] E. Ostuni, R. Kane, C. S. Chen, D. E. Ingber, and G. M. Whitesides, "Patterning Mammalian Cells Using Elastomeric Membranes," *Langmuir*, vol. 16, no. 20, pp. 7811–7819, Oct. 2000.

[184] S. M. Potter and T. B. DeMarse, “A new approach to neural cell culture for long-term studies,” *J. Neurosci. Methods*, vol. 110, no. 1–2, pp. 17–24, Sep. 2001.

[185] Y. Jimbo, T. Tateno, and H. P. Robinson, “Simultaneous induction of pathway-specific potentiation and depression in networks of cortical neurons.,” *Biophys. J.*, vol. 76, no. 2, pp. 670–678, Feb. 1999.

[186] N. P. Bansal and R. H. Doremus, *Handbook of Glass Properties*. Elsevier, 2013.

[187] D. O. Kipp and MatWeb (Online service), *Plastic material data sheets*. [Blacksburg, Va.?]: MatWeb, Division of Automation Creation, Inc., 2004.

[188] M. Thiel and M. Hermatschweiler, “Three-dimensional laser lithography,” *Opt. Photonik*, vol. 6, no. 4, pp. 36–39, Dec. 2011.